BUDAPEST UNIVERSITY OF
TECHNOLOGY AND ECONOMICS

Delft University of Technology

The effect of navigation on the flow in a river trained with groynes

Master's Thesis

Barbara Kéri

2011/2012 1st semester

Supervisors:

Dr. Sándor Baranya
prof.Dr. János Józsa
dr.ir. Robert Jan Labeur
Bas van Leeuwen MSc
prof.dr.ir. Wim Uijttewaal
ir. Henk Verheij

Preface

This report is my master thesis for the conclusion of my Master's program at the Budapest University of Technology and Economics (Budapesti Műszaki és Gazdaságtudományi Egyetem) in the program called Infrastructural Engineering MSc. It is also the conclusion of my ERASMUS scholarship at Technical University Delft (Technische Universiteit Delft).

First I would like to thank my supervisors from both the Netherlands and Hungary. As I do not want to differentiate because each of them gave me support on an indispensable level, I put their names in alphabetical order on the front page. I choose a chronological order to thank each of them.

Prof. Dr. János Józsa was lecturing me first, and then we connected through research studies about ADCP in Student Scientific Contests. He gave me several references over the years, which made it possible for me to apply for many scholarships. I am truly thankful to him because of all the support he gave me.

Dr. Sándor Baranya was my daily supervisor with the research studies we were conducted on ADCP. Later he was my supervisor on my BSc thesis. He taught me how to set my mind towards research purposes, while using software programs written for practicing engineers.

Prof.Dr.ir. Wim Uijttewaal was kind enough to host me as an exchange student for my final project. Without his understanding about my position upon arriving to Delft, probably I would not have been able to finish this thesis.

Dr.ir. Robert Jan Labeur gave me advices on numerical simulations with FINEL2D and later introduced me to Svašek Hydraulics, where I later conducted all my numerical simulations.

Ir. Henk Verheij taught me about navigation, which is one of my favourite topics in hydraulic engineering, which personally means a lot to me.

I would like to thank all the employees of Svašek Hydraulics who helped me, especially Bas van Leuween, who became my daily supervisor during my stay. He was always open to all of my questions, which made it easier for me to adapt.

During my stay in the Netherlands I was facing several problems (varying from housing to personal matters), in this last section I would like to thank to all the people who helped me: prof. László Hayde from UNESCO-IHE, the employees of TU Delft (especially the employees of the laboratory), friends from all over the world and last but not least, my family.

Thanks to Irma van Houdt for the picture on the front page.

Summary

The study deals with the investigation of flow structures in groyne fields interacting with the flow generated by navigation. Groynes are traditionally constructed to ensure adequate water depth for navigation, so the interaction of navigation and groyne fields is nearly guaranteed. The Hungarian Danube section – which is part of the 7th European transport corridor – has a great importance, however, there are several places where the minimum 25 dm navigational water depth is not available in low water regime. As the River Waal (a branch of River Rhine), which falls in the same category of navigable waterways as River Danube, in my TU Delft based research I used that particular Dutch river as case study.

The goal of this graduation project is formulated as follows: *What kind of effects does navigation have on river morphology?* This was investigated on physical basis by means of a numerical model. First, the influence of push towing on morphology is investigated by analyzing the bed shear stress distributions, then the impacts on groyne fields. It could be concluded that primary waves caused by push tows increase the bed shear stresses around the ship, moreover, groyne fields are also affected, especially their zone close to the main stream. The impact of different ship sets on shear stresses was also studied. It was found that the most significant effect was caused by the ship velocity, the sailing distance between ship and groynes, a moderate one by the ship's width and a minor one by the ship's length. A numerical morphological model could offer a more detailed insight in the morphological changes than analyzing the bed shear-stress distribution, only, a recommendation for future studies is therefore the implementation of such a model. FINEL2D's capability of predicting the flow changes at groyne fields caused by navigation have been shown, although FINEL2D only uses advective momentum transport (but suffering from some numerical viscosity) to predict the flow, while in the groyne fields inhomogeneous turbulent processes are supposed to be dominating. Nevertheless, FINEL2D showed a sufficient match with physical model results.

Összefoglalás

A diplomamunka a hajózás hatásait vizsgálja egy sarkantyúkkal szabályozott folyószakasz áramlási viszonyaira. Sarkantyúkat hagyományosan a hajózásnak megfelelő vízmélység kikényszerítése érdekében építenek, miközben belátható, hogy a hajózásnak a sarkantyúk közti területre visszahatása van, végeredményben tehát egy bonyolult kölcsönhatás-mechanizmus alakul ki. A magyar Duna-szakasznak, ami része a 7-ik európai közlekedési folyosónak, nagy a hajózási jelentősége, azonban több helyen nehezíti a hajózást az, hogy a 25 dm-es merülési mélységhez szükséges vízmélység kisvízi viszonyok mellett nincs meg. Kihasználva, hogy a hollandiai Waal folyó (a Rajna egyik ága), a Dunával azonos hajóút kategóriába esik, a Delfti Műszaki Egyetemen folytatott kutatásaimat erre a folyóra, mint itthon is hasznosítható esettanulmányra összpontosítottam.

A munka során több részkérdésre is kerestem a választ, amelyek köre röviden így fogalmazható meg: *Milyen hatásai vannak a folyami hajózásnak a hidromorfológiára?* Mindezt fizikai alapon nyugvó egyszerűbb analitikus illetve bonyolultabb 2D numerikus áramlási modell segítségével is vizsgáltam. Először a tolóhajók által kifejtett fenék-csúsztatófeszültség változásokat, illetve azok hatását elemeztem a sarkantyúk közötti területekre. A tolóhajók főként az elsődleges hullámokkal okoznak változásokat a fenék-csúsztatófeszültség eloszlásában, elsősorban eróziót a sarkantyúk közötti terület sodorvonalhoz közelebbi felén. A különböző hajójellemzők változtatásának fenék-csúsztatófeszültségre kifejtett hatását szintén vizsgáltam. Itt azt az eredményt kaptam, hogy legnagyobb hatása a vizsgált jellemzők közül a hajó sebességének, és a sarkantyúk valamint a hajó közti távolságnak van, ehhez képest a hajó szélességének hatása mérsékeltebb, a hajóhosszának pedig elenyésző. Az áramlási modellen túlmenően a morfológiai változások becslésére alkalmas modul felállítása szintén nagyon hasznos lenne, mivel a fenék-csúsztatófeszültség csupán kvalitatív eredményeket szolgáltat, míg a hordalékmozgás vizsgálata a hidrodinamikai viszonyok létrehozta mederváltozások közvetlen számítását tenné lehetővé. A FINEL2D szoftvernek a hajómozgás által okozott hidrodinamikai folyamatok reprodukálására való képességét bizonyítottam. Ugyan a FINEL2D csak az advektív gyorsulást leíró tagokat tartalmazza, így a (turbulens) viszkozitás hatása legfeljebb az advekció közelítő megoldását terhelő numerikus viszkozitással kerülhet ennek az erős turbulenciájú folyamatnak a számításába, a modell kielégítő egyezést mutatott a korábbi kisminta-modelleredményekkel.

Az 1. fejezet a témafelvetést, a 2. fejezet a Duna és Rajna folyók összehasonlítását tartalmazza. A 3. fejezet kiterjedt irodalmi áttekintést ad, részletesen kitérve a sarkantyúk áramlásra kifejtett hatásaira illetve a hajózás által okozott hatásokra. Ezen belül a 3.3 alfejezet írja le a Verheij és Vermeer által 1987-ben végzett kisminta modellezés eredményeit, melyre aztán a numerikus modellt alapoztam. A 4. fejezetben a felhasznált numerikus modellt, és a modell felállítását ismertetem. Az 5. fejezetben a kalibrálást és validálást írom le, kiválasztott pontokban a numerikus modell vízszintsüllyedésre és legnagyobb előforduló sebességre adott eredményeit a fizikai modellén túl egy analitikus megoldás eredményeivel is összehasonlítva. A 6. fejezetben a numerikus modellből kapott áramlási jellemzők eloszlását vizsgáltam. A 7. fejezetben a modell érzékenységét elemeztem különböző hajóparaméterekre. A 8. egy kritikai fejezet az eredmények

helyességéről, míg a 9. fejezet a következtetéseket és ajánlásokat tartalmazza. Az értekezés törzsét az irodalomjegyzék zárja, és ezt követik a mellékletek, ahol a FINEL2D részletes elméleti leírását, a kalibrálás és validálás eredményeit ismertetem, valamint egy képsorozat adok arról, hogy egy 3x2-es felépítésű tolóhajó a sarkantyúk közelében haladva hogyan változtatja meg a vízfelszínt és az áramlási sebességvektor-mező eloszlását.

Contents

1. Introduction

Initially the use of groynes was to make rivers more navigable via the morphological processes which, on the one hand reducing the cross section resulting in higher flow velocities in the main channel and related higher bed shear stress. The increased sediment entrainment capacity will result in river bed deepening ensuring the adequate water depth for navigation. On the other hand, the groyne fields slowly fill up with fine suspended sediment which reduces the cross-section area. At the same time, the navigation also affects the flow structure and so the morphology of rivers. The latter phenomenon is studied in this thesis.

1.1. Problem definition

This thesis deals with the effect of the inland navigation on river hydrodynamics, playing an important role in the Hungarian transport-development. As one of the most important tasks, river engineering measures have to be constructed to make the Danube more suitable for navigation; as the Danube is the 7th European transport corridor. In the Hungarian Danube reach in case of low water regime, the water depth is not satisfactory at several places (e.g. fords), i.e. does not reach the 25 dm minimum navigable water depth. The present designs contain dredging, constructing groynes and weirs. The present study focuses on the effect of navigation in a river trained by groynes.

1.2. Research objective

The goal of this graduation project is formulated as follows: *What kind of effects has navigation on river morphology?* The goal is formulated in a way that this project can contribute both for BME and TU Delft. The chosen research area is both the Rhine and the Danube hereinafter. The Rhine is already channelized: either trained with groynes or power plants are keeping the water level high enough for navigation; while the Danube is more like a free-flowing river. This free flowing river section is difficult to navigate (at several sections the water depth does not reach the 25 dm minimum) and it changes frequently while there are also several crossings, especially in the Hungarian section which is more than 400 km long.

Based on the objective, the following research questions will be answered:

(i) How does push-towing influence morphology?

a) How does it influence bed shear stresses, relative to groyne fields without ships passing?

b) What is the influence of different ship sets on bed shear stress?

c) What additional insights can be found by using a morphology set-up in the model?

(ii) Is FINEL2D able to show the changes in the flow field at groyne fields?

a) On a fundamental level, is FINEL2D capable of these predictions or is a different model or even 3D modeling needed?

b) How do FINEL2D results do compared to measurements from the physical model? (verification)

1.3. Report outline

The report is structured as follows: Chapter 2 is an introduction to the Danube and Rhine which describes the differences between the two rivers. Chapter 3 describes the literature study that was done which focused on groynes and navigation. In Chapter 3.3 the scale model study from the Rhine done by Delft Hydraulics is explained. The scale model's set-up has been used to verify the numerical simulations done by FINEL2D in Chapter 4. Model results are described in Chapter 6 while sensitivity analysis is addressed in Chapter 7. The research results are discussed in Chapter 8. Chapter 9 gives the conclusions and recommendations for further research. Finally, the last chapter gives a list of the references used.

2. Danube-Rhine comparison

River Rhine is 1200 km long and the southern part of the Netherlands can be considered as its estuary. This is shown in Figure 1. It also shows the whole river basin in the upper left corner. River Rhine is crossing several borders between countries like Switzerland, Germany, France and the Netherlands.

The Netherlands has two large rivers flowing across its borders: the Rhine and the Maas. The Rhine is divided into three rivers called: the IJssel, the Neder-Rijn and the Waal. River Waal is the main distributary branch of river Rhine and it carries more than 60% of the Rhine discharge. In earlier days it carried up to 90% of the flow. Figure 1 displays the southern part of Holland where the Rhine is distributed into the above mentioned branches.

Figure 1 Waterways in the Netherlands (source: Rijkswaterstaat, 2011)

The historical background of River Rhine is written after Yossef, 2002. The first major hydraulic engineering works after the Romans were taken in the 1700s.

Channel corrections have been carried out and groynes, dams were built. There have been several channels built from the Rhine, to let inland navigation grow.

River Danube is 2900 km long and flowing into the Black Sea. It crosses even more borders than River Rhine. It comes from Germany and flows to Austria, Slovakia, Hungary, Serbia, Romania, Bulgaria and lastly to Ukraine. A map is presented from via donau in Figure 2.

Figure 2 Danube flowing through Hungary – map (source: via donau, 2011)

The classification of waterways is introduced in Chapter 3.2. That is an older classification, and gives a good, hopeful impression that Danube in 2011 is already considered as a VII category waterway. Although in the Hungarian free flowing section several crossings are making hard to navigate with small water depths. Bakonyi, 2009 mentions that from 1992 the Hungarian Danube section has the same categorization as River Rhine, VIb and VIc. The shallow sections need maintenance e.g. dredging, hydraulic structures like groynes (VITUKI, 2009). These measurements would take account on the flora and fauna in the riverine environment. Before taking any measurements it is purposeful to look around in the world, and use the available knowledge to make those measures better.

This comparison is done to conclude that on River Rhine a lot can be seen for the future of navigation on River Danube. River Waal as the main branch of River Rhine has been chosen to investigate, which is close to the Hungarian River Danube. River Rhine has also been chosen to study because in Europe it is the biggest river which has a lot of navigation impacts.

3. Literature review

The literature study is going to separate parts as the effect of navigation on groyne fields hasn't been studied enough to base a whole chapter on it.

3.1. Groynes

3.1.1. Introduction to groynes

This is an introductory section about groynes after Yossef, 2002. The first river training measures date back to the 16th century in China. Modern river training started in Europe after the 1850's. The intentions of river training were mainly to deflect floods, reduce ice jamming, protect banks from erosion and improve navigation. The employed training structures can be categorized as bed fixation, longitudinal structures and transverse structures. Groynes are transverse structures, built to reduce the discharge cross-sections. Groynes can be categorized in several ways:

- building material: can be permeable (from piles, like wood or bamboo) or impermeable (from rock gravel or gabions),
- appearance in plan: straight, T-head, L-head, inverted hockey shape, wing or tail groynes, straight groynes with pier heads,
- action on stream flow: attracting (point downstream, attract the flow towards themselves), deflecting (short, used for local protection) and repelling (point upstream, repel the flow away from themselves),
- submergence: emerged or submerged (usually impermeable groynes are designed to be non-submerged).

The characteristic features of groyne design are described in this section after Yossef, 2002. "The most important considerations involved in groyne design are plan view shape, length of the groynes, spacing between groynes, orientation to the flow, crest elevation and slope, cross-section, construction material and scour". Plan view shapes, main construction materials and orientations are already listed above. Groyne length depends on several features like location, purpose, spacing and economics of construction. Spacing between groynes can vary between 1.5 to 6 times the groyne length; the variation is related to river width, groyne length, velocity of flow, angle to the bank, orientation to the flow, bank curvature and purpose. Crest elevation depends on the purpose of a groyne and on the possibility of overbank flow and ice. Crest widths usually vary between 1 and 6 m, while side slopes range from 1:1.25 to 1:5.

The area between groynes is called the groyne field. Yossef, 2002 determined the characteristics of the groyne fields on River Waal, the main results of these statistics are introduced below. Figure 3 shows the following dimensions (in brackets the average values on River Waal):

A: groyne field length (≈ 200 m)
B: groyne field width (≈ 60 m)
C: length along the waterline
D: beach width (≈ 25 m)

E: distance between the normal line and the thalweg
F: river width (between groynes) (≈ 260 m)
G: orientation of groyne (≈ 0°)
H: orientation of groyne field (≈ 90°)

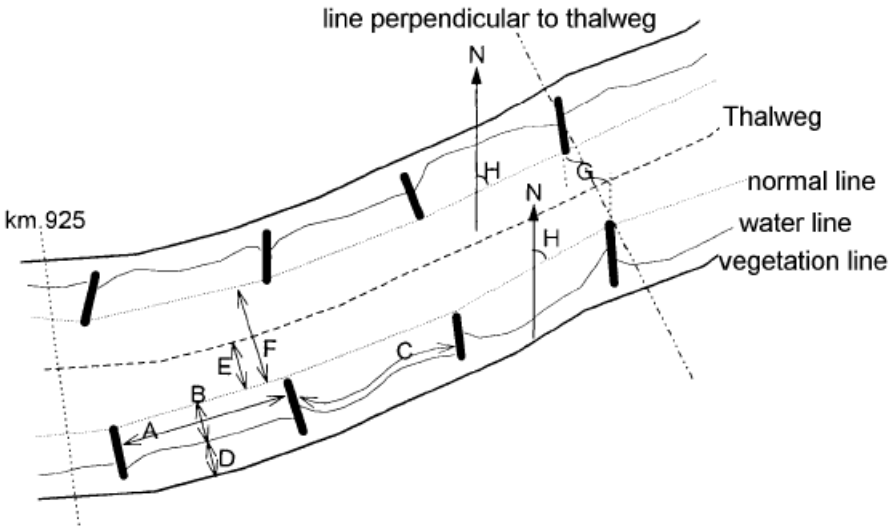

Figure 3 Definitions for the dimensions of an arbitrary groyne field (source: Yossef, 2002)

There are also two major characteristics about groyne fields: beach slope and bed material size (D_{50}). The average beach slope on River Waal is 1:25, while the average D_{50} is 350 μm (Yossef, 2002). W/L ratio, which is the groyne field width divided by groyne field length (in Figure 3 B/A), is later used as a representative feature of groyne fields. On River Waal the average W/L ratio is 0.33.

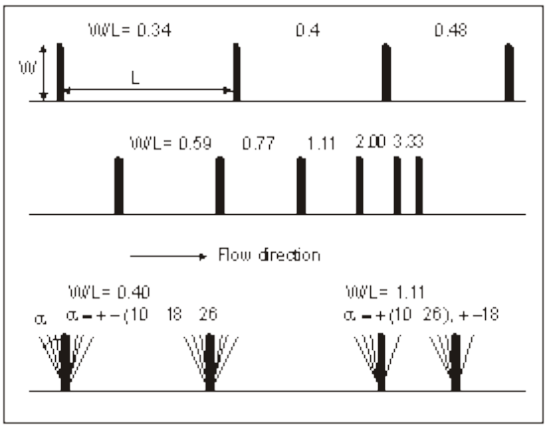

Figure 4 Representation of the W/L ratios as groyne field parameters (source: Weitbrecht and Hinterberger, 2001)

3.1.2. Flow near groynes

There are major differences between the developing flow structures around a single groyne or around a chain of groynes. As the research focuses on groyne fields, the flow around a single groyne is not detailed here.

Yossef, 2002 summarized this topic, his study is used in this section, therefore. A single groyne separates the flow field into four main zones: main flow zone, return

flow zone, shear layer and reattachment zone. From the tip of the groyne to the opposite channel bank is called the main flow zone. The return flow zone is located just downstream of the groyne with generally two large eddies. Shear layer is developed between the main flow zone and the return flow zone resulted by the velocity difference between the two zones. The reattachment zone is simplified as a point where the boundary streamline reattaches to the channel boundary. The area influenced by the groyne is called separation region which can vary from 7 times the length of a groyne to 15 times the length. The developed horizontal eddies are migrating downstream from the tip of the groyne, in the end the y merge each other. The water surface fluctuates around a groyne which, in general, means that upstream from the groyne the water level increases and downstream it decreases.

The level of submergence greatly affects the flow patterns in groyne fields. If groynes are non-submerged, the groyne fields are not part of the wetted cross-section of a river, thus this flow feature is not influenced by the discharge in the main channel. Additionally, flow pattern changes with the change of its location along the river (inner curve, outer curve or straight part – see: Figure 5) and/or the groynes orientation (Yossef, 2002).

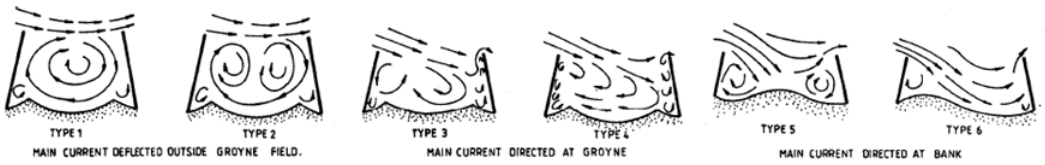

Figure 5 Types of flow pattern in groyne fields (source: Przedwojski et al, 1995)

The flow field results in various flow structures according to groyne field geometry (Lehmann et al., 1999). Figure 6 displays three categories, which can describe the main flow structure from geometry.

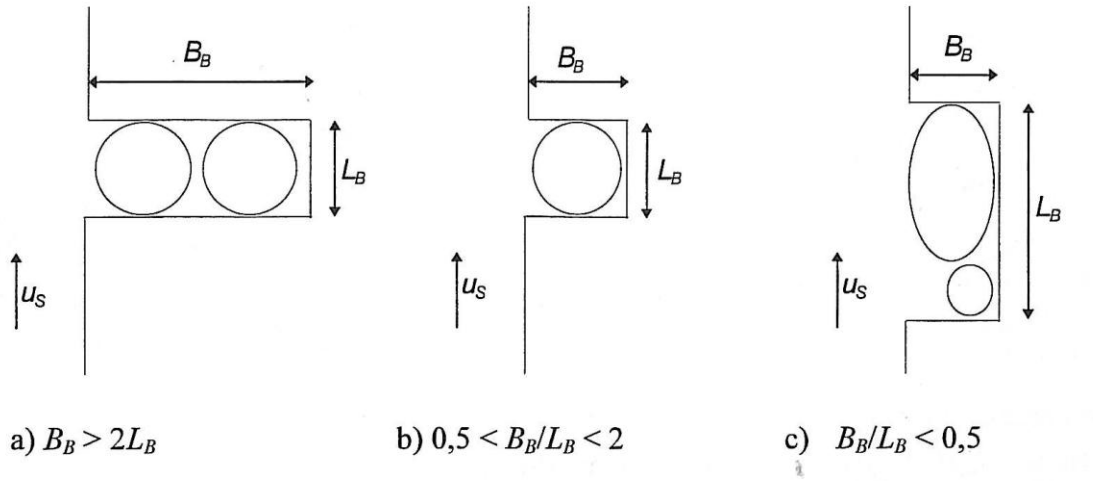

Figure 6 The influence of groyne field geometry on the eddy structures (source: Wallast, 1998)

The groyne field length is going to be described in the next sentences as L_B in Figure 6 (later just L) while the groyne field width is B_B (later just W). In the followings the three categories are defined according to Figure 6 after Lehmann et

al., 1999, where L_B marks the length of the groyne field, while B_B is the width of the groyne field:

a, $B_B/L_B>2$

At least two eddies appear in this case. The first eddy will directly develop in the shear layer between the still water and the main flow, while other eddies will be driven through the energy input through the shear layer between the eddies.

b. $0.5 \leq B_B/L_B \leq 2$

At this B_B/L_B ratio only one eddy appears, which can be formed as an ellipse with a maximum length of the half width of the groyne field.

c. $B_B/L_B<0.5$

These are the so called elongated groyne fields. More eddies form here, having a rapid exchange with the main stream. The smaller, secondary eddy from the two will only have exchange with the large eddy.

Since the typical groyne fields in the Netherlands (and also in the Hungarian Danube) belong to class *C*, this one will be studied in this research. The large eddy, in such a case, is called primary eddy, while the small one is called secondary eddy (Yossef, 2002). Yossef, 2002 also concluded that "the flow pattern when groynes are not submerged is predominantly two-dimensional. The small scale three-dimensional turbulence plays a minor role in the mass and momentum exchange process between the groyne field and the main channel". "With the exception for the area near the groyne head where the flow is strongly three-dimensional."

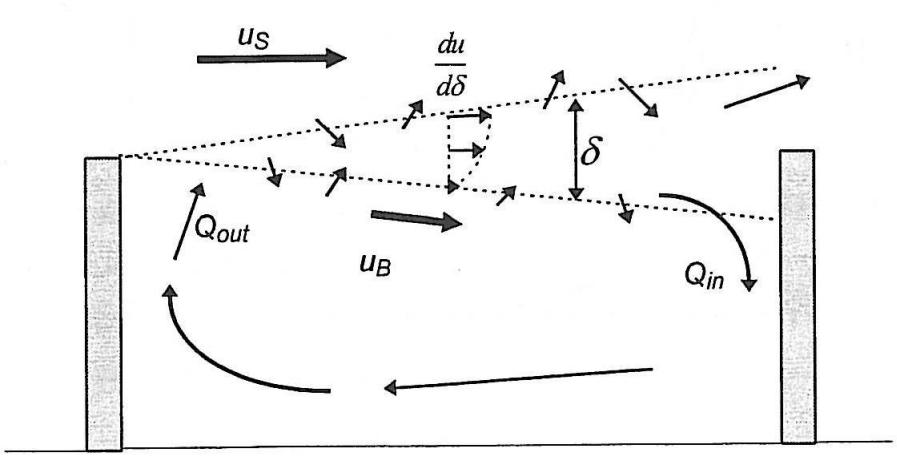

Figure 7 Formation of a rotational movement in groyne field due to the flow in the main channel (source: Lehmann et al., 1999)

Exchange processes between the main flow and the groyne fields are described after Lehmann et al., 1999. Flow in the groyne field is influenced by various forces. Beside water level changes and density differences (their influence is not considered further here) the flow in the groyne field is mainly produced by forces that are transmitted in the shear layer between the slow dead zone flow and the fast main stream caused by shear stresses. The presence of a velocity gradient indicates that shear stresses act in this area. This leads to that the contact surface in a flow direction directs the motion of the water particles in the groyne field. A

mixing layer is formed between the main flow and groyne field, which is located in the downstream area of the groyne, water enters (Q_{in}) and transfers water from the groyne field (Q_{out}). When the spacing of the groynes is greater than a critical distance, than an eddy system can form in the groyne field, which can lead to complete mixing of the groyne field (see Figure 7).

The two eddy's exchange process with the main stream, which are formulating in an elongated groyne field (see Figure 6, c), is described after Lehmann et al., 1999. The primary eddy, which has a faster rotational velocity, has an exchange with the main flow, while the slower secondary eddy has no direct connection with the main flow, just with the primary eddy, thus it will only have an exchange with the main flow through the primary eddy. If a water particle gets into the secondary eddy, it will spend more time in the groyne field than otherwise.

3.2. Navigation

"Navigation is a water resource use of significant historical importance – social and economic development would not have been possible without navigation." (PIANC, 2003) Inland navigation has an ancient past by being one of the oldest modes of transport. Inland waterway systems primarily shaped in areas where large rivers flow, but there are many canals built around those areas (e.g.: the Netherlands, UK, USA). Inland navigation varies widely in every country, mainly because of the geographical situation (Verheij et al., 2008). The main advantages of inland waterways according to Verheij et al., 2008 are the high level of safety, the environmental friendliness, the low costs per tonkm and the capacity.

Later in the study several ship sizes are studied according to the classification of ships in Figure 8. (Several classification methods exist but this one is a world-wide known classification.) At the same time the ship classification plays an important role in the categorization of waterways. (Verheij et al., 2008)

Type of inland waterways		Classes of navigable waterways	Motor vessels and barges					Minimum height under bridges (m)
			Type of vessel: general characteristics					
			Designation	Length (m)	Beam (m)	Draught (m)	Tonnage (T)	
Of regional importance	To West of Elbe	I	Péniche barge	38.50	5.05	1.80-2.20	250-400	4.00
		II	Campine barge	50-55	6.60	2.50	400-650	4.00-5.00
		III	D.E.K.	67-80	8.20	2.50	650-1000	4.00-5.00
	To East of Elbe	I	Grosse Finow	41	4.70	1.40	180	3.00
		II	Barka Motorowa 500	57	7.50-9.00	1.60	500-630	3.00
		III		67-70	8.20-9.00	1.60-2.00	470-700	4.00
Of international importance		IV	R.H.K.	80-85	9.5	2.50	1000-1500	5.25 or 7.00
		Va	Large Rhine Vessels	95-110	11.40	2.50-2.80	1500-3000	5.25
		Vb						7.00 or 9.10
		VIa						7.00 or 9.10
		VIb		140	15.00	3.90		7.00 or 9.10
Type of inland waterways		Classes of navigable waterways	**Pushed convoys**					Minimum height under bridges (m)
			Type of convoy: general characteristics					
			Designation	Length (m)	Beam (m)	Draught (m)	Tonnage (T)	
Of regional importance		I						3.00
		II						3.00
		III		118-132	8.20-9.00	1.60-2.00	1000-1200	4.00
Of international importance		IV		85	9.5	2.50-2.80	1250-1450	5.25 or 7.00
		Va		95-110	11.40	2.50-4.50	1600-3000	5.25
		Vb		172-185	11.40	2.50-4.50	3200-6000	7.00 or 9.10
		VIa		95-110	22.80	2.50-4.50	3200-6000	7.00 or 9.10
		VIb		185-195	22.80	2.50-4.50	6400-12000	7.00 or 9.10
		VIc	6 barges, long 6 barges, wide	270-280 193-200	22.80 33.00-34.20	2.50-4.50 2.50-4.50	9600-18000 9600-18000	9.10
		VII		285 195	33.00-34.20	2.50-4.50	14500-27000	9.10

Figure 8 Classification of waterways by PIANC (source: Verheij et al., 2008)

The next section will give a brief description on ship types, based on Verheij et al., 2008. One can encounter several types of ships on inland waterways, but the most common ones are: motor ships and the so-called push tow convoys. Motor vessels can be traditional vessels, bulk vessels, container vessels, RORO vessels, car carriers and tankers. A pushed tow convoy contains a push boat and push barges. The push boat provides the propulsion. The barges and the push boat are stiffly connected so they are maneuvering as one vessel. Pushed convoys were invented in the USA, and first used on the Mississippi River and the Ohio River in the 19th century. They were introduced in Europe only in 1957 (PIANC, 1988). However, there are differences between the convoys used in Europe from the ones used in the US. The European rivers are generally narrower, shallower and have higher flow velocities, and accordingly American convoys are bigger and have larger draughts (can be seen on Figure 9).

Figure 9 American pushed convoys on the Mississippi (source: USACE – St. Louis district)

The standard dimensions of a barge are 76.50 m length, 11.4 m width and a maximum draught of 4 m; while the typical dimensions of a tugboat are about 35.50 m length, 14.45 m width and 1.83 m draught.

The Rhine, as was already shown, is a VIb category waterway, but it has sectional restrictions (see Figure 10).

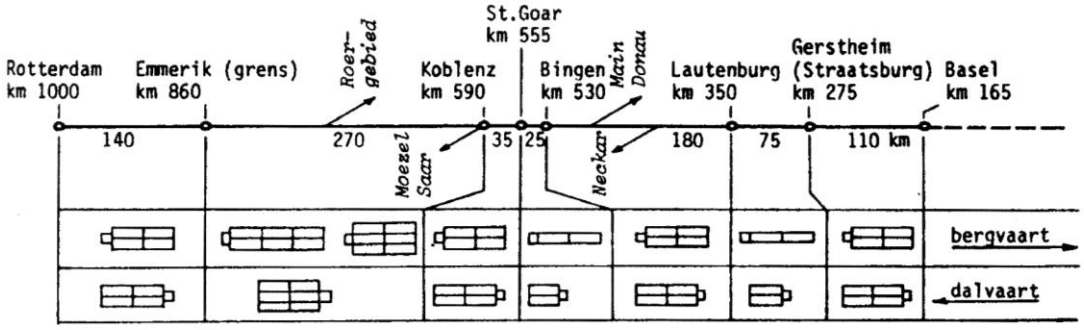

Figure 10 Maximum allowed size of pushed convoys on the Rhine (1980) (source: Verheij et al., 2008)

The interaction between ships and waterways is described after Verheij et al., 2008. A sailing ship causes certain water movements; "the ship's bow will constantly push water to the front and aside, while at the same time a corresponding amount of water is being supplemented at the stern, behind the ship."

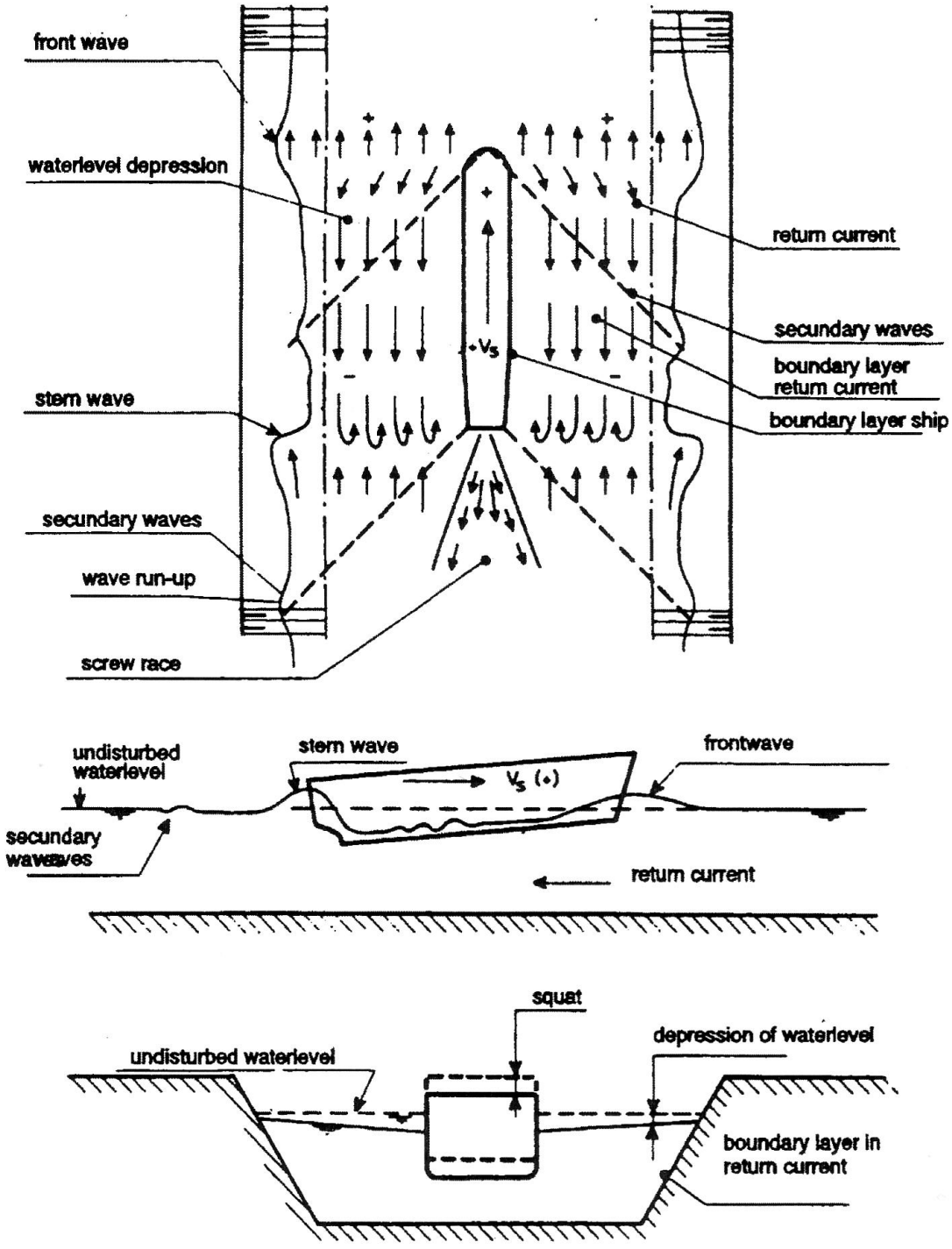

Figure 11 Water movement around a ship on a restricted waterway (source: Verheij et al., 2008)

The hydraulic phenomena about the ship induced water movement can be described as three characteristic features: primary waves, secondary waves and propeller jet after Verheij et al., 2008. The primary water motion is connected to the displacement of water caused by the ship, so it contains the water level depression and return current together. The return current is induced by the displacement of water along and under the ship. This primary wave system is dominant in waterways where the cross-sectional blockage caused by ship is

significant (Schiereck, 2001). The secondary wave system contains also ship-induced waves, but these are short waves. The height of these waves highly depends on the speed of a ship, but also on the shape and the dimensions of a ship's hull. Usually the smaller and faster ships cause major secondary water movement, while the larger ones are more important for primary movements (Schiereck, 2001). Propeller jets are getting more and more important as time passes – as the shipping industry emphasizing the capacity and so the propulsion of ships. More powerful propellers cause higher flow velocities. The propeller wash plays a significant role when ships are maneuvering at low velocities (Schiereck, 2001).

In this section the ship-induced water-movement – most important for the bank stability - is summarized after Pilarczyk et al., 1990. As a loaded ship moves in the fairway axis the most important phenomena are the return current and the supply flow (the direction of both of them is parallel to the axis). The direction for both of them is parallel to the axis, but the supply flow has the same direction as ship's sailing direction, while the return current has an opposite directionality. The transversal stern wave is caused by the return current which is the aft boundary of the water level depression. The propeller race has no direct impact on the banks. The size of the secondary waves depends on the ship's speed which is not significant in cases with push-tow units.

PIANC, 1988 was investigating the extra load on rivers when six barge push tows were introduced on the River Rhine. It concluded that from the already used four barge combination only small increase will appear in bank erosion. Brinke et al., 2004 investigates the erosion in groyne fields. It concludes that only large vessels (>60 m) can cause significant erosion on beaches and the secondary waves caused by smaller vessels don't have a major impact. This conclusion may be inconsiderate.

3.2.1. Empirical method of calculation of return current

A theoretical approach by Schijf (based on the method of preservation of energy) is discussed in the next section which determines the water-level depression and the return current after Verheij et al., 2008. The three-dimensional flow is simplified to a one-dimensional flow. "The list below enumerates the assumptions made in the one-dimensional approach:

- a straight, infinitely-long prismatic canal section;
- a prismatic amidships cross-section over the total length of the ship;
- a constant speed of the ship;
- a uniform return current over the total wet-waterway profile, next to and below the ship;
- a uniform water-level depression over the total width of the canal;
- sinkage of the ship equal to the water-level depression;
- no trim of the ship;
- no energy losses; omitting of shear stress and inertia losses;
- no influence of ship-initiated waves or phenomena caused by helical motion.

A ship-fixed co-ordinate system is assumed, which means that the axes of the co-ordinates are considered to move together with the ship."

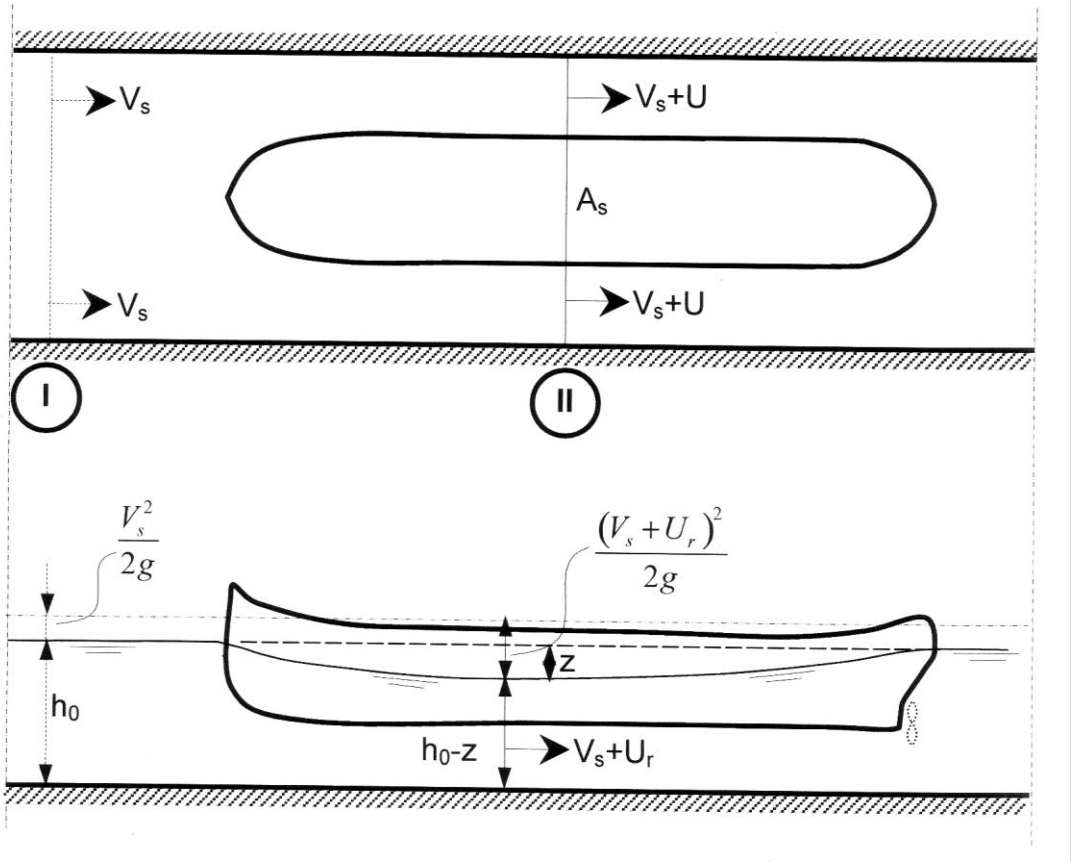

Figure 12 Ship fixed co-ordinate system (source: Verheij et al., 2008)

Using the Bernoulli equation between the two marked cross-sections I and II (Figure 12):

$$z = \frac{V_s + U_r\ ^2}{2g} - \frac{V_s^2}{2g} = \frac{V_s \cdot U_r}{g} + \frac{U_r^2}{2g}$$

z= maximum water-level depression at amidships section [m]
V_s= ship's service speed [m/s]
U_r= maximum return current velocity along ship at amidships section [m/s]

The continuity equation can also be applied to the marked cross-sections:

$$Q = V_s \cdot A_c = \ V_s + U_r \ \cdot \ A_c - A_s - W_s \cdot z$$

$A_c = W_s \cdot h_0$= wet cross-section area of undisturbed canal [m²]
$A_s = B_s \cdot D$= ship's underwater amidships cross-section [m²]
h_0= water depth of undisturbed canal [m]
W_s= width at water-level of undisturbed canal [m]
B_s= ship's beam at amidships section [m]
D= draught of ship at amidships section [m]

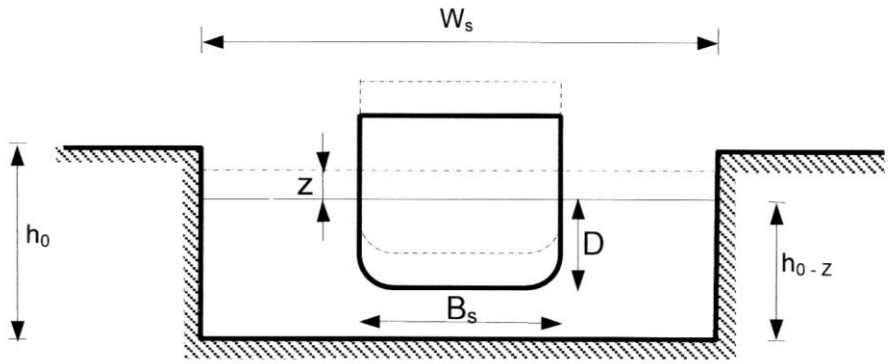

Figure 13 Amidships cross-section A_S (source: Verheij et al., 2008)

The limiting speed, the related limit return current velocity and the limit water-level depression can be computed after the deduction of the above presented equations. Although for a specific speed the return current velocity can be determined:

$$\frac{\alpha \cdot \left(V_s + U_r\right)^2 - V_s^2}{2g \cdot h} - \frac{U_r}{V_s + U_r} + \frac{A_s}{A_c} = 0$$

α= correction factor for the non-uniform distribution of the return current [-]

h= A_c/W_s = average waterway depth [m]

Then the maximum water-level depression can be computed:

$$z = \frac{\alpha \cdot \left(V_s + U_r\right)^2}{2g} - \frac{V_s^2}{2g}$$

This hydraulic model was first developed for rectangular canal cross-sections but basically can be used on any form of cross-section with a proper schematization. The schematization is shown in Figure 14 with a trapezoidal cross-section.

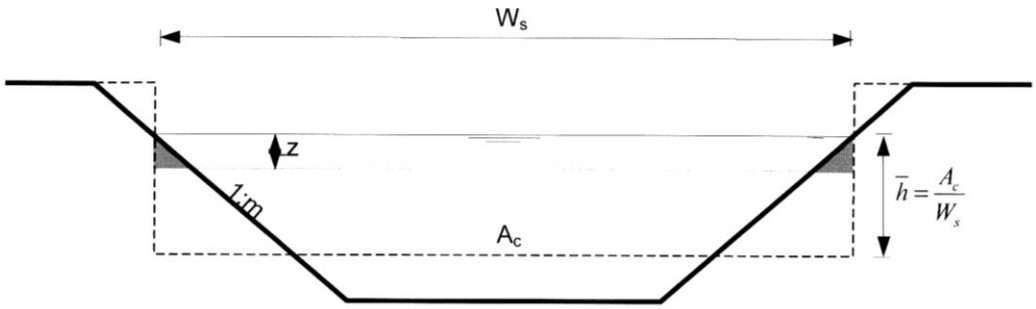

Figure 14 Average water depth in a trapezoidal cross-section (source: Verheij et al., 2008)

This model is applicable also on waterways with current (like natural waterways); this is shown in Figure 14. The only difference is that the above described velocities are relative to the current velocity. (The directions are defined from left to right as positive and from right to left as negative.)

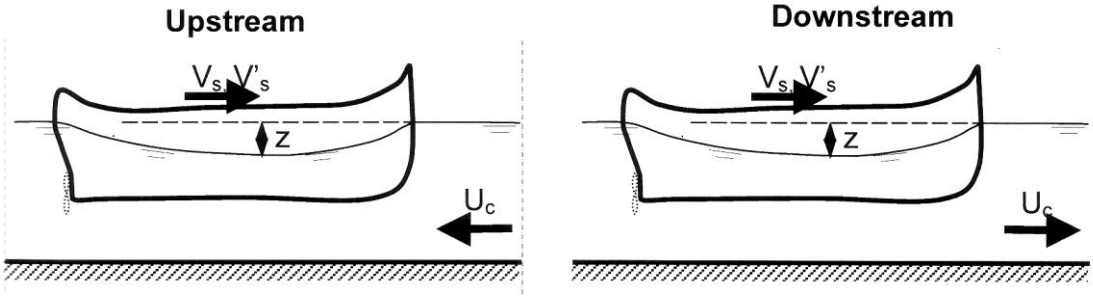

Figure 15 Waterway with a current (source: Verheij et al., 2008)

$$V_s^{'} = V_s - U_c$$

The return current velocity U with respect to the banks:

$$U_r = U_r^{'} - U_c$$

This method can be used if $U_r^{'} > U_c$.

3.2.1.1. Method extended to groyne fields

Figure 32 - Figure 35 shows also the analytically calculated data points. The calculation is already described in Chapter 3.2.1 - Empirical method of calculation of return current. The specific formulas are the next:

$$\frac{u'}{U_c + U_r} = \alpha_1 \cdot \left(\frac{h_0}{h_{ref}}\right)^{-1.4}$$

$$\frac{\Delta h'}{\Delta h} = \alpha_2 \cdot \left(\frac{h_0}{h_{ref}}\right)^{-0.9}$$

u'= water velocity [m/s]
$\Delta h'$= water level depression in the groyne field [m]
Δh= average water level depression in the river in front of the groyne [m]
h_0= average water depth in the river [m]
h_{ref}= average water depth in the river at a discharge just before the groynes become submerged [m]

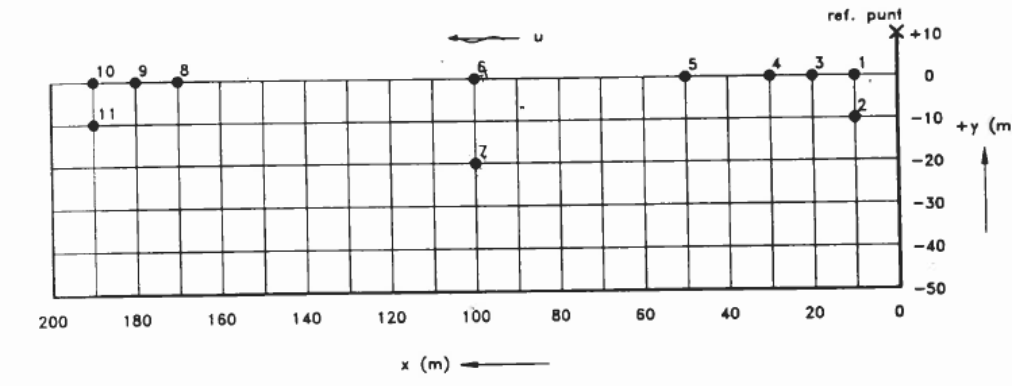

Figure 16 Locations where the analytical solution for groyne fields are shown (source: Termes et al., 1991)

Number	x (m)	y (m)	α_1 (-)	α_2 (-)
1	10	0	0.55	0.56
2	10	-10	0.57	0.59
3	20	0	0.34	0.39
4	30	0	0.32	0.39
5	50	0	0.36	0.39
6	100	0	0.37	0.53
7	100	-20	0.19	0.48
8	170	0	0.38	0.39
9	180	0	0.32	0.48
10	190	0	0.34	0.48
11	190	-10	0.24	0.48

Table 1 Values of alpha's in the case of groyne fields (source: Termes et al., 1991)

Table 1 shows the values of alpha's which should be used with the equations above.

3.3. Earlier experiments

Verheij and Vermeer (1987) have conducted extended research regarding interaction between groyne fields and navigation induced flow. There have been field measurements in the River Waal. The measurements were used to set up a scale model. The main goal of the scale model's research was to imitate the prototype study and use it later for calibration. Further goals were:

- Investigate the potential extra erosion due to the six barge configuration (in those times started to appear six barge push tow configurations instead of four barge configurations).
- Research the influence of the groyne field dimensions.
- Qualitative analysis of sediment transport.
- Develop a prediction method for bed development over time.

In the scale model research, six variables were examined: discharge, groyne field length, barge configuration, barge speed, barge weight, and the distance between the barges and groyne field. Due to the fixed bed conditions morphodynamical investigations were not carried out, sediment transport processes were investigated with tracer material.

3.3.1. Physical model set-up

A River Waal section near Druten (Figure 20) was chosen as an example for the scale test, where the field tests were taken. The physical model did not represent the groynes on the opposite bank. All together four groynes were built in the model, resulting three groyne fields. The river bed around the three groynes and in the two researched groyne fields (a longer with 200 m length and a smaller with 100 m length) were based on the actual bathymetry, the other groyne field was schematized. The scale model was built of concrete.

The scale factor was 1:25 and the Froude Law has been taken into account as scaling law.

Flow velocity and water level measurements were taken in the two groyne fields. Tracer experiments were also conducted in the groyne fields.

3.3.2. Ship in the physical model

The model boats were push tows in the formation of 1x2, 2x2 and 3x2 (only the length was changed, not the width of the set-up). These model boats had their own propulsion. The applied draught was 3 m, the boat velocities were 2.4 m/s and 2.7 m/s. Engine power was included in the propeller jet, although boats were pulled with fixed speed and track in the scale model.

3.3.3. Results of the physical model

Figure 17 displays a schematized drawing of the main flow patterns as a pushed convoy passes the groynes, showing the primary result of the scale model. It shows three phases during the passage of a push tow sailing upstream which was summarized by Yossef, 2002: "The return current is maximum immediately after the bow passes a groyne. The return current is furnished by water from the upstream groyne field and the groyne field alongside. An eddy develops at the groyne head and the small vortex at the downstream end of the groyne field apparently disappears entirely. As the push boat passes by the supply flow refills the groyne field. When the stern of the push-boat passes the particular groyne field, the supply flow is forced to flow out of the groyne field by the upstream groyne, perpendicular to the axis of the fairway. The natural eddy immediately downstream of the groyne is transported downstream by the main current."

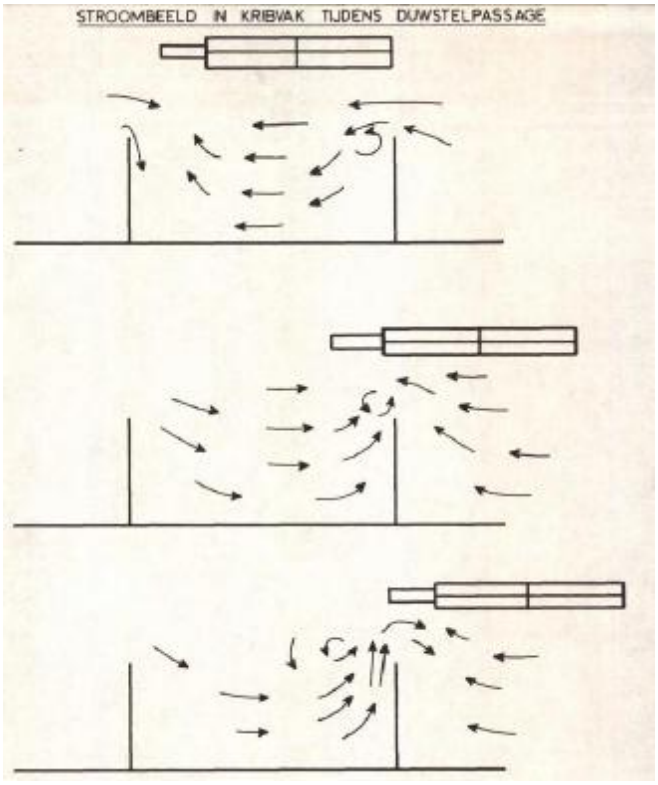

Figure 17 Schematized flow patterns as a 2x2 pushed convoy passing groynes (source: Verheij et al., 1987)

Maximum velocities and water level drops were measured in the scale model (later referred to as measured data). Velocity was measured at 38 fixed points along the groyne field. Water level drop was measured at only 21 points.

Table 2 from Appendix B: Calibration and validation shows the recorded water level depressions from the scale model in four separate cases. The accuracy of the measurements instruments were 0.02 m – wave height meter-, and 0.02 m/s for the velocity meter. This covers the measuring uncertainties and rounding errors etc.

As seen in the above table, water level depression measurements were only recorded as round millimeters which, from the 1:25 scale of the model, means the results can only be in increments of 2.5 cm. This is important when looking at the numerical model results, which seem to be more accurate than the scale model's results. These rounding errors are shown in Figure 32 and Figure 33.

Measured flow velocities in the scale model were 20 % higher than the field test measurements directly downstream from the groynes if the passing distance was small (y_s=50 m). Otherwise results were approximately equal to data gained from field tests.

The conclusions of this study are summarized below:

- The fastest current occurred downstream of the groyne, perpendicular to the river axis, after the ship passed.
- Ship induced flow is less relevant during high discharges.
- Downstream of the groyne the tracer material which was used as a mimic for sediment is transported out to the main channel.
- The six barge configuration led to 35-50 % higher maximum flow velocities than four barge configurations.
- With the six barge configuration more tracer material slips into the main channel than with four barges.
- Introduction of the six barge configuration will most likely lead to larger and deeper scour holes.

Verheij and Vermeer recommend further study to determine if the most important features for sediment transport are the eddies in the groyne field or outward flow during the ship-pass.

These experiments were later applied in my research that is the reason of the previous detailed description.

4. FINEL2D model set-up

4.1. FINEL2D short model description

4.1.1. General overview

The FINEL2D is a finite element, two-dimensional numerical flow model developed by Svašek Hydraulics. The model has several modules: hydrodynamic, sediment transport (for sand and silt) and morphology. The model is capable of handling the sand-mud interaction which can be an important function in estuaries and tidal basins. The wave model SWAN (developed by TU Delft) is also integrated into the FINEL2D model, which can be applied to e.g. nearshore wave modeling. The specific purpose why this model was used in this thesis is the next module: the ship induced water movements can be modeled.

4.1.2. Equations

The depth-integrated shallow water equations are the basis of the hydrodynamic module of the FINEL2D. The model equations

Continuity equations:

$$\frac{\partial h}{\partial t} + \frac{\partial uH}{\partial x} + \frac{\partial vH}{\partial y} = 0$$

X direction:

$$\frac{\partial Hu}{\partial t} + \frac{\partial Hu^2}{\partial x} + \frac{\partial Huv}{\partial y} + f_c Hv + gH\frac{\partial h}{\partial x} - \frac{1}{\rho}\tau_{x,b} + \frac{1}{\rho}\tau_{x,w} + \frac{1}{\rho}\tau_{x,r} = 0$$

Y direction:

$$\frac{\partial Hv}{\partial t} + \frac{\partial Huv}{\partial x} + \frac{\partial Hv^2}{\partial y} - f_c Hu + gH\frac{\partial h}{\partial y} - \frac{1}{\rho}\tau_{y,b} + \frac{1}{\rho}\tau_{y,w} + \frac{1}{\rho}\tau_{y,r} = 0$$

$$H = h + z_b$$

Where:

H = water depth [m]
h = water level [m]
z_b= bottom level[m]
u = depth averaged velocity in x-direction [m/s]
v = depth averaged velocity in y-direction [m/s]
f_c= Coriolis coefficient [s^{-1}]
g = gravitational acceleration [m/s^2]
ρ = density of water [kg/m^3]
τ_b = bottom shear stress [N/m^2]
τ_w = wind shear stress [N/m^2]
τ_r= radiation shear stress [N/m^2]

FINEL2D uses an unstructured triangular grid. The size and shape can be varied in the model area, hence specific areas of interest can have higher resolution grid

sizes. FINEL2D uses explicit time discretisation. (For a more extended model description see the Appendix A: FINEL2D technical description after Svašek.)

As FINEL2D does not apply any turbulence model – the viscosity is only considered as numerical viscosity, which depends on the gridsize. FINEL2D is a robust, first order model, which is a good application where flow is dominated by advective processes.

The ship can be implied in a model in several ways. On the one hand, as the ship immerses volume, it means in a two-dimensional description that the water column is smaller. So it can be interpreted as the bed level increases with the same distance as the draught of the ship. On the other hand, it can be implied as an increased pressure on the water surface. The ship is defined in FINEL2D according to the first method, i.e. the bed level is modified.

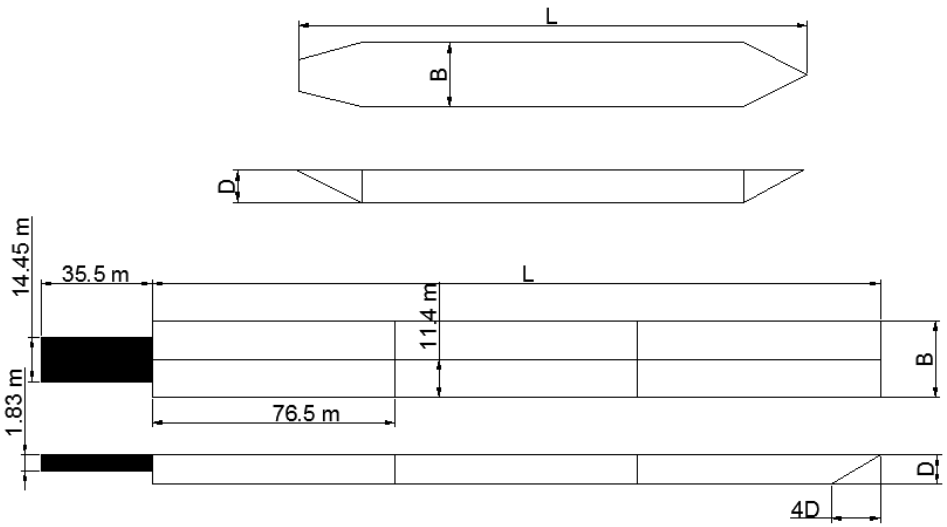

Figure 18 Ship shape implementation from FINEL2D

The first ship implementation in FINEL2D had the shape of a motor vessel (see Figure 18, upper ship, first plan view then profile), while the applied model uses barges and a tugboat. The applied tugboat and barge sizes are introduced in Chapter 3.2. Two examples of the push tow setups are displayed in Figure 19. The FINEL2D code has been changed in order to define the correct ship geometry of the physical model (described in Chapter 3.3Earlier experiments). This changed shape can be seen in Figure 18, where the tugboat has constant sizes (only changeable by changing the code – that's why it is hatched black), while the barges can be changed. The variability of the ship geometry means that e.g. only one or several barges are connected to each other. The pictures below in Figure 18 show a 3x2 barge setup, the plan view and the profile view, respectively.

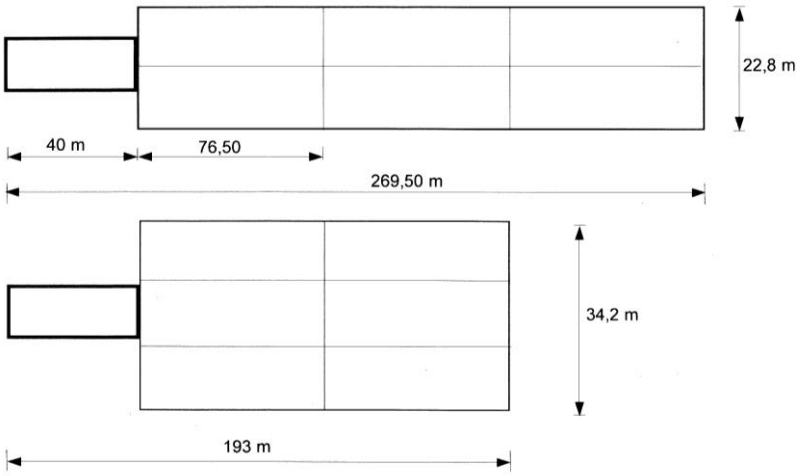

Figure 19 The possible set of a six barge push tow (source: Verheij et al, 2008)

4.2. Input

The model set-up is chosen to be as close to the earlier described scale model – with actual scale - (Verheij and Vermeer, 1987) as possible.

4.2.1. Model area

The model area is a schematized version of a River Waal section area close to Druten. This can be seen in Figure 20 just north from Druten; the yellow line represents the border.

Figure 20 Druten's location in the Netherlands (source: Google Earth)

4.2.2. Grid and bathymetry

The dimensions of the modeled area have to be large enough to avoid boundary affecting the area of interest (the groyne fields). The dimensions used can be seen in Figure 21. The length of the modeled area was 6000 m while the width was 412 m.

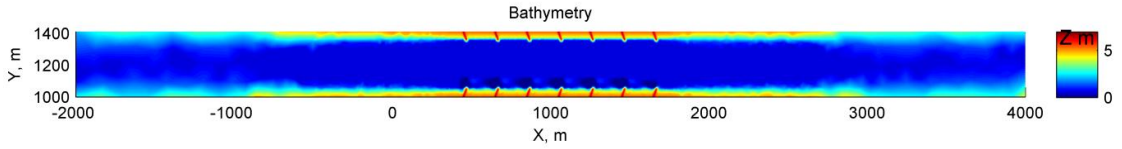

Figure 21 Used bathymetry

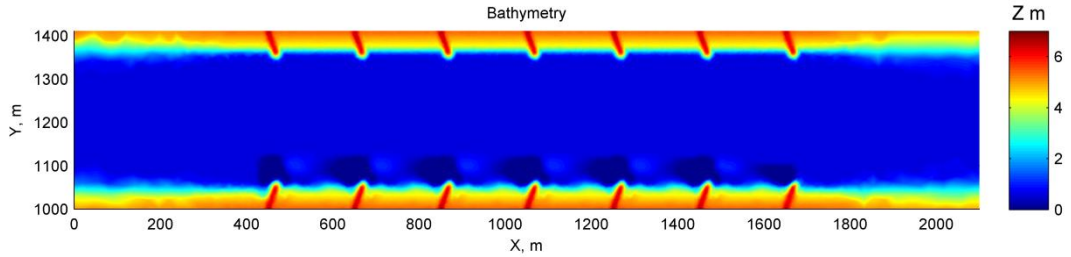

Figure 22 Bathymetry of the channel

Figure 22 and Figure 23 shows the study area where the actual bathymetry was used - based on field measurements (Verheij and Vermeer, 1987 – Chapter 3.3) for the groyne fields along the left bank. The difference between the schematized and the actual bathymetry is easily noticeable by looking at the groyne fields at the right bank. They have a smooth schematized bathymetry while on the opposite side the groyne fields have the irregular, real bathymetry given from field measurements.

FINEL2D is capable of defining groynes as weirs. When groynes are emerged it is not worthwhile to use this application. If groynes are submerged (water is flowing over the crest of groynes) hydrodynamics is described in a more suitable way applying weirs, and not taking groynes into the bathymetry. However, submerged groynes create strong secondary flows where a three-dimensional description would be needed. (3D application would be needed in case of scour holes, because in such locations the logarithmic velocity profile is not valid anymore. Therefore the calculated velocities will not be accurate in a 2D model.)

The computational grid for the area of the interest is shown in Figure 24. The FINEL2D uses triangle cells for the discretization of the study domain.

Spatially varied cell sizes were applied. Upstream and downstream of the groyne fields larger grid sizes were defined. Preliminary model runs suggested a relatively homogeneous distribution of cell sizes in the zone of the groyne fields (see Figure 24).

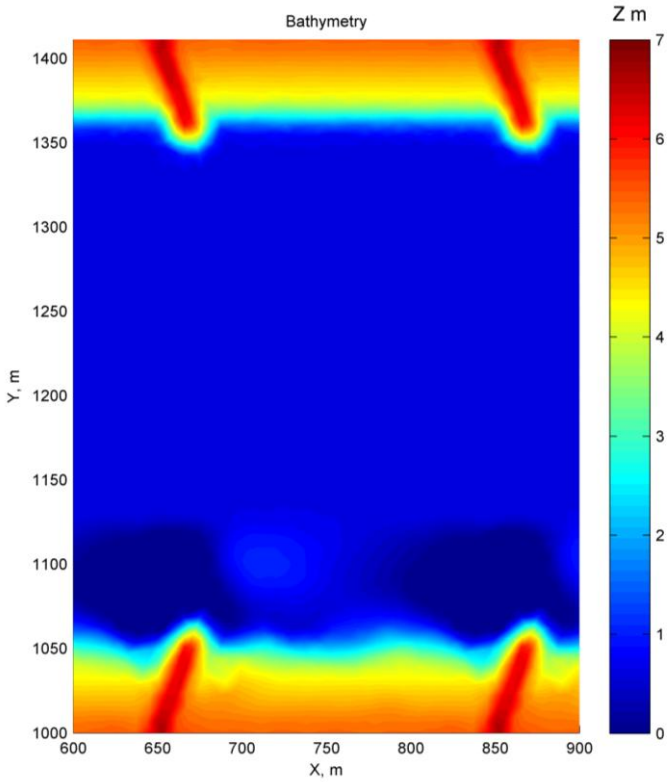

Figure 23 Bathymetry zoomed to the area of interest

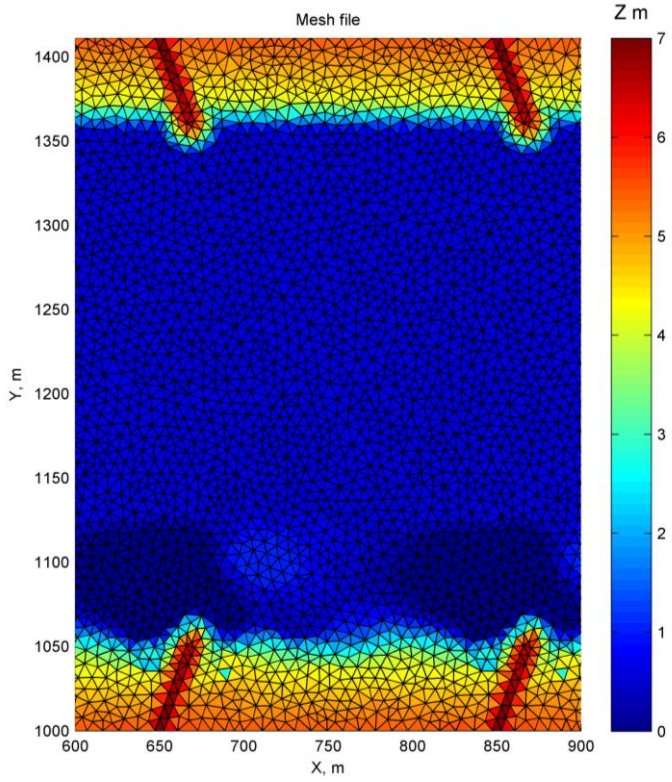

Figure 24 Mesh at the area of interest

The reference level for the bathymetry is "NAP". This is the Dutch reference level for geographical height ("Nieuw Amsterdams Peil").

5. Calibration and validation

The scale model's results were used for the verification process.

In the experiments (Verheij and Vermeer 1987) several data series were collected from a groyne field. Among those the maximum water level drop series have been chosen for the numerical model verification process. Figure 25 displays a top view where the groyne's crest and base are shown with dashed lines. Data was collected from 21 locations distributed evenly in the scale model (Figure 25).

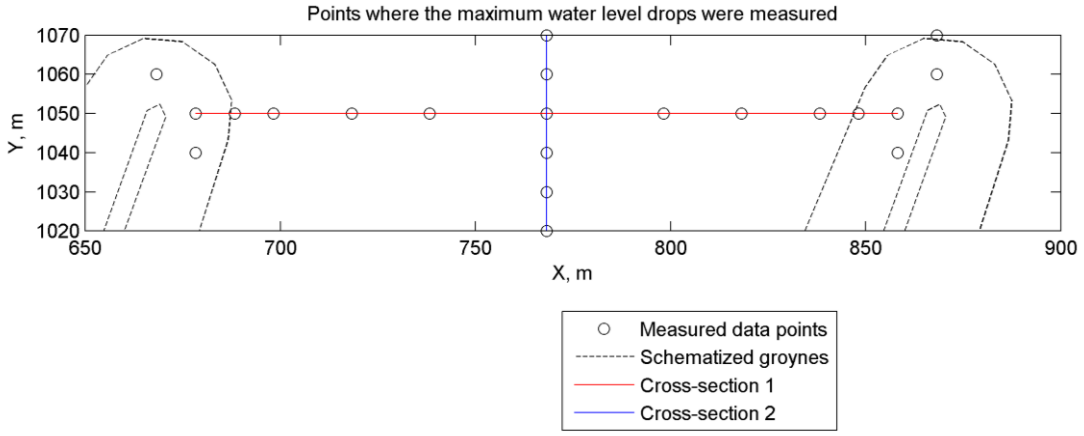

Figure 25 Points where the water level drop were measured in the scale model

For calibration and validation purposes the water level drop series have been used (Table 2 from Appendix B: Calibration and validation). Only those series were used which had sufficient data for the verification process. In the column titles the descriptive parameters of the barges can be seen as the allocation of the barges (as 2x2 or 3x2), the ship velocity (v_s) and the sailing distance from the groyne tips (y_s). The x and y coordinates are already transformed to the coordinate system which used in the numerical set-up. As seen in the table the water level drop might be negative, which means e.g. the influence of a higher primary wave. Although by taking the absolute value of it, it seems closer to all the other data and later to the simulation results.

The red and blue lines in Figure 25 indicate cross-sections shown of the chosen groyne field. In cross-section 1 there are 11 measuring points while in cross-section 2 there are 6 measuring points. These cross-sections are used to visualize the verification process.

In the calibration process two parameters were changed: cell size and bed roughness. As FINEL2D has no turbulence model implemented, only numerical diffusion is possible through numerical viscosity, which parameter is calculated based on the cell size.

The estimation of the numerical viscosity at the groyne fields is as follows (the formula applies to a rectangular grid, but used as an approximation for an unstructured mesh):

$$\nu = \frac{U \cdot \Delta x}{2} = \frac{1 \cdot 8}{2} = 4 \text{ m}^2/\text{s}$$

While the Elder viscosity would be – approximately:

- in the groyne fields: $\nu = \frac{1}{6}\kappa\frac{U}{15}H = 0.0267$ m²/s
- at the main channel: $\nu = \frac{1}{6}\kappa\frac{U}{15}H = 0.0024$ m²/s

The mixing layer's viscosity may be essential. It depends on the length scale and the velocity scale. Estimation for the mixing layer's viscosity is shown here (Fischer et al., 1979):

- $\nu_t = 0.2 \cdot u_* \cdot h \approx 0.2 \cdot \frac{U}{15} H = 0.048$ m²/s

Figure 26 shows one of the figures from Verheij and Vermeer 1987. It displays the flow structure in groyne fields without any ship passing.

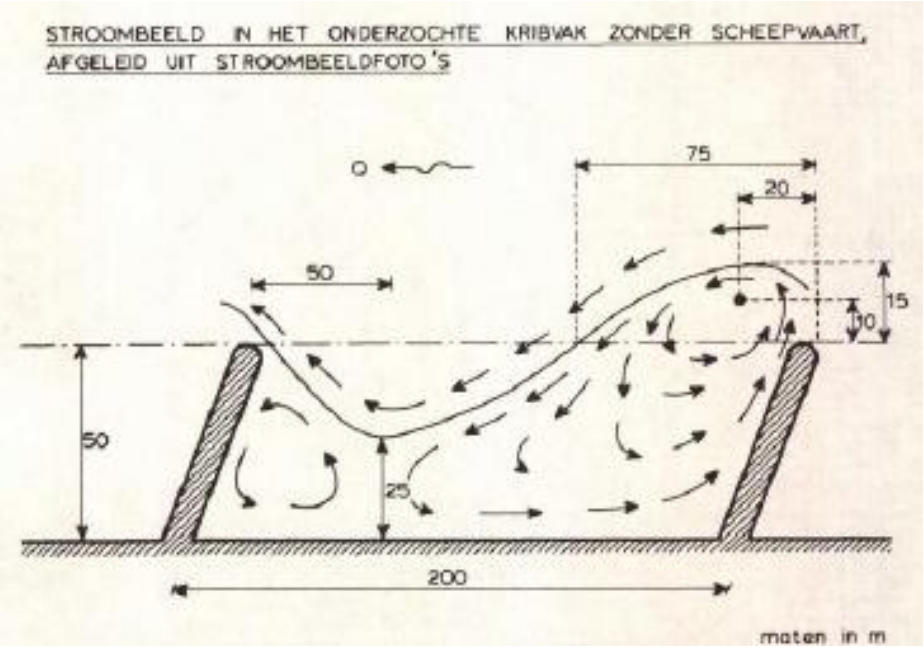

Figure 26 The evolving eddies in the groyne field in the physical model without ship movements (source: Verheij et al., 1987)

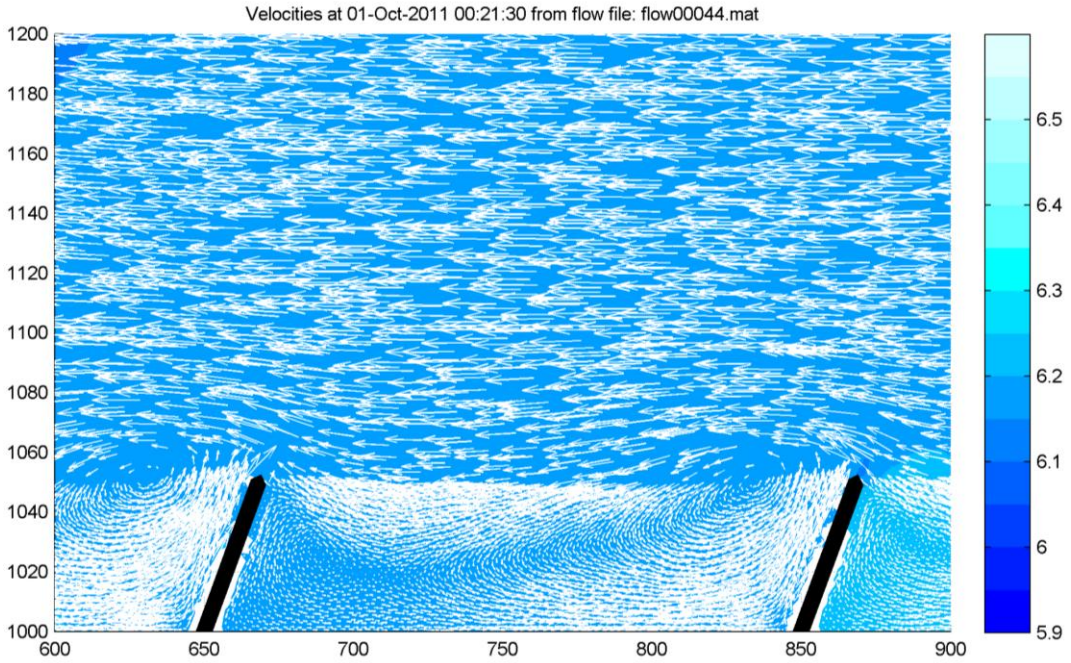

Figure 27 The eddy structure on a very fine grid without ship movements

Figure 27 indicates that FINEL2D is capable to reproduce the evolving eddies in the groyne field. Although in the calibration process a coarser grid resulted in a better agreement with the measurements (quantitative verification). (In Figure 27 the grid has a universal resolution, but for clarification only every fifth velocity vector is shown where y > 1050 m). Figure 27 and Figure 28, showing a good agreement with experimental results, suggest that considering only numerical diffusion the calculated flow characteristics are well predicted.

The later used version (Figure 28) shows also two eddies, but from a plan view it doesn't seem to have conformity as good as the previous, finer grid. The coarser gridsize has been used because quantitatively it was closer to the datasets used during verification.

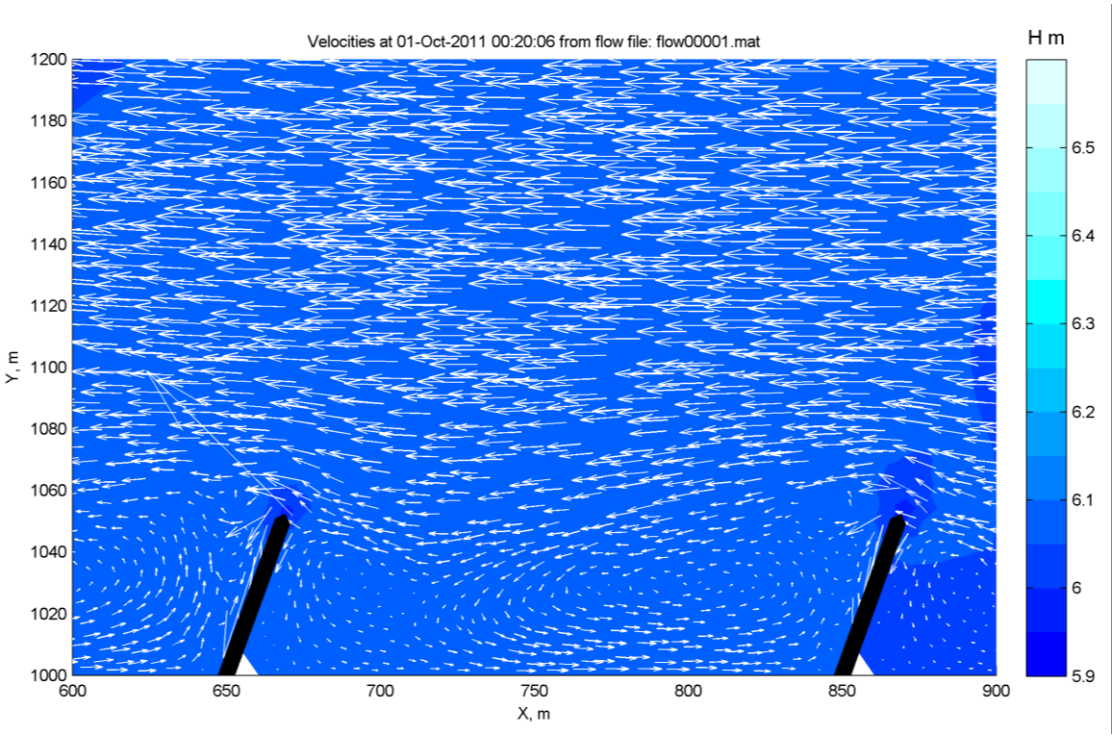

Figure 28 The eddy structure on a coarser grid which was used in the calibration process

The qualitative goodness of the datasets was not changing according to any linear, or parabolic trend. Figure 29 shows the maximum area of a grid cell on the x axis, while y axis shows the number of measurement points, where the error of the predicted water level drops are less than 50 % or 20 %. Based on these results an average cell size of 40 m was chosen as an optimal choice.

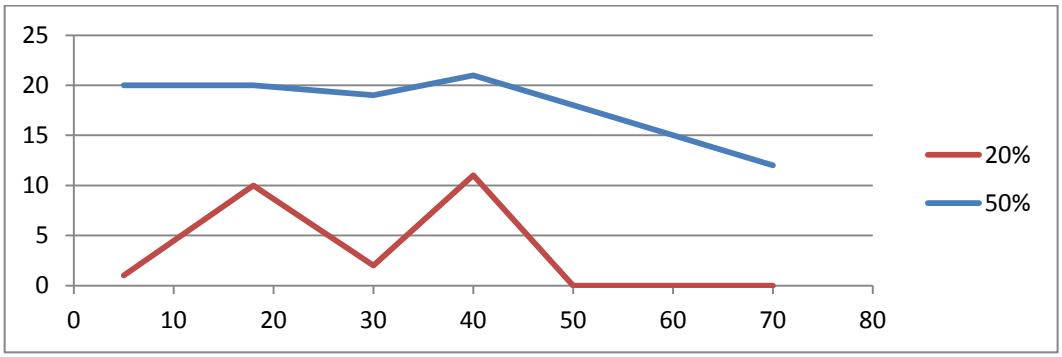

Figure 29 Calibration process gridsizes vs. goodness (Horizontal axis: average area of cells, m²; vertical axis: nr. of measurement points where the error is within the given extent)

Regarding the bed roughness (using the so called Chézy roughness - C) the best agreement with the experimental results could be achieved using C= 100 $m^{1/2}/s$.

From the several groyne fields defined in the model geometry the one between the second and third groyne was chosen to be studied. This decision was stated after the experiments of Sukhodolov et al., 2008 and Uijttewaal et al., 2001: "A single groyne field appears inadequate to mimic a virtually infinite series of groyne fields, because the length needed for the river flow to adapt to a situation with groyne field is much larger than the length of one or two groyne fields."

5.1. Calibration

In the calibration process the roughness, the grid size and the use of the propeller was varied to identify the best agreement between the measured and modeled data. From those variables, grid size had the most significant influence on the results. The propeller usage and roughness barely affected the results.

Throughout the process the deviations of the calculated results from the measurements were used to indicate the goodness of the calculations. Four categories were applied: the difference between the modeled and measured value is maximum 100% / 50% / 20% /10% from the measured values. The calibration became accepted when the deviation in all the measurement points fell within 50% error range.

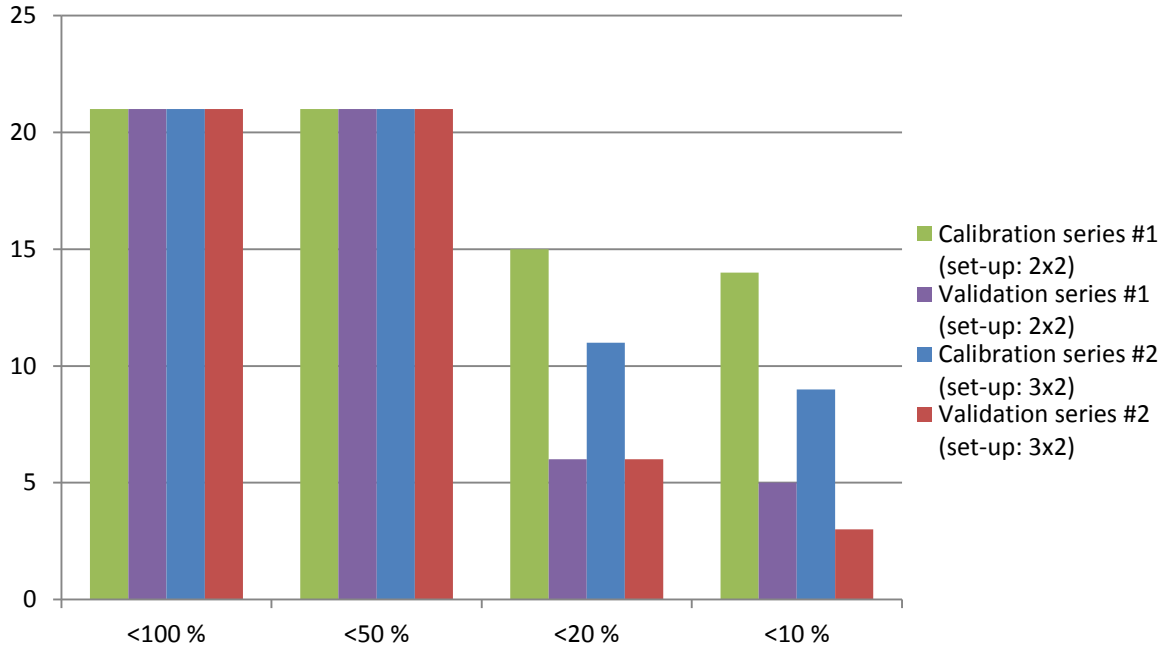

Figure 30 Deviations of the calibration and validation cases of data series

Figure 30 displays modeled data series in the above described four categories. From the four data series there is no data with a difference greater than 50 %.

5.1.1. 2x2 set-up

In Figure 31 green circles identify the location of the measuring points. Data points where the differences between the measured and modeled values are higher than 10% are identified with a black x. The values around are identified by color:

- blue - measured upscaled water level drop values from the scale model, in meters
- red - modeled water level drop values from the numerical model, in meters
- black - differences between measured and modeled water level drop values, in meters.

There are only 7 points of the 21, where the predicted water level drop values deviate more than 10%. In the right half of the groyne field, the measured values

are higher than the modeled ones, marking an over-prediction of the water level drop. On the contrary, modeled values are higher than the measured ones on the left half of the zone.

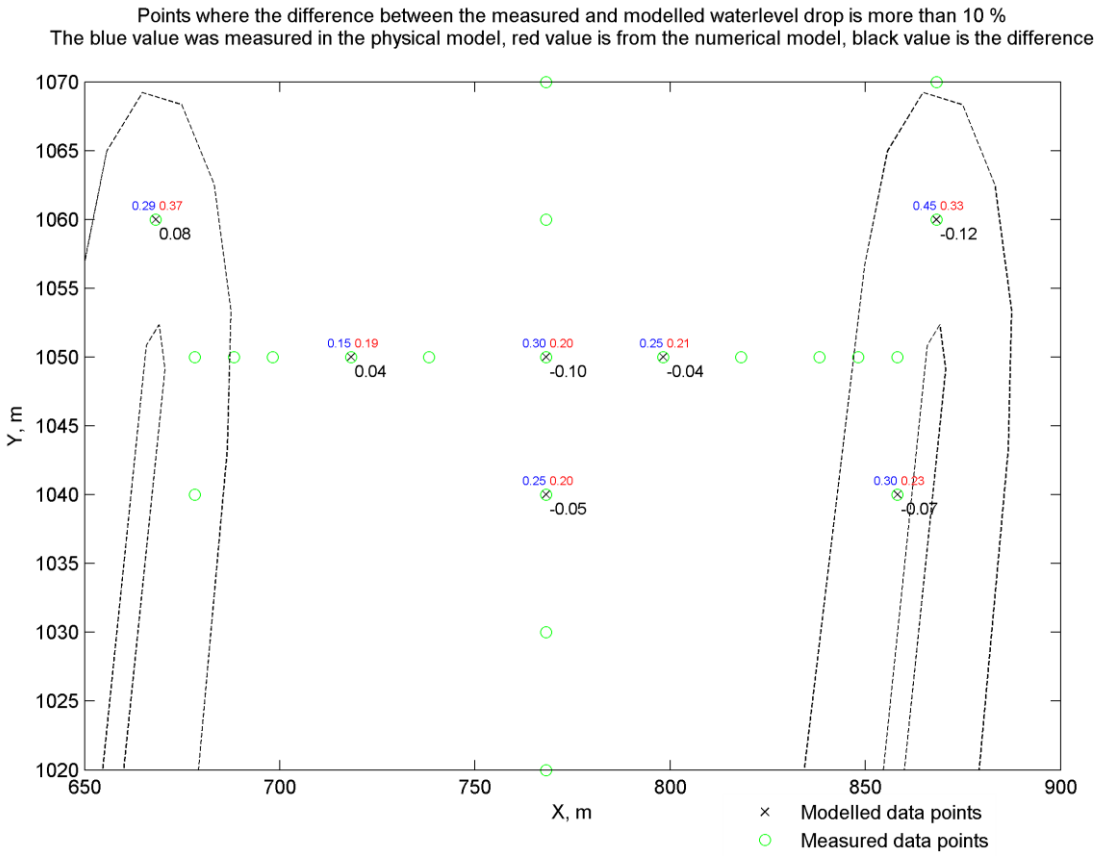

Figure 31 Points where the difference between the measured and modeled water level drop is more than 10 %

Figure 32 and Figure 33 display the maximum water level drop measured and modeled from the sections indicated in Figure 25, showing section 1 (Figure 32) and section 2 (Figure 33), respectively. Both figures show the modeled data with stars and the measured data with plus signs. The red x-s show the analytical solutions results, which were calculated according to the Chapter 3.2.1.1. This solution would give results in a 5% error rate, but the simplifications taken into account in these calculations would give from the author's point of view more than 5 % error rate.

Figure 34 shows velocities with opposite directions at the upstream end of the groyne field. This means that close to the groyne the physical model and the numerical model using a fine grid gives higher velocities when the directionality is reverse from the numerical model using a coarser grid.

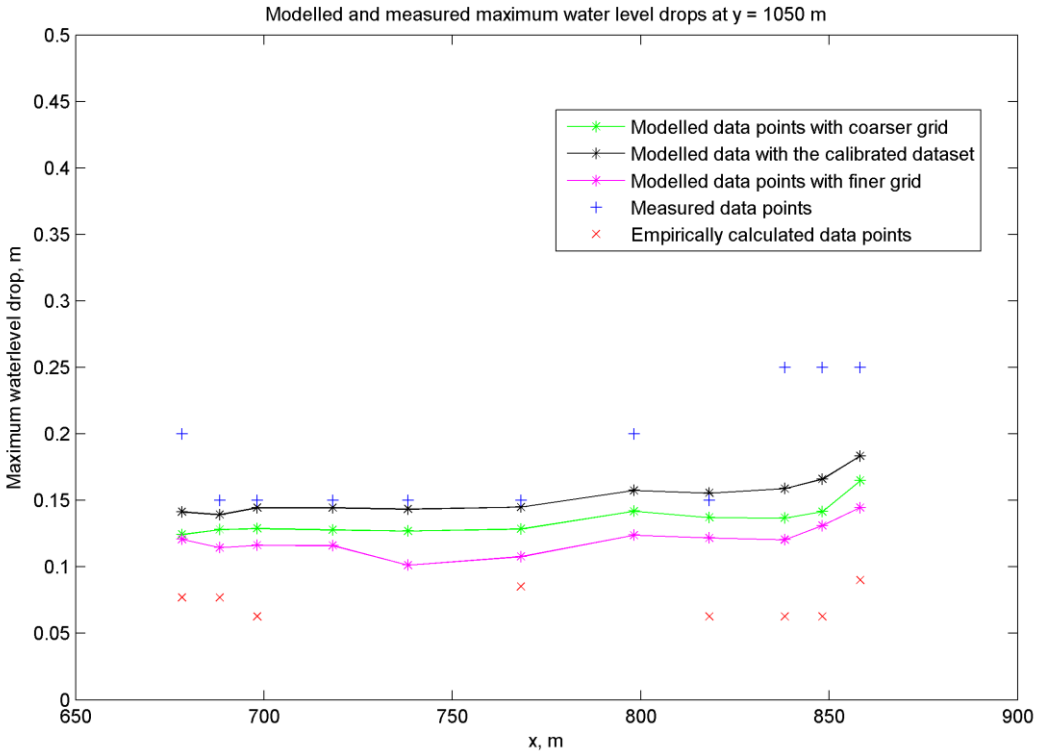

Figure 32 Cross-section 1

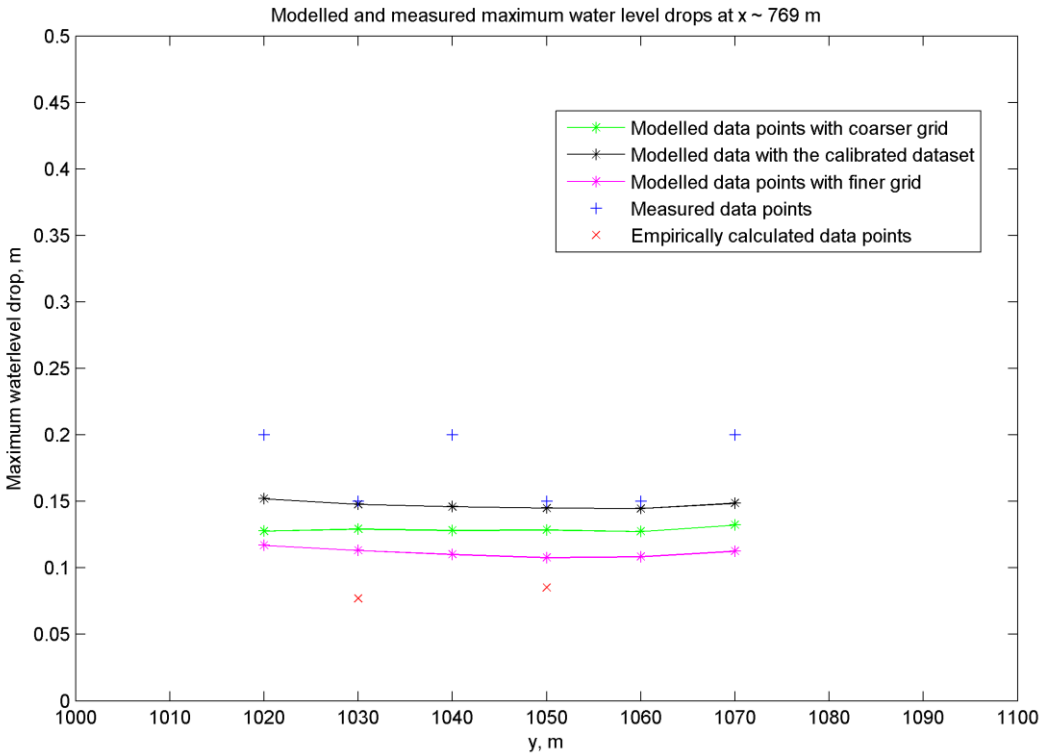

Figure 33 Cross-section 2

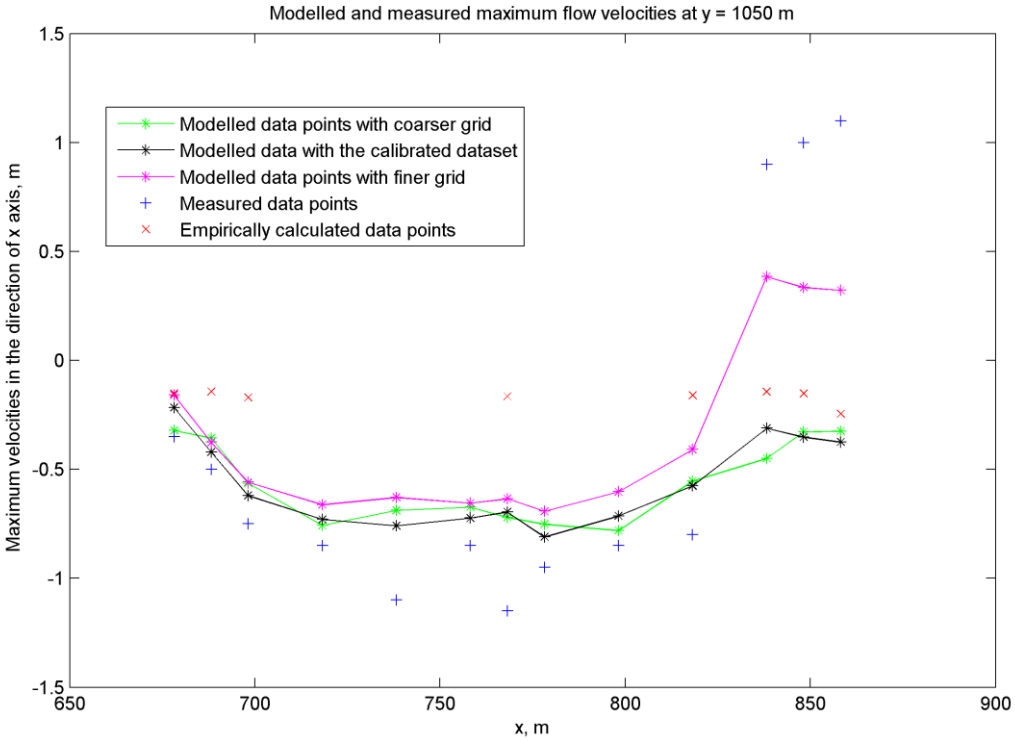

Figure 34 Cross-section 1

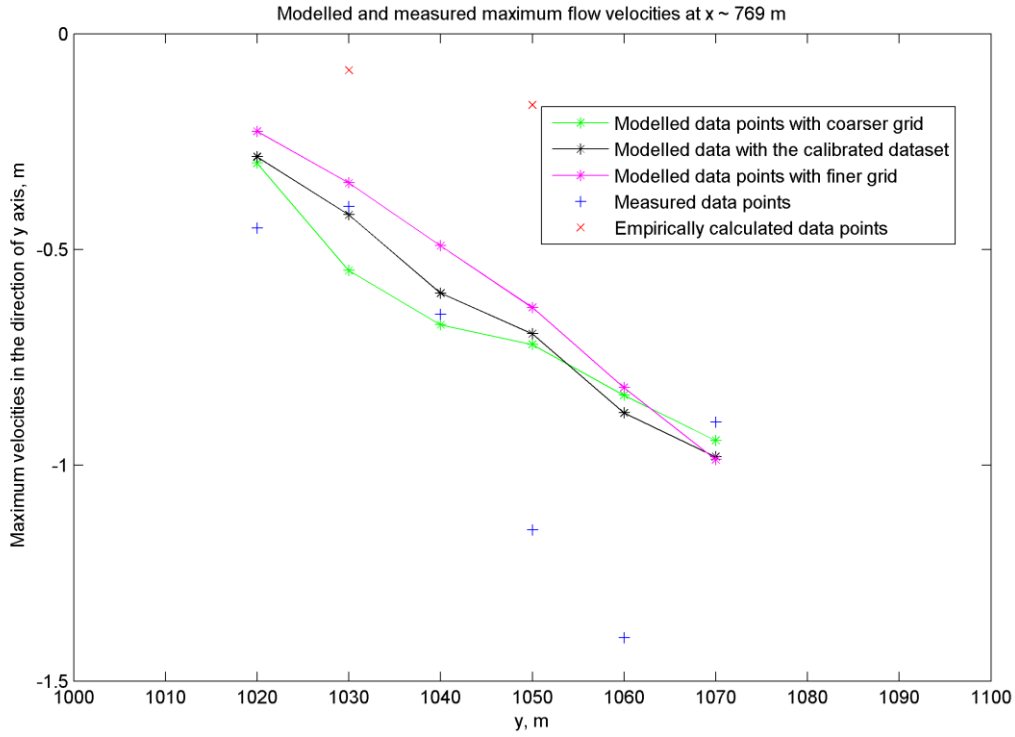

Figure 35 Cross-section 2

5.1.2. 3x2 set-up

As the results show in Appendix B: Calibration and validation this set-up resulted in somewhat worse agreement as the 2x2 set-up, however, most of the data fell within an acceptable range.

The differences between the modeled and measured water level drops can be related to three main phenomena. Firstly, the differences between the scale model set up and the numerical model set up. Secondly, the deviation can be resulted by the laboratory model (e.g. measurement uncertainty, scaling problems). Thirdly, the applied numerical model (data sampling frequency, absence of turbulence model, 2D description of flow field).

5.2. Validation

Although Figure 36 shows that at most of the measuring locations the difference between modeled and measured data is higher than 10%, the agreement is still acceptable considering the 0.02 m measurement uncertainty, which, in fact, means 0.8 mm in the scale model.

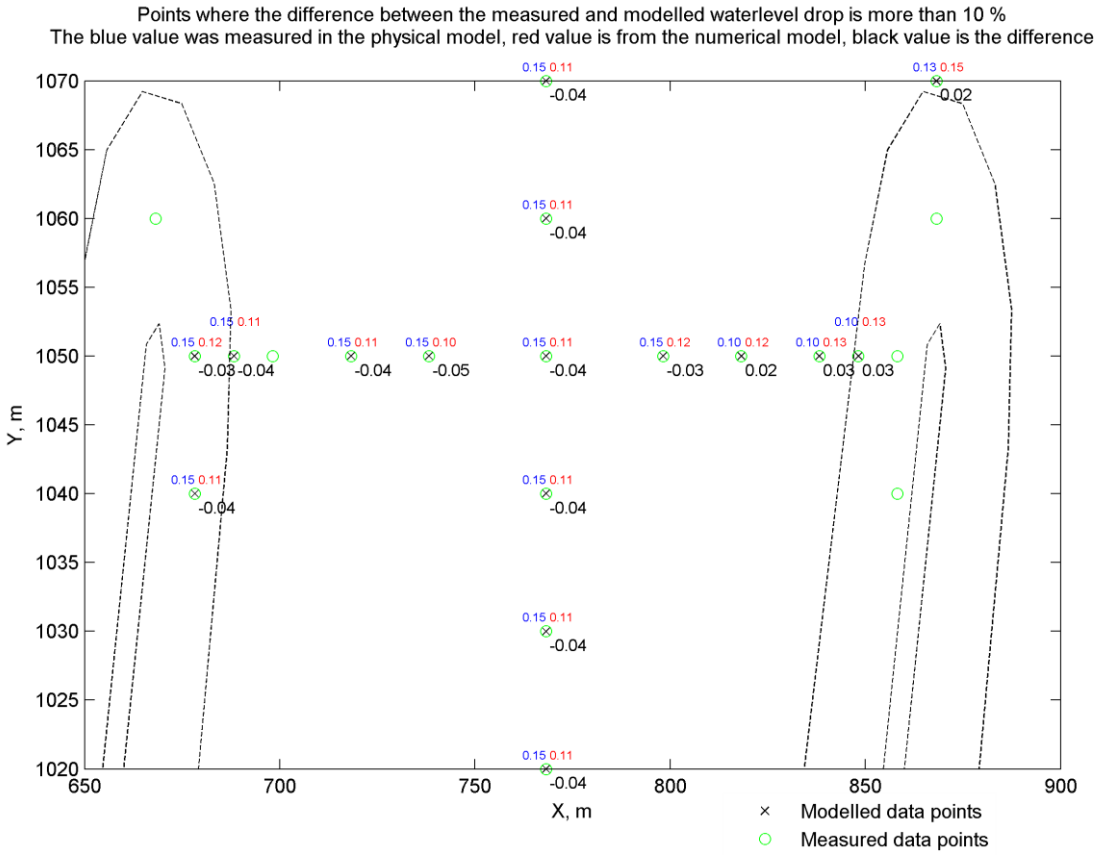

Figure 36 Points where the difference between the measured and modeled water level drop is more than 10 %

It is interesting to see the difference between Figure 33 and Figure 38. In Figure 38 the values are smoother and do not deviate from the average as much as in Figure 33.

The Appendix B: Calibration and validation shows more detailed figures about the verified datasets.

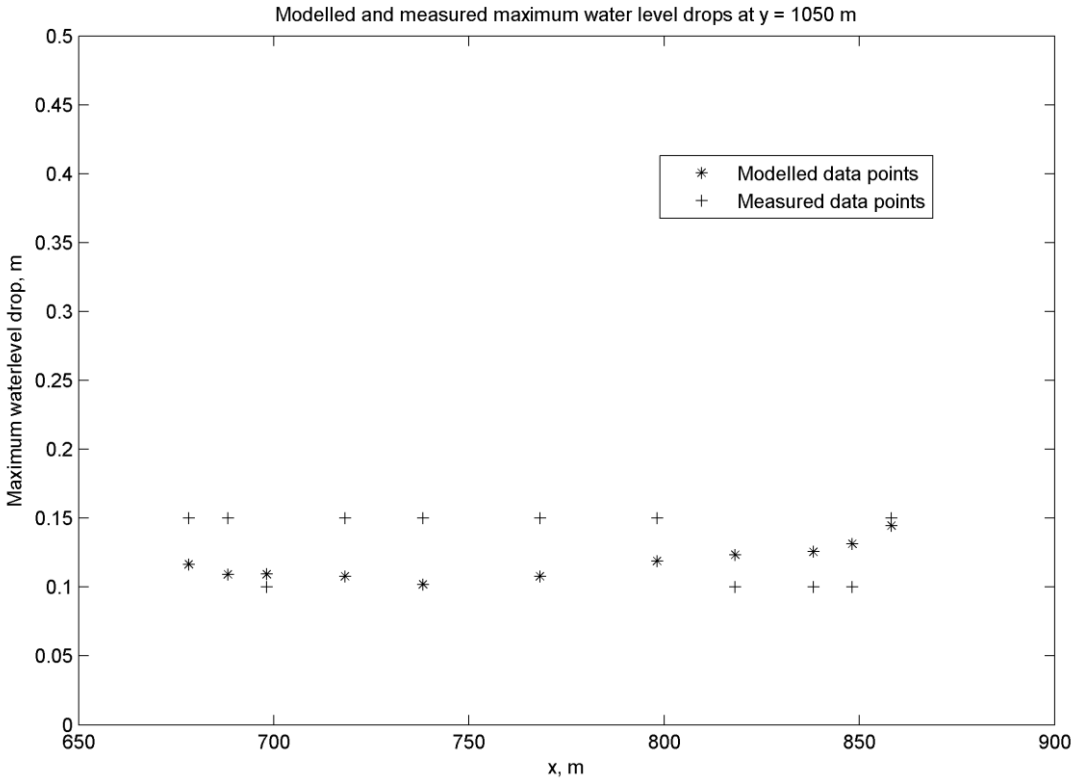

Figure 37 Cross-section 1

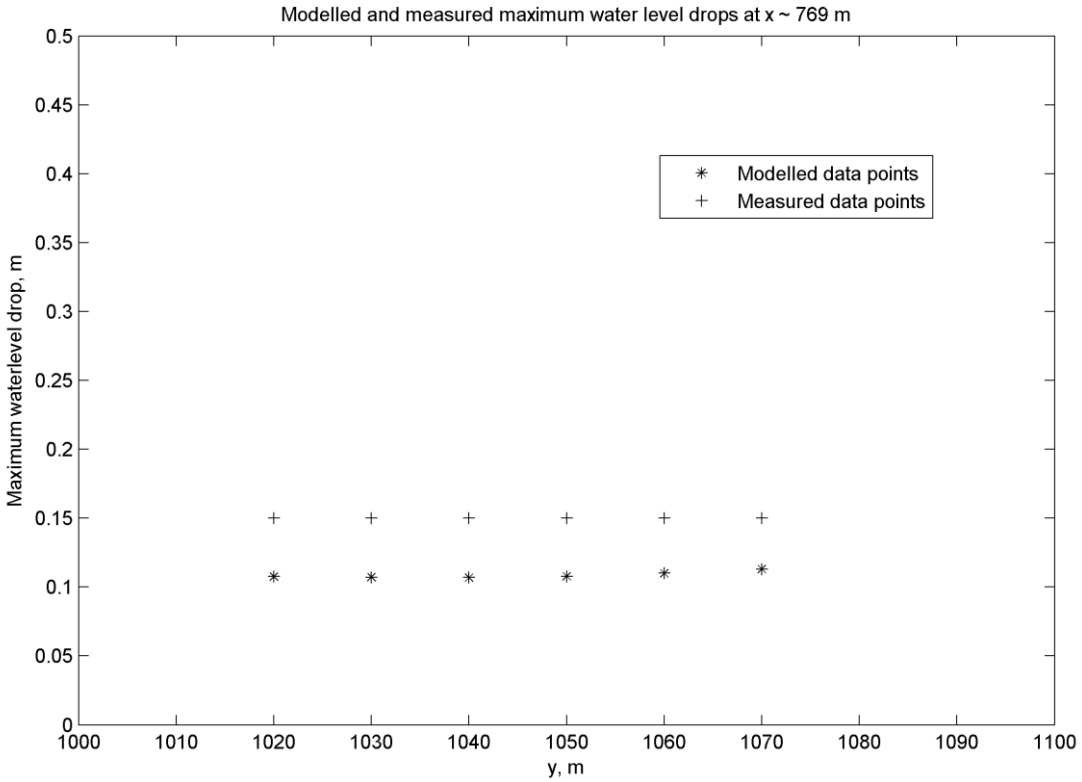

Figure 38 Cross-section 2

6. Simulation results

In this chapter only the most relevant results are shown, several other picture where the ship is passing can be seen is in the Appendix C: FINEL2D simulation results. Those pictures show the velocity vector field and water surface field.

In the first part of this chapter instantaneous velocity and streamline fields of the unsteady calculations are shown. In the second part, assessing the effects of the ship induced waves on the river bed, the distributions of the maximum shear stresses values are introduced.

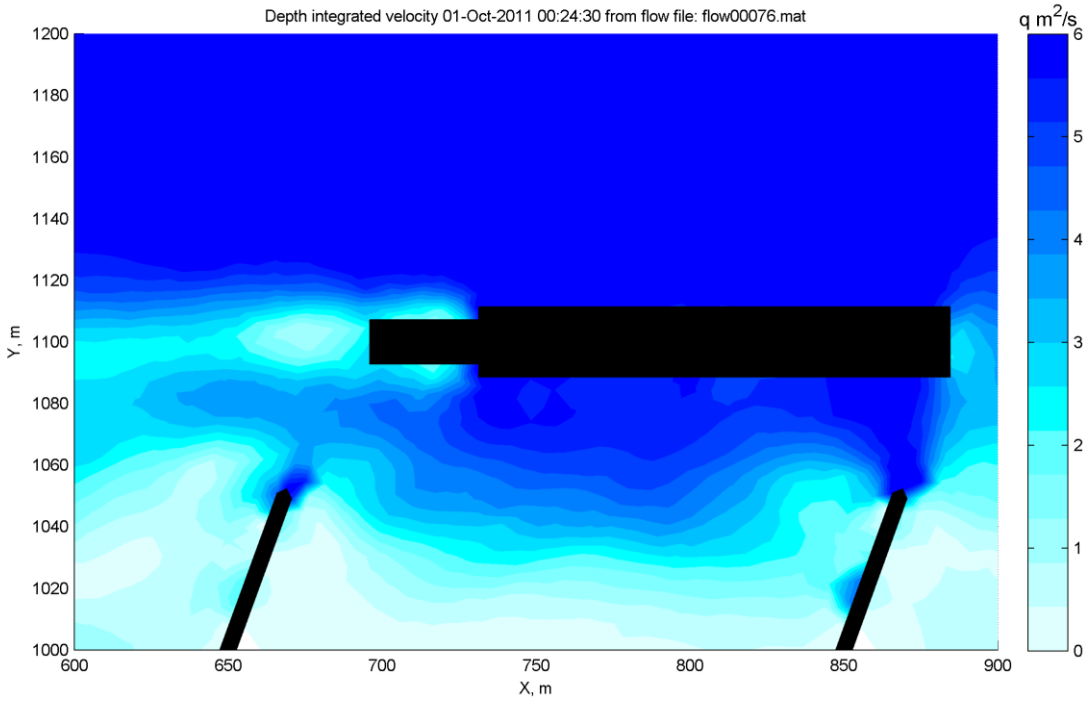

Figure 39 Depth integrated velocities as the ship is passing

Figure 39 displays the depth integrated velocities as the ship is passing. Easily remarkable how the ship is pulling the primary waves with it, and how far they can reach in the groyne field. Approximately, a 10-15 m wide zone is affected in the groyne fields.

Figure 40 shows streamlines without the ship (this screenshot is taken after the ship passed). The two eddies are well developed, then it is changing as the ship passes.

Figure 41 shows streamlines as the ship passes next to the groyne fields. The propeller's impact downstream from the tugboat is easily observable as the streamlines are not flowing straight downstream, but have a disturbance.

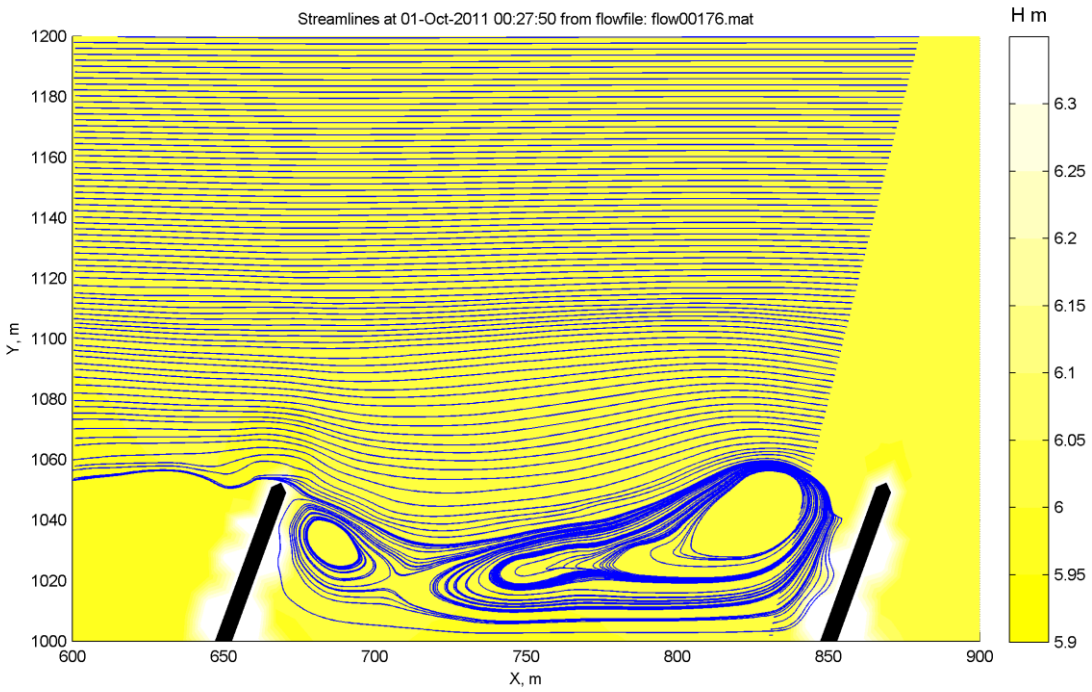

Figure 40 Streamlines after the ship passed

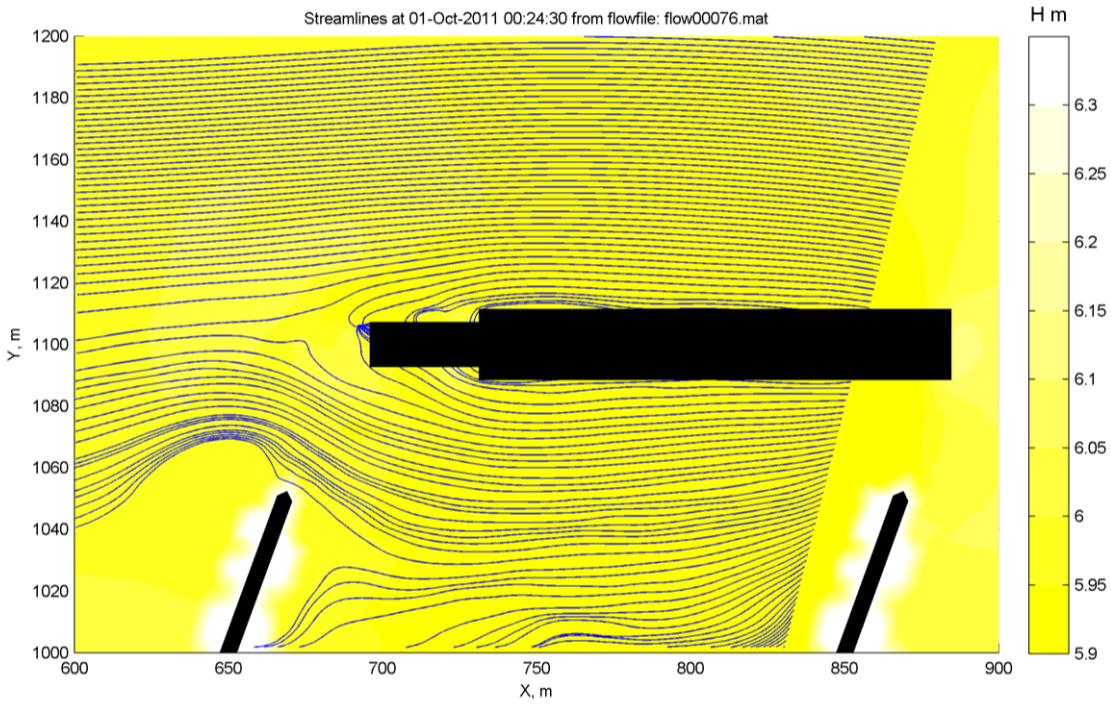

Figure 41 Streamlines as the ship is passing

Figure 17 showed the effect of passing ships on groyne fields. One should notice that those figures do not have a current velocity, while the next figures (Figure 42 - Figure 44) have, so they will only show the difference caused by a ship in channel with current.

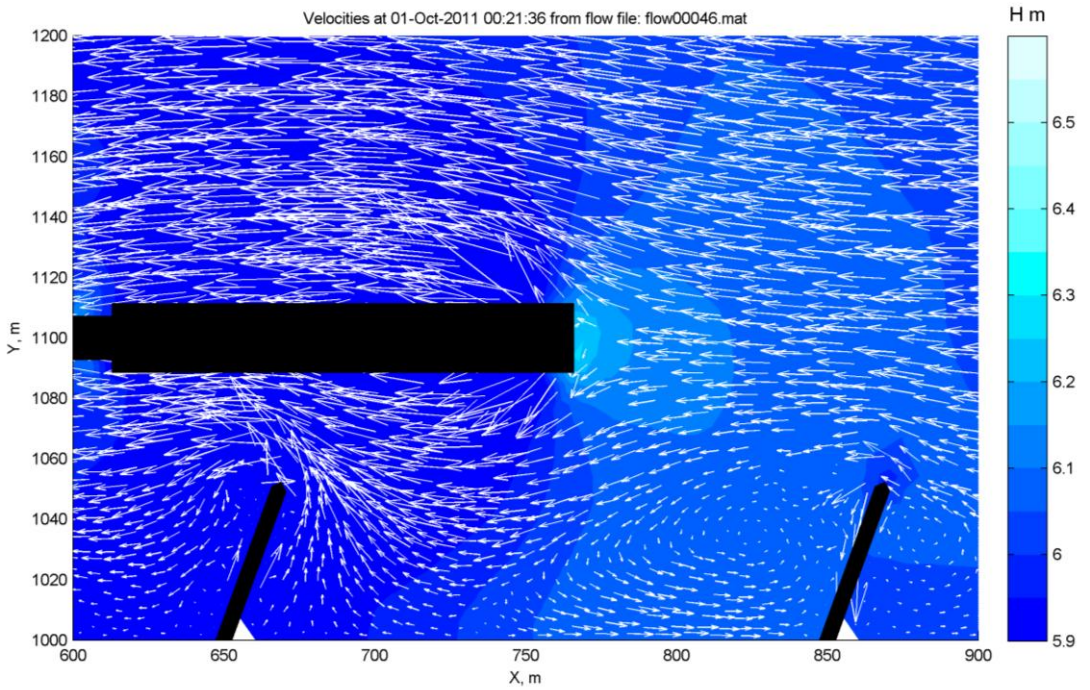

Figure 42 Ship passes the groyne fields – phase #1

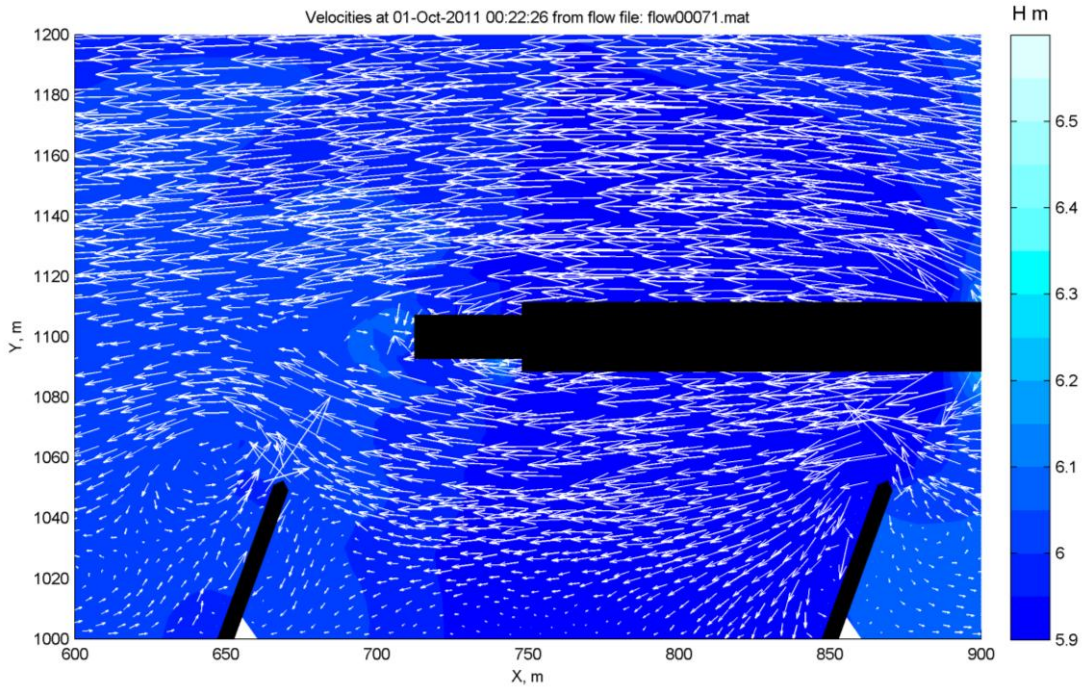

Figure 43 Ship passes the groyne fields – phase #2

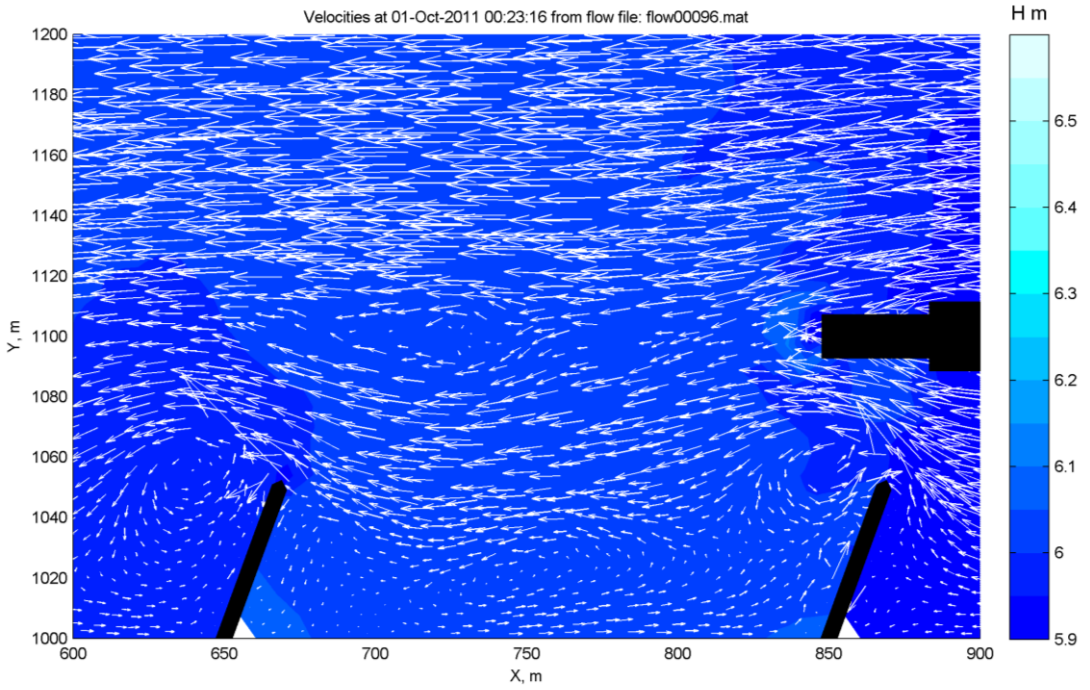

Figure 44 Ship passes the groyne fields – phase #3

Figure 42 - Figure 44 display as a 2x2 push tow is passing the chosen groyne fields with a velocity of v_s=2.7 m/s and in y_s= 50 m distance from the groyne tips.

Figure 42 - Figure 44 show the water level distribution fields and velocity distributions. One can see how the push tow pushes the front wave in Figure 42, while the water level depression is appearing next to the ship caused by the return current. The propeller shows its own impacts, so the velocity vectors downstream from the push tow have varied directionality. The figures above were chosen to be as close to the phases shown in Figure 17 as possible.

As the ship is approaching the groyne field, the secondary eddy vanishes and the flow has directionality towards the main flow. The second figure (Figure 43) shows that the push tow is pushing water in the groyne field, while the velocity magnitude close to the groyne tips is increasing. While the ship approaching to the next groyne fields the primary eddy is starting to develop again.

6.1. Transects

As van der Wal, 2001 showed in his study, the cross-sectional velocity profile has negative values in groyne fields. This is shown in Figure 45. (In the research the difference is shown between permeable and standard groynes – this is already accounted in Chapter 3.1.1.)

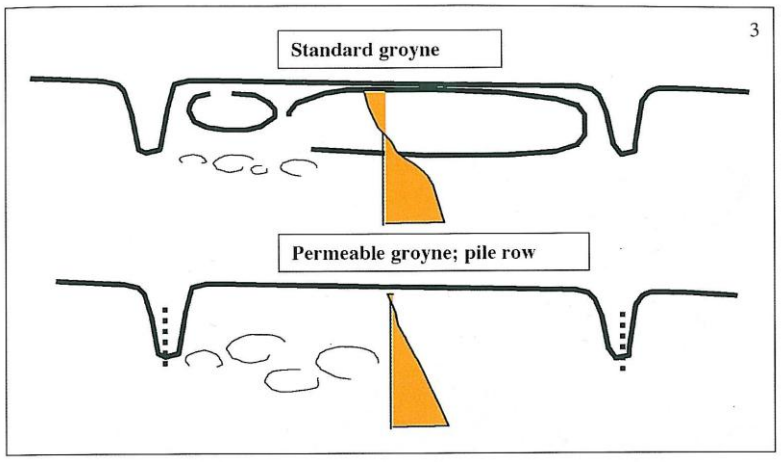

Figure 45 Comparison of flow pattern for standard and permeable groyne (source: van der Wal, 2001)

Figure 46 shows a chosen cross-section through the primary eddy.

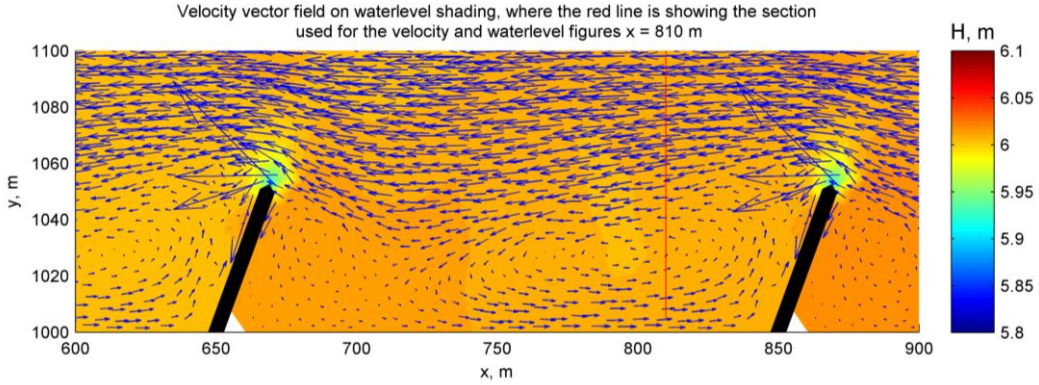

Figure 46 Cross-section through the primary eddy

Figure 47 shows how the cross-sectional velocity profile changes as the ship is passing. Originally (without any ship movement) the cross-sectional view of the velocities in the groyne fields is changing directionality (from the main flow point of view) – this is what is displayed by van der Wal, 2001 in Figure 45. The color of the lines varies from blue to red, in the middle, with lilac one can see how the velocity directionality is changing as the ship passes (the eddies vanish because of the interaction with the primary wave).

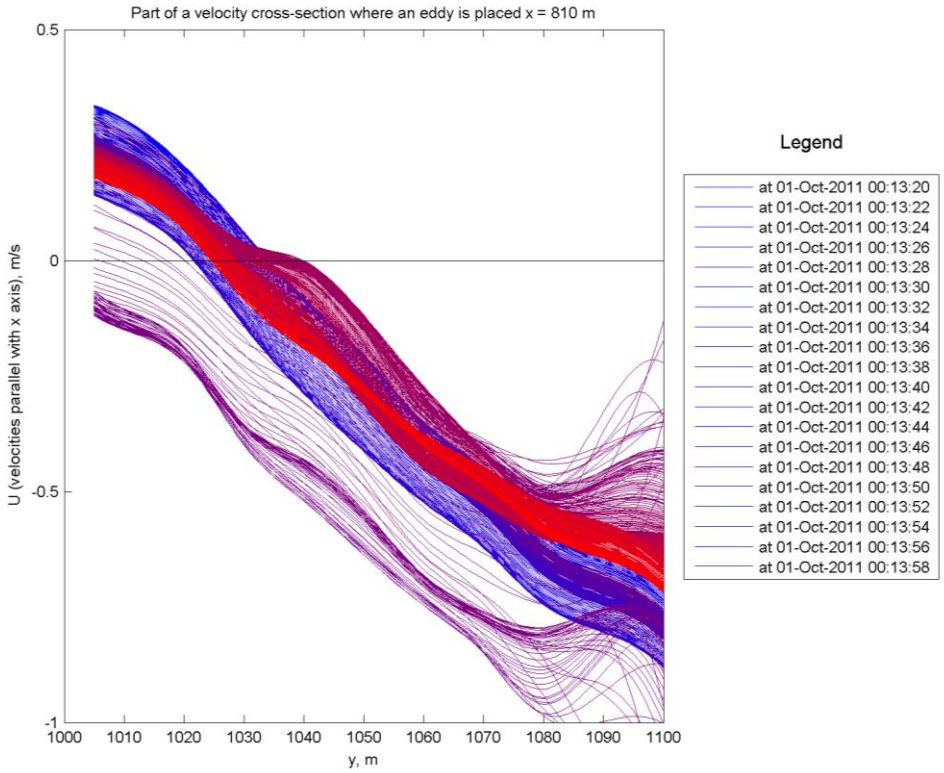

Figure 47 Velocity changes through time as the ship passes in the cross-section shown in Figure 46 through the primary eddy

Another section is also chosen to display the exchange between the groyne field and the main flow. This is shown in Figure 48.

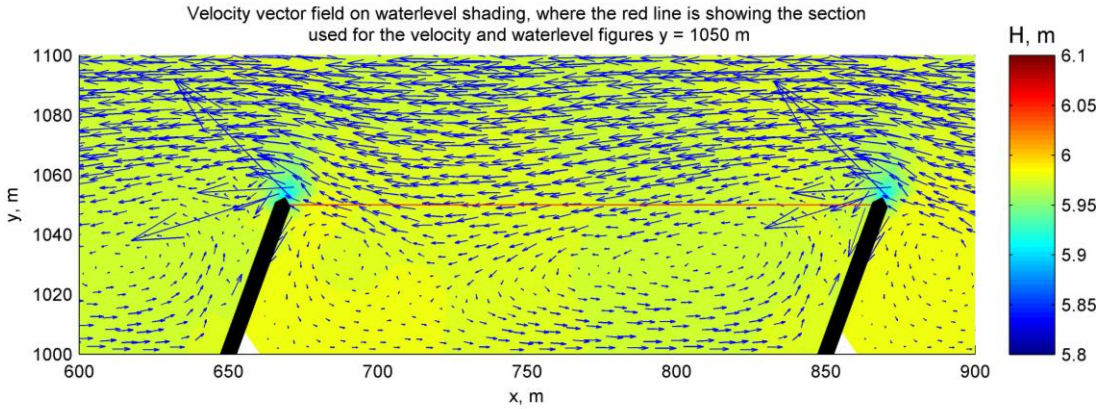

Figure 48 Transect at the normal line

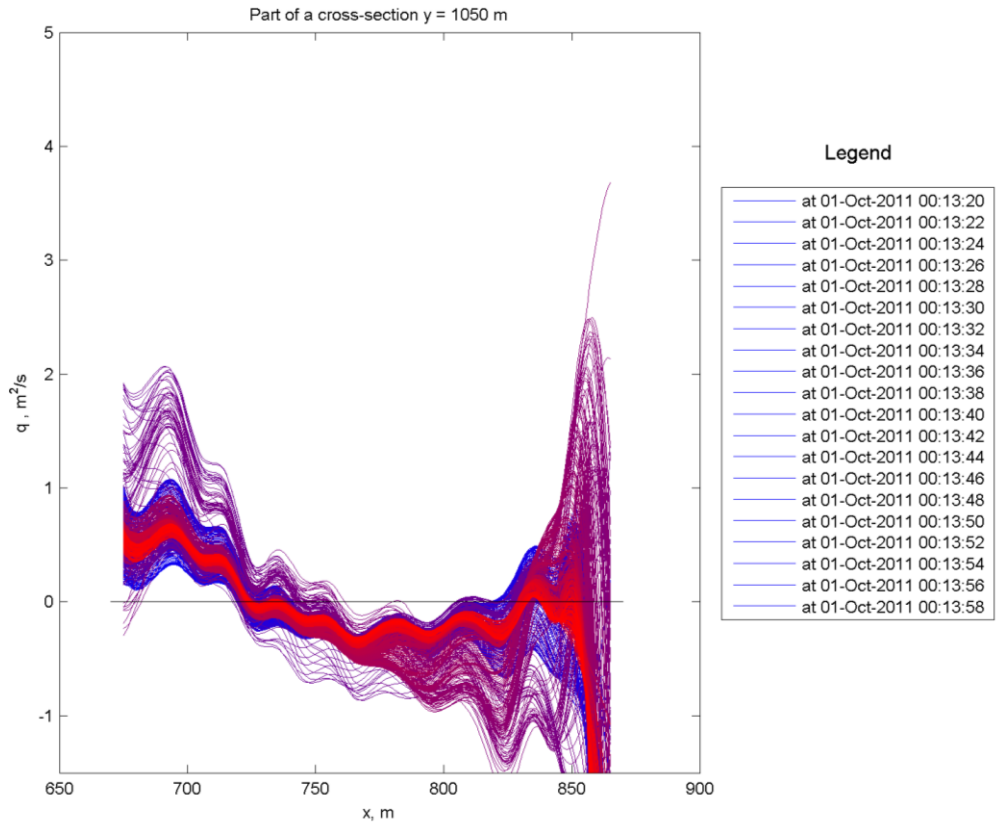

Figure 49 Changing the depth integrated velocity by the transect above (Figure 48)

Figure 49 shows how the depth integrated velocity is altering at the cross-section at *y*=1050 m, as the ship passes. The color scale is the same as in Figure 47. Around the groyne tips probably the estimated flow velocity is higher than in reality because of the nearly dry cells. The very small water depth causes uncertainties, and gives a genuinely high water velocity. The depth integrated velocities are calculated from the perpendicular velocities to the normal line, i.e. parallel with the *y* axis.

Later, the exchange process has been shown as the ship passes in Figure 50. Here, because of the high velocities around the groyne tip the discharge through the normal line between two groynes is shown.

This approximation shows that there is only outflow from the groyne field, which is not possibly true. A better approximation would be to not take into account the areas next to groyne tips, as there the water depth is really small. This is shown in Figure 51. One can see that inflow and outflow is altering. As the ship passes outflow is more dominant, than otherwise. This outflow possibly washes out the settling sediment from the groyne fields.

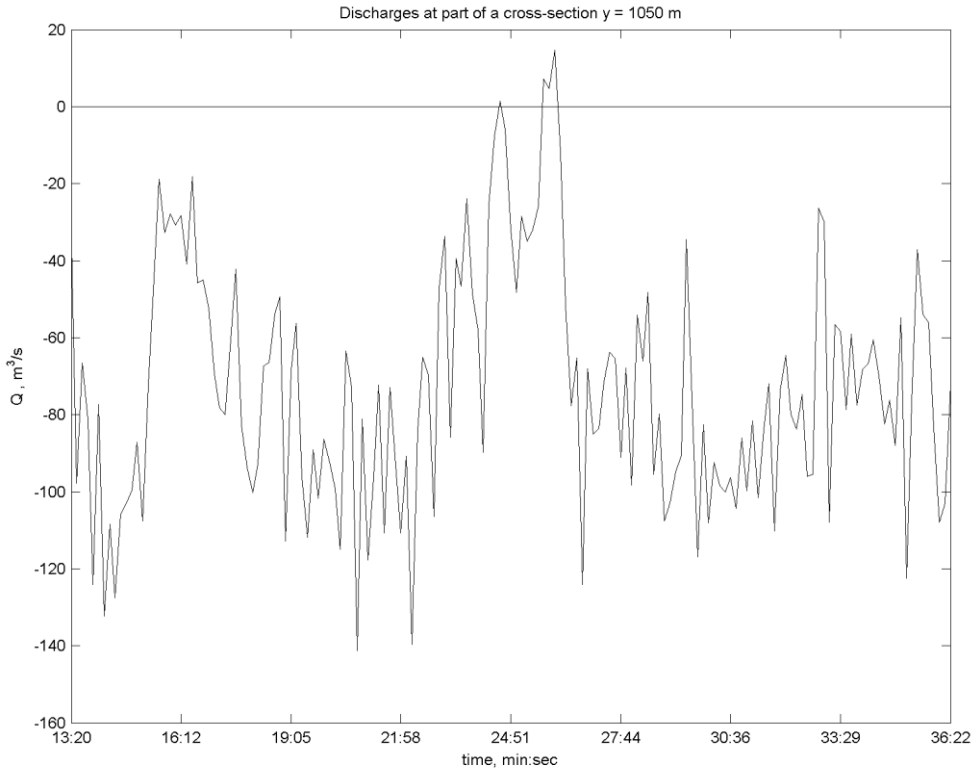

Figure 50 Discharges in cross-section shown above with groyne tips (Figure 48)

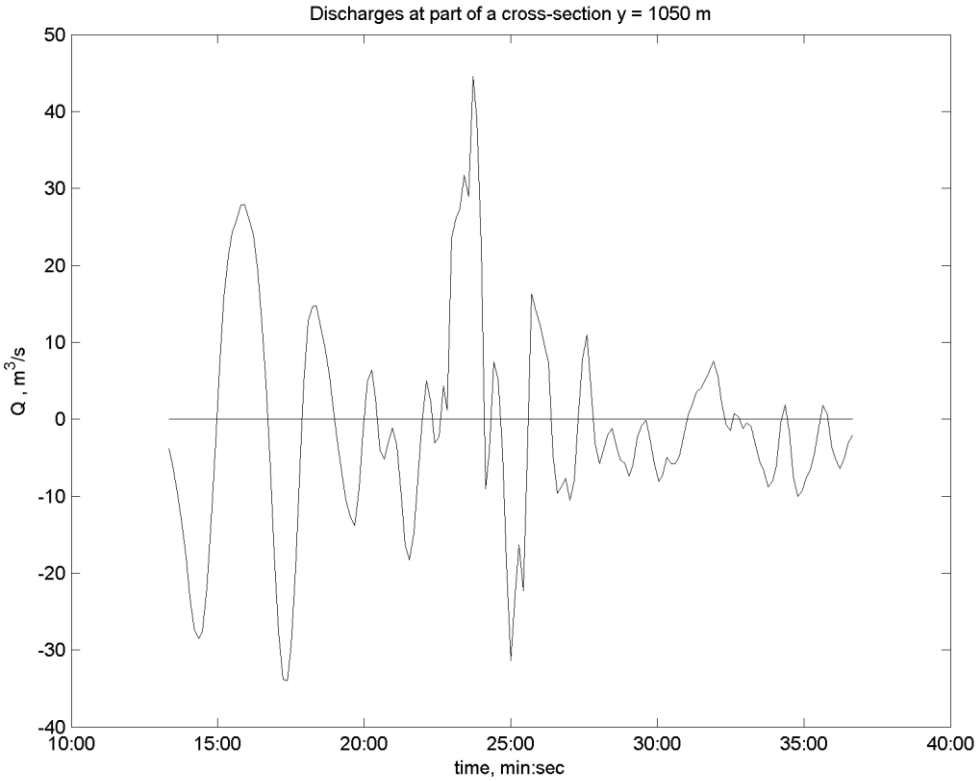

Figure 51 Discharged in cross-section above (Figure 48) without the groyne tips

6.2. Shear stresses

Shear stresses are examined to describe the processes which take place in groyne fields as the impact of navigation. Shear stress is calculated with the following formula:

$$\tau_b = \frac{\rho \cdot g \cdot u^2}{C^2}$$

Shear stress is increasing around and under the push tow, because of the implementation of the ship (increased bed level). Due to this description, strong gradients in the bed level field develop resulting in inappropriate shear stresses values. Therefore, it is suggested no to take those values into account in a two cell distance around the ship.

Figure 52 shows an instantaneous bed shear stress field as the ship passes the groyne field. The plot shows increased shear stress values around the groyne tip from due to the high velocity gradient in characteristic to this zone. The data at these locations should be applied with care.

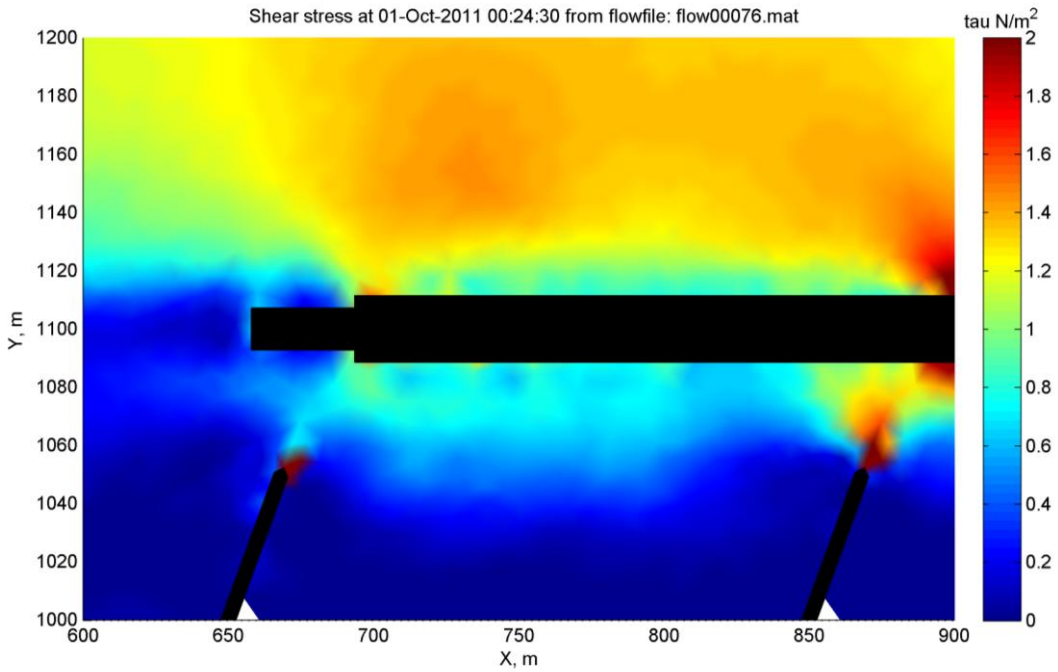

Figure 52 Shear stresses as the ship passes

Figure 53 displays the shear stress differences between the scenarios with and without the ship at a certain time. The shear stresses under and right around the ship should not be considered. It can be seen in Figure 53 that a 15-20 m wide zone in the groyne field is influenced by the ship, where the bed shear stress increases with approximately 0.5 N/m^2. On the contrary, the area close to the river bank is slightly affected by ship motion.

Figure 54 shows the shear stresses without ship, while Figure 55 shows the maximum occurring shear stresses as the ship passes by to groyne fields. The pattern of the increased values along the ship track can be clearly observed.

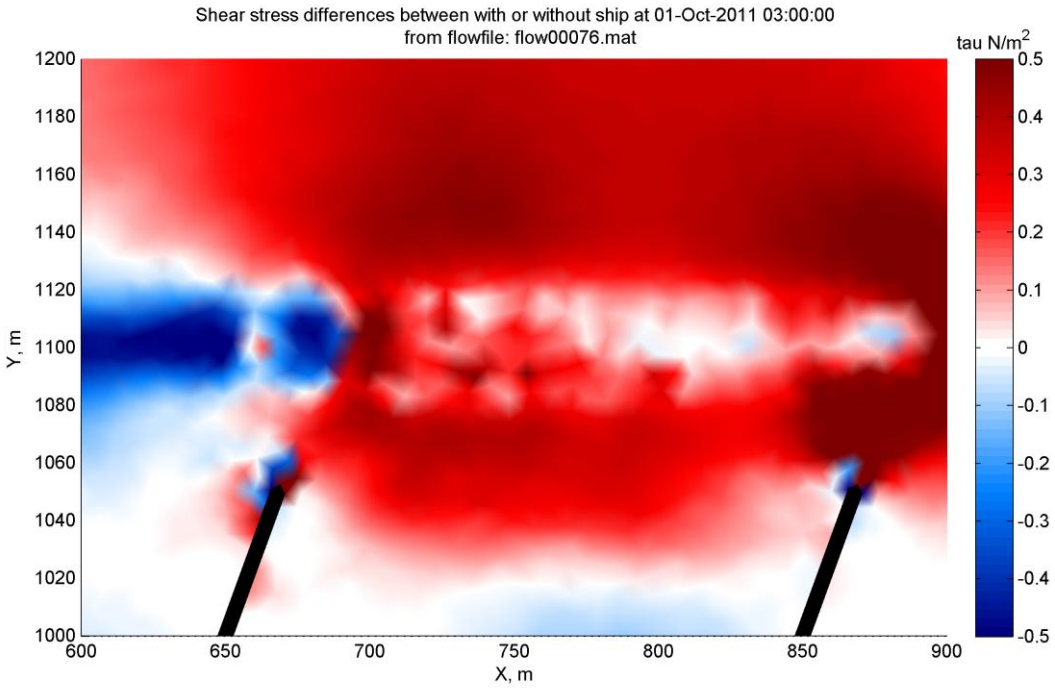

Figure 53 Difference of the shear stress between with and without ship-passing

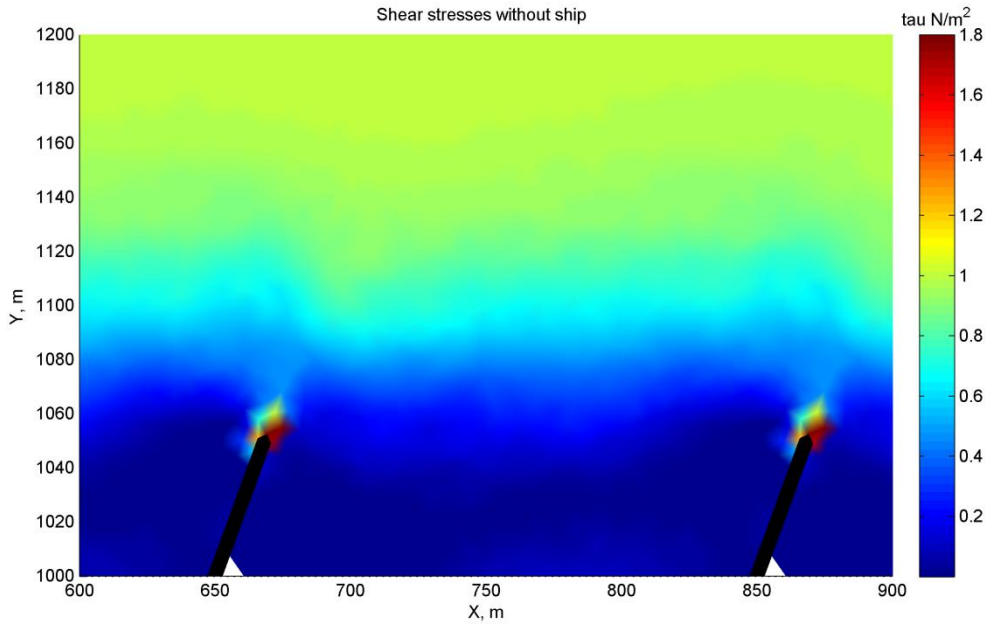

Figure 54 Shear stress magnitude without ship

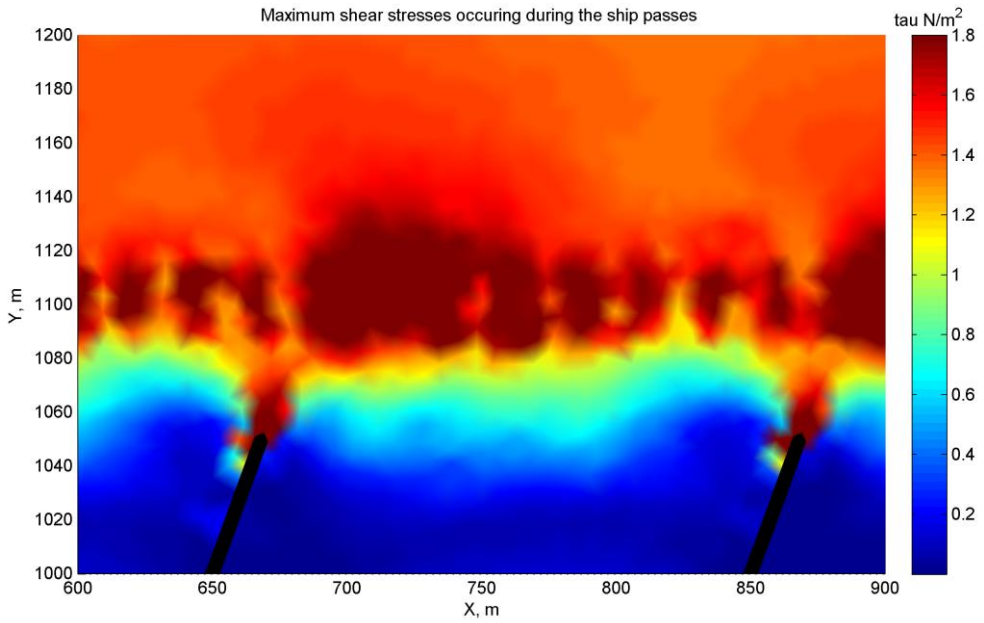

Figure 55 Maximum occurring shear stresses as ship passes

Figure 55 shows that the primary wave is barely entering the groyne field farther. It has a similar pattern as shown in Figure 53.

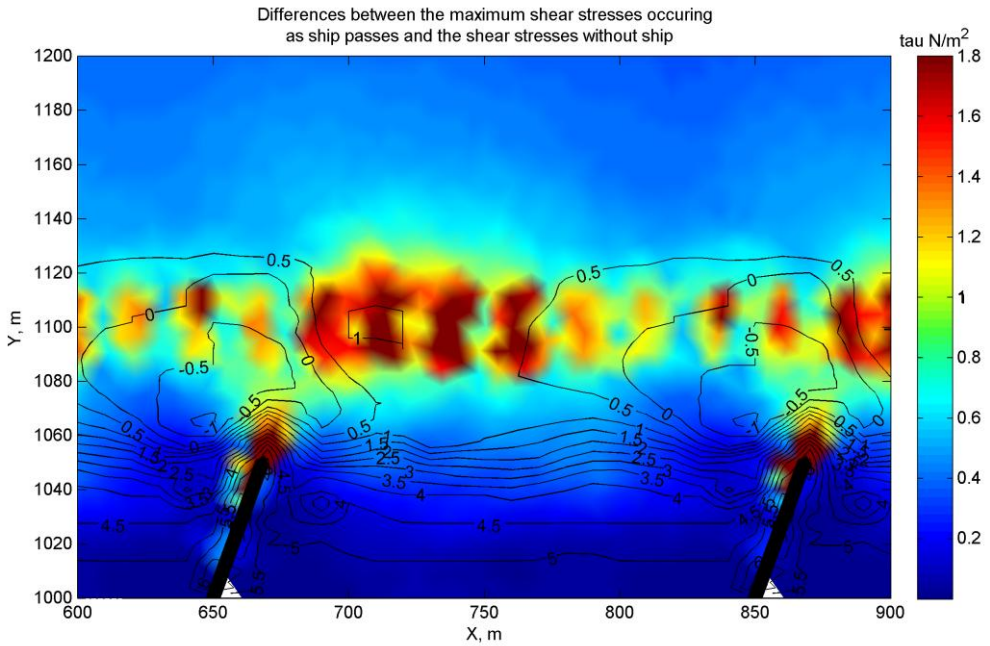

Figure 56 Differences between the maximum occurring shear stresses as the ship passes and the shear stresses without the ship showing the contour lines of the bathymetry

Figure 56 shows the differences between the maximum shear stresses and the situation without ship movement. The contour lines are also displayed to show how it can affect the shear stresses. It seems that the high shear stresses occurring in the ship track can be caused by changes in the bathymetry – it means the scour holes and the deposition.

7. Sensitivity analysis

This chapter focuses on the effect of different ship properties, analyzing their impact on hydrodynamics.

The figures below introduce the values of several hydrodynamic features in five selected points from the groyne field. The location of the selected points is displayed in Figure 57. Three points have been chosen along the y=1050 line, which is shown as the red line in Figure 25 . While another point from the inside of the groyne field has been chosen (on the blue cross-section in Figure 25) y=1020 m. The fifth point was chosen to show what happens around the toe of the groyne. These points have the same marker makeup as the figures shown later on.

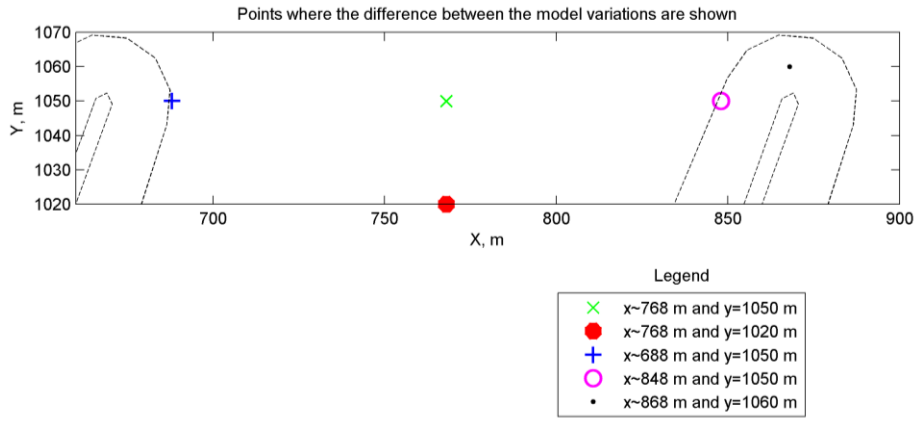

Figure 57 Points from the groyne field where the next pictures were observed

7.1. Sensitivity analysis of water level drops and maximum velocities

On the next pictures the first column displays the differences between the water level drops, while the second column shows the differences between the maximum velocities.

The first set of pictures (Figure 58) shows the differences with three different ship velocities. These were: v_s = 2.4 m/s, 2.7 m/s and 3 m/s. Easily noticeable that if the ship velocity is increasing than water level drop is larger and the flow velocities are getting larger, too.

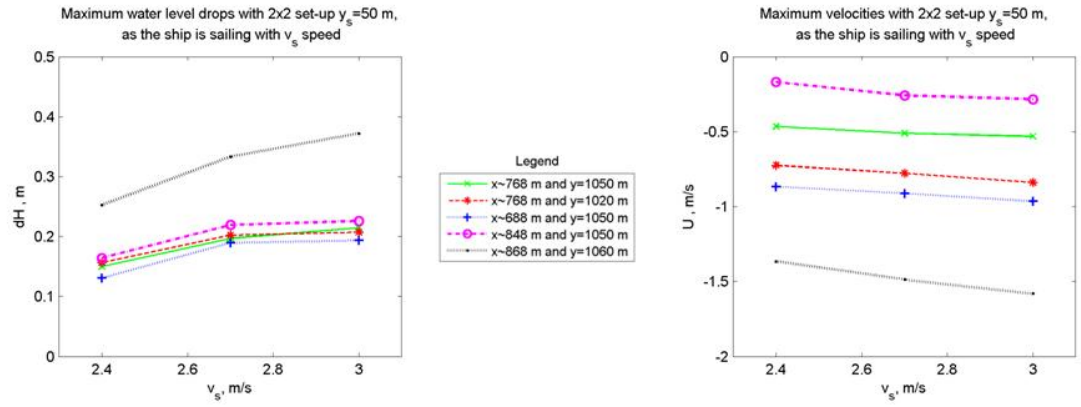

Figure 58 Maximum water level drop and velocity sensitivity for ship velocity changes

Figure 59 displays three different ship distances from the groyne tips. The y_S had also three values from 50 m to 150 m (sailing along the axis). This set shows the further the ship is sailing from the groyne fields the less impact it has.

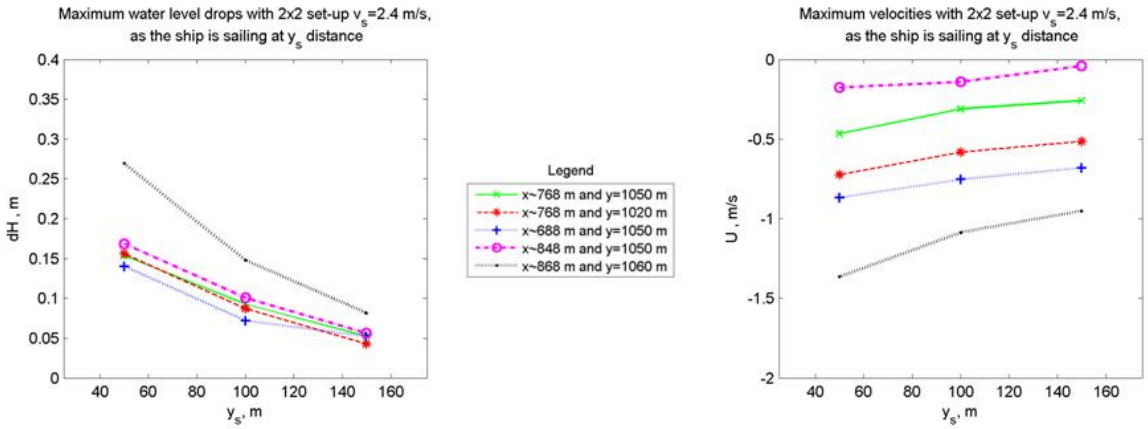

Figure 59 Maximum water level drop and velocity sensitivity for ship and groyne distance changes

Figure 60 shows the differences in case of three ship widths, B= 11.4 m, 22.8 m and 34.2 m, respectively. It seems that outside of the groyne field the strongest effect is caused by the ship width. The studied width values were taken from the PIANC ship classification (Verheij et al., 2008).

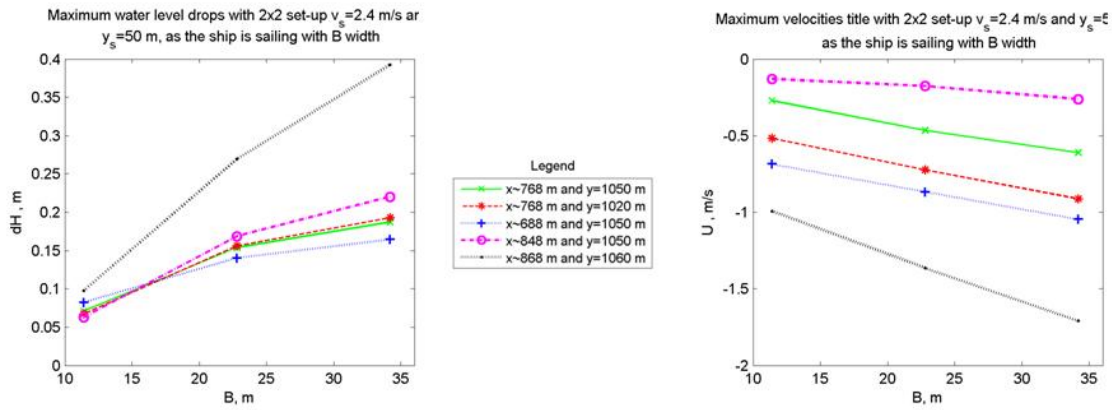

Figure 60 Maximum water level drop and velocity sensitivity for ship width changes

Figure 61 shows the effects of different ship draughts where *D*= 2.5 m, 3 m and 3.5 m, respectively. The ship draught marks also a greatly noticeable effect on the flow properties. The effect of draught changes is almost linear.

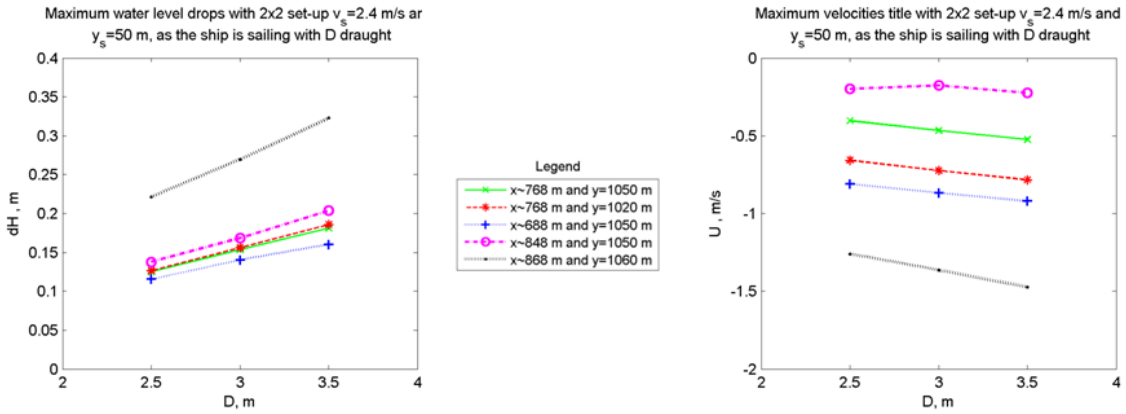

Figure 61 Maximum water level drop and velocity sensitivity for ship draught changes

Figure 62 shows the effect of different ship lengths: *L*= 76.5 m, 153 m and 229.5 m, respectively. The length of the ship has a barely noticeable impact on the flow field. These lengths are taken from PIANC ship classification (Verheij et al., 2008).

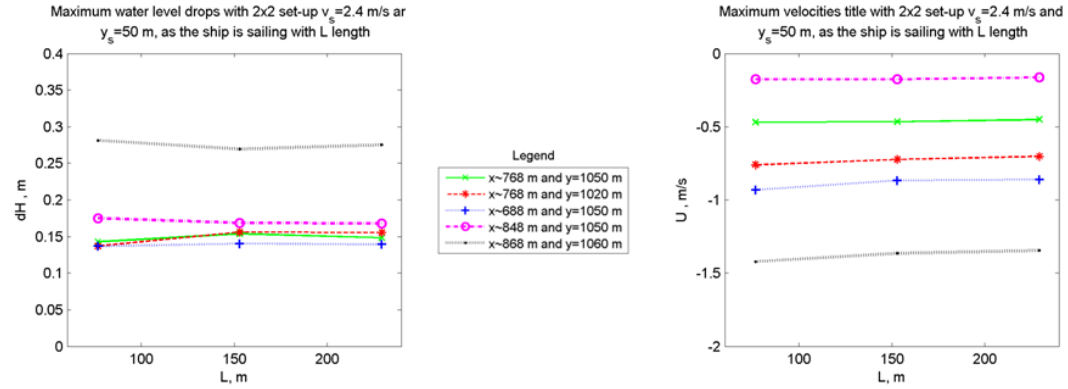

Figure 62 Maximum water level drop and velocity sensitivity for ship length changes

7.2. Shear stress sensitivity analysis

The sensitivity analysis regarding river morphology can be assessed by analyzing the calculated shear stress field, since morphological changes are not considered here. The next figures, therefore, show the maximum shear stresses in the above defined points (Figure 57).

The y axis is the same again, making the results easier observable on the figures.

Maximum shear stress shows that the middle of the groyne field is more sensitive than the sides (Figure 63 - Figure 66).

Ship velocity changes do not indicate too strong effects (Figure 63).

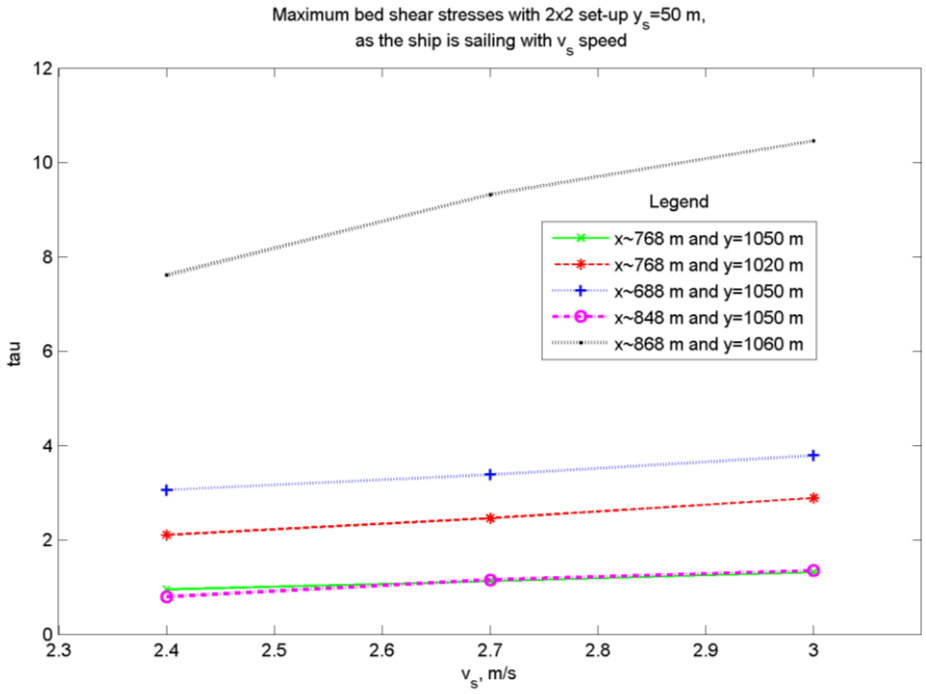

Figure 63 Maximum shear stress sensitivity for ship velocity changes

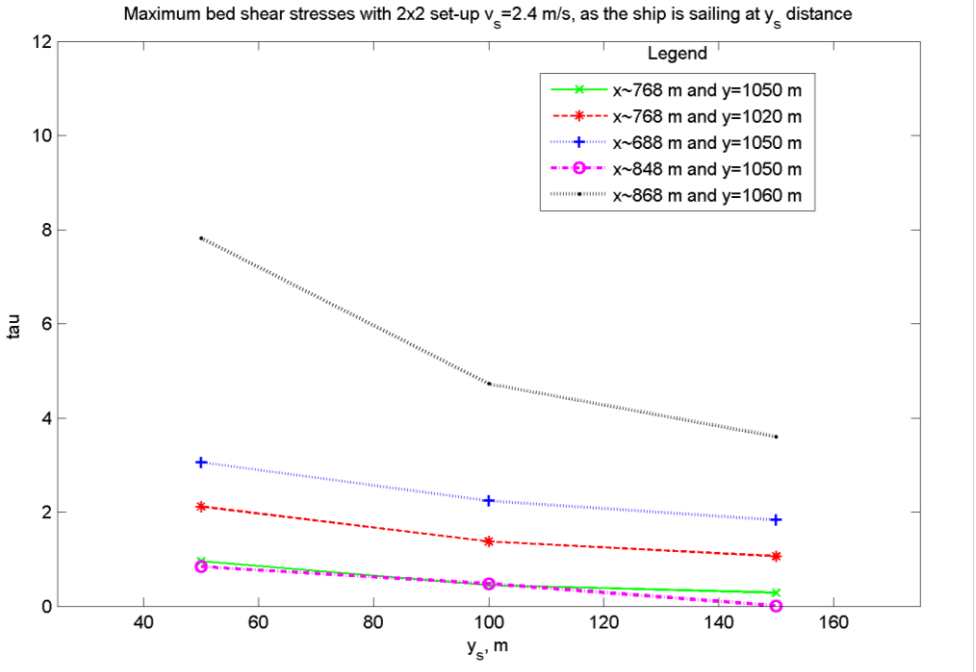

Figure 64 Maximum shear stress sensitivity for ship and groyne distance changes

The sailing distance from the groyne toes (Figure 64) indicates larger differences than the ship velocity, although the highest sensitivity experienced is caused by the ship width changes, as shown in Figure 65.

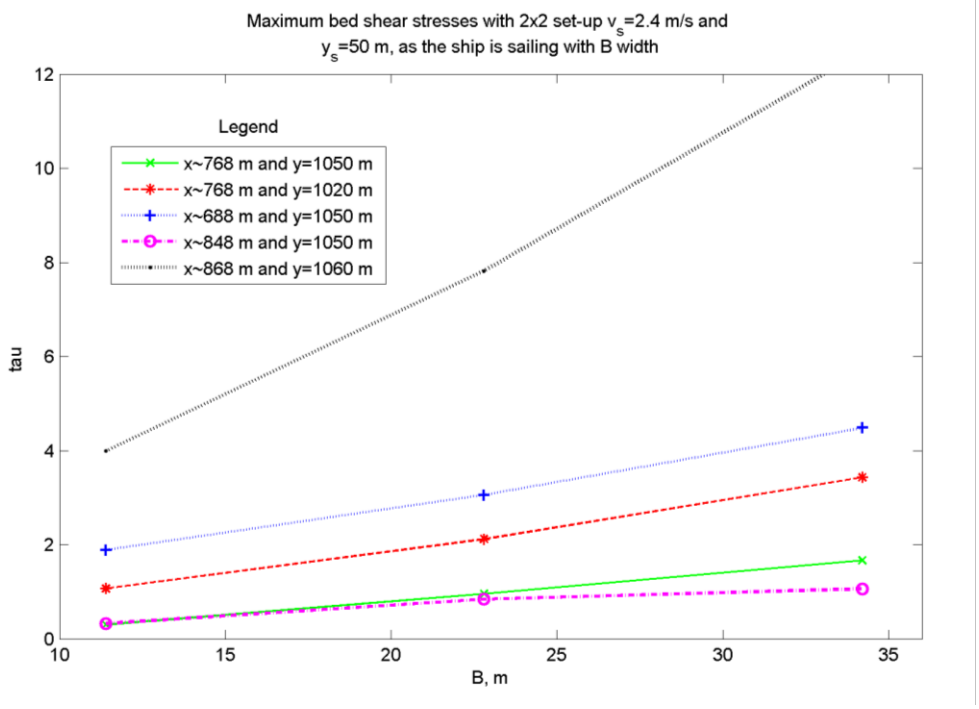

Figure 65 Maximum shear stress sensitivity for ship width changes

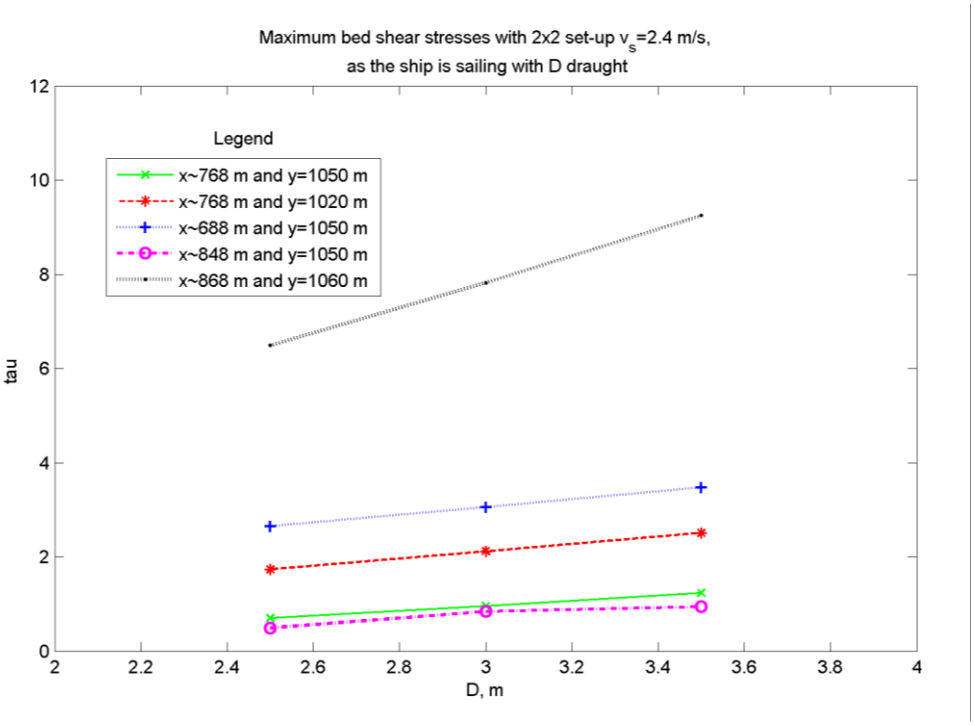

Figure 66 Maximum shear stress sensitivity for ship draught changes

Ship draught changes do not show big differences either (Figure 66).

7.3. Conclusion of the sensitivity analysis

The sensitivity analysis's summary on flow field properties shows that most of the impacts are related to the width of the ship and sailing distance from the groyne

toes. Draught has still a stronger impact than the ship velocity, whereas the length has no significant effect.

As is expected, stronger effects can be observed at the point outside of the groyne field (fifth point shown by green on the figures) than inside. Also, the mid zone of the groyne field is more influenced than margins of it.

The sensitivity of shear stress on the groyne field hydrodynamics can be ordered according to the following list:

- ship width
- ship draught
- sailing distance from the groynes
- ship velocity

These results agree well with the ones found by Verheij and Vermeer, 1987.

8. Discussion

When applying numerical models one should always consider the limitations of such a tool. Due to the simplifications, perfect agreement with measurements can, certainly, never be achieved. Even so, validated numerical models can be suitable and cost-effective tools for engineering purposes such as the analysis of ship induced currents in rivers.

8.1. Discussion of results

The numerical model results in the verification process resulted in satisfactory agreement with the experiments, however, the slight deviations can be explained by several reasons, among which, the differences between the physical and numerical model play an important role. The physical model's upscaled setup was not completely the same as the one defined in the numerical model. The main error source can be that the length of the study domain and thus the number of groynes differed. In the numerical model more groynes were defined because the aim was to study a groyne field, where the flow characteristics are not influenced by the main flow, as it does in the surroundings of the most upstream groyne field (see Uijttewaal, 2001). The numerical setup has also other simplifications, like the groyne schematization. Digitalization of the bathymetry may also contain errors as it has been done based on a scanned report.

Based on the simulation results several distributions of hydrodynamic parameters were introduced and analyzed. Velocity distributions showed e.g. how the passing ship affects the velocity fields or how it results in the lapse of eddies (both the primary and the secondary eddy). Water level fields showed the front waves and the return current well. The influence of the propeller jet was best displayed with the velocity vector fields.

The results showed that a 15-20 m wide zone (closest to the main flow) is influenced by the ship in the groyne field. It can be stated that the shear stresses increase in this zone, so it is probable that this primary wave might result in additive erosion. It was also shown that the propeller jet has negligible effect on the groyne fields.

The results of the sensitivity analysis were assessed analyzing three variables: water level drop, maximum velocities and maximum shear stresses. Both the water level drops and maximum velocities matched the ones found by Verheij and Vermeer, 1987. The sensitivity of shear stress on the groyne field hydrodynamics can be best given in the following order: ship width, ship draught, sailing distance from the groynes and ship velocity.

The applicability of such results is good, but there are several considerations to take into account:

- ship sizes
- drift angle

Although the used push tow sizes are from well-known international classification, one can see that these ship sizes will vanish in the close future, while bigger barges will appear. This would also be one subject of further research. It can also be

presumed that on River Danube as navigation will improve these barges will probably be still used.

Some simplifications of the real conditions were already made in the scale model. Such simplification was the neglecting of the drift angle (see Figure 67). Drift angle is an angle how push tows passes farther from the river axis (even without being in a bend); this β is usually around 2-5°, which makes the cross-section larger, than the amidships cross-section. (It means that closer to riverbank a push tow's route is closer to parallel to the banks, while the push tow is not.)

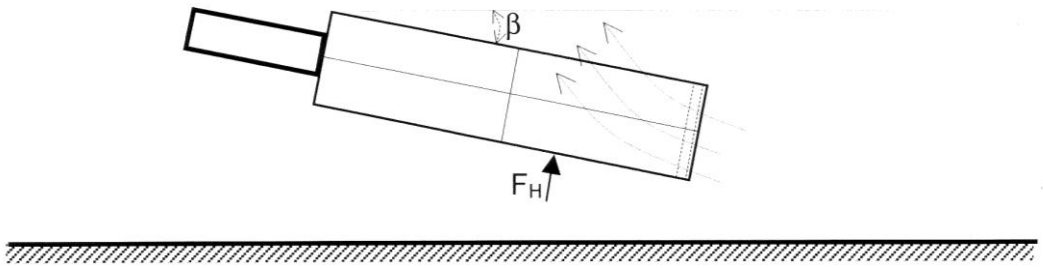

Figure 67 Drift angle shown on a 2x2 barges configuration as the ship is sailing close to the bank (source: Verheij et al., 2008)

This drift angle can be calculated as Figure 68.

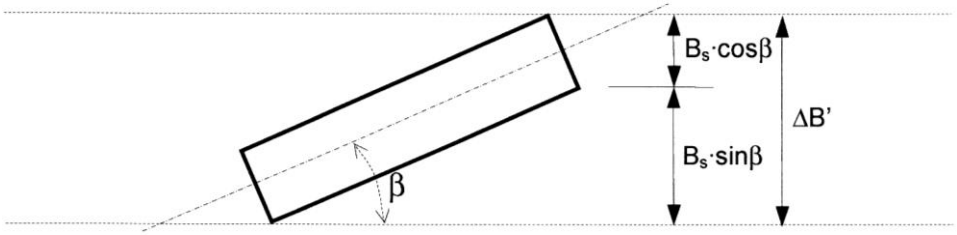

Figure 68 Largest width occupancy (source: Verheij et al., 2008)

8.2. Discussion of the numerical model

The numerical model is only capable of simulating the primary wave system and the jet. It means that secondary wave system is not examined in this research.

8.2.1. Turbulence

FINEL2D does not apply any turbulence model, it is only a robust, first order model. It can be well applied if the advective processes are dominative, but turbulence has not such a great impact. However, according to this study (see Chapter 5) FINEL2D calculates the two eddies, which qualitatively gives a good agreement with the experiments. Turbulence is modeled with the numerical diffusion, which basically comes from the cell size. Apparently smaller cells result in higher viscosity, thus the turbulent flow is expected to be better simulated in such a case.

8.2.2. Three dimensional application

A three dimensional approach would be needed if scour holes were located in the study domain. The problem with scour holes is that the program will only consider using the logarithmic velocity profile for the whole water depth, while in reality in the scour hole the velocities are probably not fitting this curve, e.g. it has an opposite directionality.

To determine the impact of scour holes, the simulations have been done also by a schematized bathymetry. This bathymetry doesn't have the depositions and scour holes as the real bathymetry. This can be seen in Figure 69.

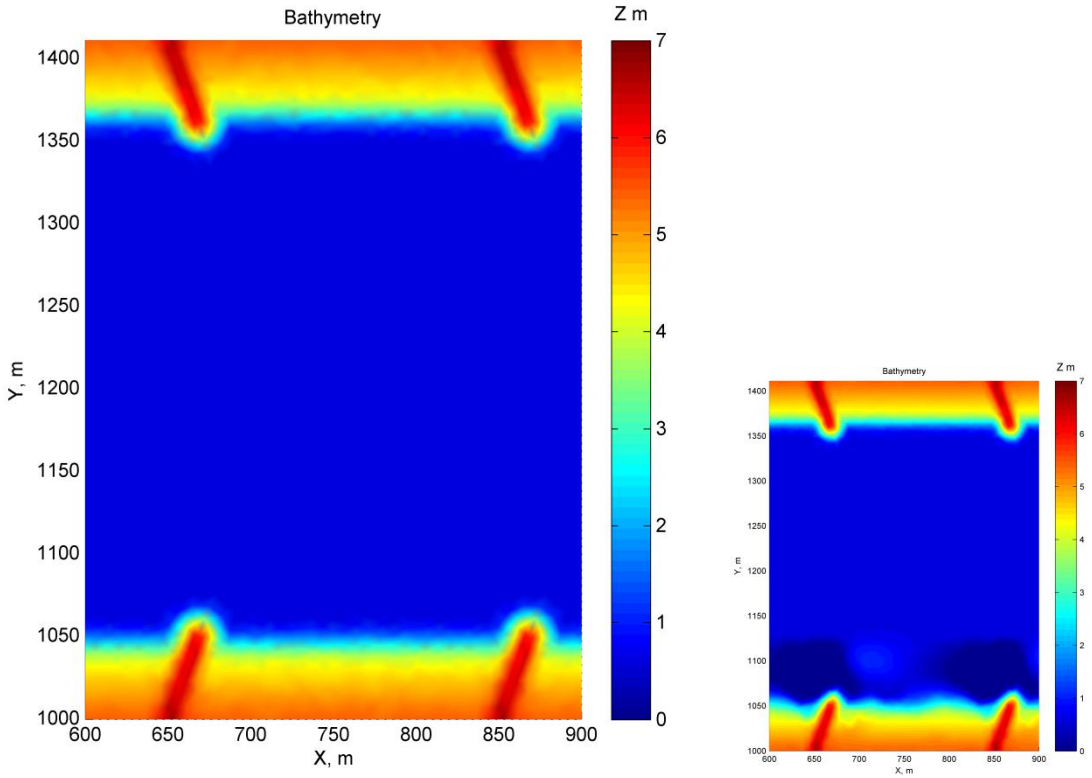

Figure 69 Schematized bathymetry vs. real bathymetry (small picture)

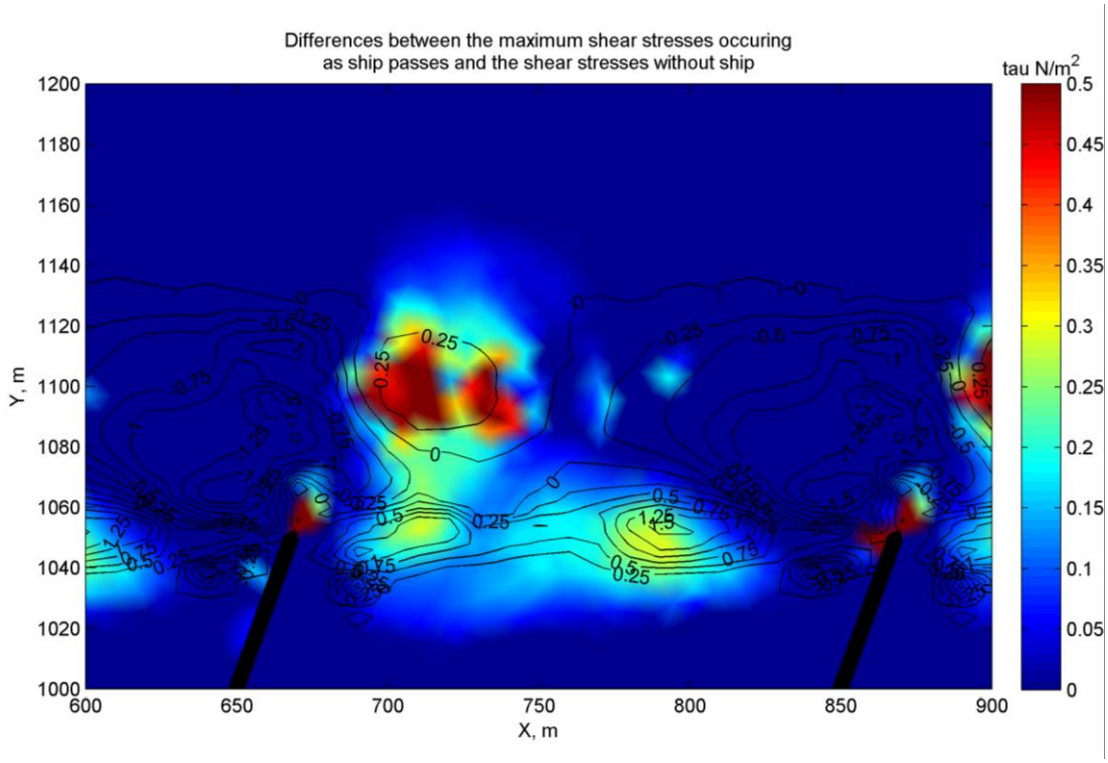

Figure 70 The difference between the differences with and without ship scenarios with schematized and real bathymetry

To show the differences appearing in shear stresses another figure (Figure 70) has been generated, where one can see that the differences are not between the places where scour hole appeared, only at the places where depostion appeared. This shows that for the better understanding of scour holes a three-dimensional application would be needed.

Submerged groynes would require a three-dimensional description, because they are creating strong secondary flows, but this needs further discussion in another study.

Time scale of the dynamic processes according to the ship passing is also considered. First, the time scale of the ship passing is coming from the length of a groyne field, the length of the ship and the ship's velocity, this means for a 3x2 setup around 200 seconds. The dynamic processes a time scale describable with the depth and shear velocity; it will probably be approximately 50 s. As the ship passing takes much longer than the evolving of the dynamic processes, it is adequate to use this numerical solution. A 3D application would apply this better as the shear stress would expand only to a thinner, lower layer.

9. Conclusions and recommendations

9.1. Conclusions

The goal of this project is: *What kind of effects has navigation on river morphology?*

(i) How does push-towing influence morphology?

a) How does it influence bed shear stresses, relative to groyne fields without ships passing?

In general, bed shear stresses in the groyne field are increasing as a ship passes. Modeled bed shear stresses show that the primary wave caused by a passing ship does not lead to large differences within the groyne fields. The influenced zone can be described as the closest 30 m to the main channel in the groyne field. Additional morphological dynamics can be expected mainly around the normal line. Differences can be expected resulted by the used bathymetry.

b) What is the influence of different ship sets on bed shear stress?

As the literature study has shown the main differences between different ship sets are in velocity, distance from groyne fields, ship width and draught; ship length has a barely detectable effect. This is corroborated by model results presented in Chapter 7.

c) What additional insights can be found by using a morphology set-up in the model?

Modeling erosion/sedimentation processes would give insight in the morphological set of groyne fields. This is recommended for further research because by analyzing the shear stresses only qualitative results can be estimated while a morphological set-up would give quantitative results. Although the different bed materials could be taken into account – as groynes are not built from river bed material, and react to the erosion in another way than the river bed.

With the usage of a morphology set-up additional information can be gained like the movement of suspended sediment or flow can influence the sediment transport while the sediment transport can influence the bathymetry which can influence the flow field again.

(ii) Is FINEL2D able to show the changes in the flow field at groyne fields?

a) On a fundamental level, is FINEL2D capable of these predictions or is a different model or even 3D modeling needed?

FINEL2D is a robust, first order model, which does not apply a turbulence model. FINEL2D is a good application where flow is dominated by advective processes and less applicable where flow is turbulence dominated. The latter is the case in the groyne fields with the two evolving eddies.

However, in practice the model shows adequate results in both a qualitative and quantitative sense as compared to measurements. Apparently the combination of advective and numeric diffusive processes in the model lead to similar flow fields as the actual advective and true diffusive processes do in the scale tests. It is thus contended that the model can be used to study the relative effects of ship size, passing distance etc. Determining the numeric diffusion was part of the calibration process, which apparently gives a good approximation of the turbulent diffusion.

The process has been simplified to two dimensions, but in reality a three dimensional description would give a better approximation. There are two main situations where vertical details needed: scour holes and submerged groynes. Submerged groynes would create secondary flows so strong that they would need a better (three-dimensional) description which is not the case with emerged groynes. Scour holes where the applicability of the logarithmic velocity profile is questionable also raise the question of the use of 3D applications.

b) How do FINEL2D results do compared to measurements from the physical model?

The starting model runs showed that FINEL2D is capable of applying the evolving flow in groyne fields. Two eddies appear on the stationary situation. These flow characteristics change when the ship passes corresponding to the physical model results by Verheij and Vermeer (1987).

On a quantitative level the verification process showed that FINEL2D is capable of simulating the water level drops (at more than half the locations the result was within 10% of the measurements); while the velocity changes had a larger deviation than the water level decrease (half of the results were within 100% of the measurements).

9.2. Recommendations

Data from field measurement for verification purposes would make this kind of research easier, e.g.: mean water level, velocity and morphological measurements. For velocity and water level measurements ADCP would be propose to use. (ADCP can take measurements with high time resolution, which would make the errors smaller, but of course in the velocity the turbulence would take a more considerable part, so a moving average should be used while data processing.) Before application it is recommended to consider the sensitivity of ADCP for waves.

Measurements could be also applied on the Danube. Although possibly the hydrodynamic processes are the same, but hydromorphological attributes would not be the same.

FINEL2D already has a morphology and sediment module but it is not capable – in the present state – describing the evolving processes caused by a passing ship. For this further research case programming is needed.

FINEL2D is capable of describing the relevant processes, however there are several processes which can be described better by a three dimensional approach.

It is recommended for further research to inquire into scenarios with bends (not just in a straight channel) or with more than one ship passing.

A model using a better physical representation (not just the primary wave but also the secondary waves and the propeller wash) could also be a further research area. But this may not be as useful as it sounds, because it would make the model very slow, and these features may not be as important.

References

Bakonyi P. (2009): Navigation and Hydropower. VITUKI (manuscript), Budapest (in Hungarian)

Brinke, W.B.M., F.H. Schulze and P. van derVeer (2004): Sand exchange between groyne field beaches and the navigation channel of the Dutch Rhine: the impact of navigation versus river flow. River Research and Application Vol. 20, pp. 899-928.

Dam, G., M. Klein and L. de Wit (2009): Technical and user manual FINEL2D, version 6.15, Svašek Hydraulics.

Fisher, H.B., E.J. List, J. Imberger and N.H. Brooks (1979): Mixing in Inland and Coastal Waters, Academic Press.

Lehmann, D.C., W.S.J. Uijttewaal, A. van Mazijk and V. Wietbrect (1999): Auswirkungen von Buhnenfeldern auf den Transport gelöster Stoffe in Flüssen. TU Delft and Universität Karlsruhe, Socrates Forschungprojekt, Delft (in German)

Ockenfeld, K. and H. Guhr (2003): Groyne fields – sink and source functions of "flow-reduced zones" for water content in the River Elbe (Germany). Water Science and Technology, Vol. 48 No. 7 pp 17-24

PIANC Netherlands Section (1988): Six-barge pushtow trials. Excerpt from Bulletin No 62, Den Haag.

PIANC (2003): Guidelines for sustainable inland waterways and inland navigation. EnviCom, Report of WG 6

Pilarczyk, K.W., H. Havinga, G.J. Klaassen, H.J. Verhey, E. Mosselman and J.A.A.M. Leemans (1990): Control of bank erosion in the Netherlands (State-of-the-art). Delft Hydraulics, publication 442, Delft.

Przedwojski, B., R. Blazejewski and K. W. Pilarczyk (1995): River training techniques fundamentals, design and application, A.A. Balkema, Rotterdam.

Rijkswaterstaat (2011): Water management in the Netherlands. Online edition, February 2011

Schiereck, G.J. (2001): Introduction to Bed, bank and shore protection. Delft

Sukhodolov, A., I. Schnauder, C. Anlanger, H.P. Rauchand and W.S.J. Uijttewaal (2008): Field experiments on flow hydrodynamics and exchange processes in groyne fields. In: Proceedings of the International Conference on Fluvial Hydraulics, Izmir, Turkey, pp. 865-874

Termes, A.P.P., M.van der Wal and H.J. Verheij (1991): Water motions due to navigation on rivers and in groyne fields. Delft Hydraulics, report Q903, Delft (in Dutch)

Uijttewaal, W.S.J, D. Lehmann and A. van Mazijk (2001): Exchange processes between a river and its groyne fields: model experiments. Journal of Hydraulic Engineering, Vol. 127, No. 11, pp. 928-936.

Verheij, H.J. and K. Vermeer (1987): Groyne field erosion due to push tow navigation (six and four barges) on the River Waal (Kribvakerosie door zes- en vierbaksduwvaart op de Waal). Delft Hydraulics, report Q93, Delft (in Dutch)

Verheij, H.J., C. Stolker and R. Groenveld (2008): Inland Waterways (Ports, waterways and inland navigation). TU Delft, lecture notes CT 4330, Delft

via donau (2011): Danube waterway map. online edition www.via-donau.at

VITUKI (2009): Studies on improving navigability in River Danube. Budapest, online edition: www.vituki.hu (in Hungarian)

van der Wal, M. (2001): Approach to groyne innovation in the Netherlands. Neue Ergebnisse über physikalische und ökologische Prozesse an Buhnenfeldern (New insights in the physical and ecological processes in groyne fields)– workshop publication Magdeburg, pp. 33-37.

Wallast, I. (1998): Exchange of dissolved matter between groyne field and main stream (in Dutch). MSc-thesis, Delft University of Technology, The Netherlands.

Weitbrecht, V. and C. Hinterberger (2001): Ergebnisse von physikalischen und numerischen Experimenten an umströmten Buhnenfeldern. Neue Ergebnisse über physikalische und ökologische Prozesse an Buhnenfeldern (New insights in the physical and ecological processes in groyne fields)– workshop publication Magdeburg, pp. 63-77.

Yossef, M.F.M. (2002): The effect of groynes on rivers. TU Delft, Literature review, Delft.

Appendix A: FINEL2D technical description after Svašek

This appendix is part of the work of Dam et al., 2009.

Introduction

FINEL2D is a computer model for the simulation of flow and morphology in rivers, estuaries and coastal areas. The two-dimensional shallow-water equations are solved to simulate the flow.

MORFIN is the name of the morphological modules for sand and silt transport within FINEL2D. Results of the wave model SWAN (shear stresses due to waves) can be included. Because the flow characteristics of cohesive (fine silt and partly organic material) and non-cohesive material (sand) are not the same, different approaches for computing the transport rates are applied: MORFIN-SAND and MORFIN-SILT. For areas with both sand and silt the module SAND-SILT is available.

Based on the computed flow and wave field, MORFIN computes sediment concentrations, causing local sedimentation or erosion. After the bottom levels are updated with these erosion and sediment figures, the new flow field is assessed, and above-mentioned steps are repeated throughout the computations.

The simulation of the morphology is based on one of the empirical sediment transport models, like Bijker, or Van Rijn. Sand-silt interaction can also be accounted for. The influence of waves on the flow and morphology can be taken into account by the coupling of FINEL2D with the wave model SWAN.

The Finite Element Method is the numerical basis for solving the equations. This method allows for the use of an unstructured grid of triangles. Such a grid is flexible and can be generated automatically.

In this short note, the concepts for the flow modelling and the sediment modelling are explained. First the finite element method is explained, second the mesh generation, third the flow module and finally the sediment transport module is discussed.

Finite Element Method

The numerical basis of FINEL2D is the Finite Element Method (FEM). This method differs from the difference method, used in many other software packages. Typical for FEM is that the model domain is divided into a number of triangular elements rather than rectangles. The physical variables, the two horizontal velocity components and the water level, are represented by discrete values in each element. Basis functions are subsequently used to take into account the interaction between the discrete values. Various textbooks discuss the concepts, advantages and disadvantages of the Finite Element Methods, see for example Donea and Huerta, 2003 for a general overview.

Mesh generation

The computational mesh can be generated using KeGeM (KeGeM: Klik en Genereer een Mesh (Click and generate a mesh)). This MATLAB graphical user interface

makes an input file for the mesh generator SEPRAN. Another option is using grid generator TRIANGLE. In both options the borders of the flow domain can easily be followed and the resolution can be adjusted locally. This means a high resolution can be obtained at areas where this is required and low resolution can be used in areas where this is allowed.

Governing flow equations

The depth-integrated shallow water equations are the basis of the flow module. For an overview on shallow water flows we refer to Vreugdenhil (1993).

continuity:

$$\frac{\partial h}{\partial t}+\frac{\partial uH}{\partial x}+\frac{\partial vH}{\partial y}=0$$

momentum balance in x-direction:

$$\frac{\partial Hu}{\partial t}+\frac{\partial Hu^2}{\partial x}+\frac{\partial Huv}{\partial y}-fHv+gH\frac{\partial h}{\partial x}-\frac{1}{\rho}\tau_{x,b}+\frac{1}{\rho}\tau_{x,w}+\frac{1}{\rho}\tau_{x,r}=0$$

momentum balance in y-direction:

$$\frac{\partial Hv}{\partial t}+\frac{\partial Huv}{\partial x}+\frac{\partial Hv^2}{\partial y}+fHu+gH\frac{\partial h}{\partial y}-\frac{1}{\rho}\tau_{y,b}+\frac{1}{\rho}\tau_{y,w}+\frac{1}{\rho}\tau_{y,r}=0$$

with $H=h+z_b$

so $\frac{\partial h}{\partial x}=\frac{\partial H}{\partial x}-\frac{\partial z_b}{\partial x}$, $\frac{\partial h}{\partial y}=\frac{\partial H}{\partial y}-\frac{\partial z_b}{\partial y}$

and $\frac{\partial h}{\partial t}=\frac{\partial H}{\partial t}$, because $\frac{\partial z_b}{\partial t}=0$

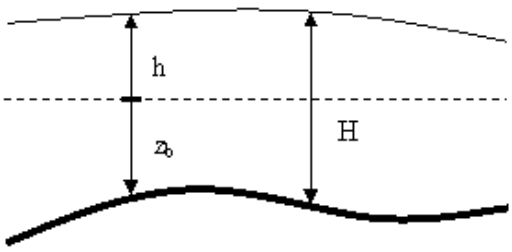

Figure A.1: Definition of variables

u = depth-integrated velocity in x-direction [m/s]

v = depth-integrated velocity in y-direction [m/s]

h = water level [m]

z_b = bottom level (positive downwards) [m]

H = water depth [m]

f = Coriolis coefficient [1/s]

g = gravitational acceleration [m/s^2]

ρ = density of water [kg/m^3]

τ_b = bottom shear stress [N/m^2]

τ_w = wind shear stress [N/m^2]

τ_r = radiation stress [N/m^2]

In addition to advection and pressure gradients, external forces like the Coriolis force, bottom shear stress, wind shear stress and radiation stress due to surface waves can be taken into account. It is noted that turbulent shear stresses are not taken into account; the application of the model is therefore restricted to advection dominated flows only. For applications where turbulent stresses play a role, the implicit version of FINEL2D is advised to be used.

Shallow water equations in FINEL2D explicit

As solution method in FINEL2D explicit, the discontinuous Galerkin method is adopted (Hughes, 1987) in which the three flow variables (waterlevel and two velocity components) are taken constant in each element, see Figure A.2. This method has great advantages in dealing with drying and flooding of elements.

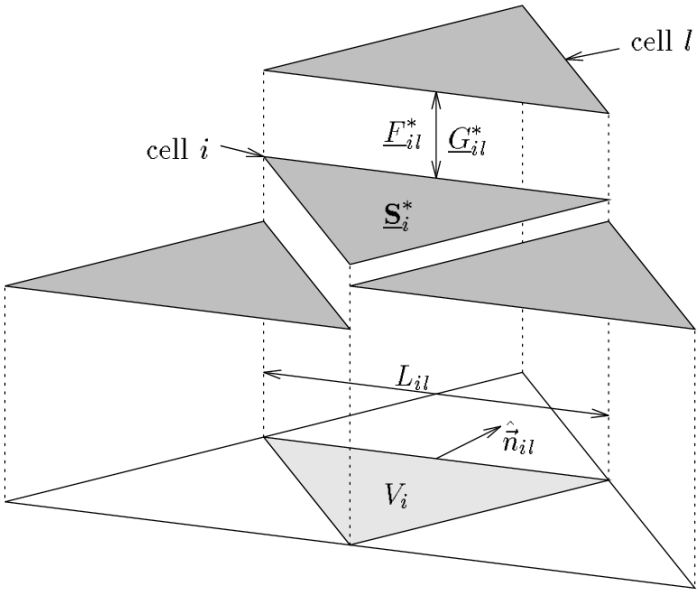

Figure A.2: Discontinuous Galerkin method
(constant flow variables in each element)

The momentum equations only contain first order derivatives in space. The three governing equations can be written as:

$$\frac{\partial}{\partial t}U + \frac{\partial}{\partial x}F_x + \frac{\partial}{\partial y}F_y = S_1 + S_2 \qquad (1)$$

with

$$U = \begin{pmatrix} H \\ uH \\ vH \end{pmatrix}, \quad F_x = \begin{pmatrix} uH \\ u^2H + \frac{gH^2}{2} \\ uvH \end{pmatrix}, \quad F_y = \begin{pmatrix} vH \\ uvH \\ v^2H + \frac{gH^2}{2} \end{pmatrix}, \quad S_1 = \begin{pmatrix} 0 \\ gH\frac{\partial z_b}{\partial x} \\ gH\frac{\partial z_b}{\partial y} \end{pmatrix}, \quad S_2 = \begin{pmatrix} 0 \\ \frac{1}{\rho}\tau_{x,tot} - fv \\ \frac{1}{\rho}\tau_{y,tot} + fu \end{pmatrix}$$

This set of equations can be integrated over an element resulting in:

$$\int_{\Omega}\frac{\partial}{\partial t}U\mathrm{d}\Omega+\int_{\Gamma}(F_x\cdot n_x+F_y\cdot n_y)\mathrm{d}\Gamma=\int_{\Omega}(S_1+S_2)\mathrm{d}\Omega$$

with

Ω = element surface

Γ = element boundary

n = unit vector normal to the element contour, directed outward

The fluxes (F_x, F_y) contain the advective terms with the pressure gradient. The first source term (S_1) contains the influence of the bottom slope. This term is needed because in the fluxes the gradient of the water depth H is taken instead of the water level h. The second source term (S_2) contains the external forces like the Coriolis force, bottom shear stress, wind shear stress and wave forces due to gradients in the wave radiation stresses.

As the variables are calculated in the centre of the elements and not along the edges of the elements, the fluxes (F_x, F_y) are not known beforehand, but can be found by the solution of a local Riemann problem. An approximate Riemann solver according to Roe is applied. The bottom slope within an element is zero, because the flow variables are taken constant in each element. On the sides of the elements the bottom slope can be determined simply by the difference in bed level of both elements. Therefore also the first source term S_1 (bottom slope) is taken into account in the Roe solver. The second source term S_2 (Coriolis force and several shear stresses) need not be taken into account in the Roe solver, but can be calculated in each element separately and then be integrated over the element surface.

Roe solver in FINEL2D explicit

The Riemann solver according to Roe is applied to calculate the change of flow variables in time in every element due to the fluxes over the boundaries. The fluxes are caused by advective transport and a pressure gradient (momentum equations (1) incl. first source term). Using the chain rule in differentiation, the momentum equations with only the first source term on the RHS can be rewritten as:

$$\frac{\partial}{\partial t}U+\frac{\partial F_x}{\partial U}\frac{\partial U}{\partial x}+\frac{\partial F_y}{\partial U}\frac{\partial U}{\partial y}=S_1$$

with $\frac{\partial F_x}{\partial U}$ and $\frac{\partial F_y}{\partial U}$ as 3 x 3 matrices containing the flux Jacobians. Omitting the source term on the RHS this can be rewritten into:

$$\frac{\partial}{\partial t}U+A\nabla\cdot U=0 \text{ with } A=\left(\frac{\partial F_y}{\partial U},\frac{\partial F_y}{\partial U}\right)\cdot\vec{n}$$

Matrix A has three real eigenvalues which form the characteristics of the system. The information in the system moves along every characteristic with velocities:

$$\lambda_1 = un_x + vn_y + c, \qquad \lambda_2 = un_x + vn_y - c, \qquad \lambda_3 = un_x + vn_y$$

$$c = \sqrt{gH}$$

First two eigenvalues correspond to gravity waves moving at a velocity $\vec{u} \pm \sqrt{gH}$, last eigenvalue corresponds to a vorticity wave moving at a velocity $\vec{u}$.

On every element boundary an abrupt change in flow variables can be found, like sketched in figure A.3. This can be interpreted as a bore. In subcritical conditions two characteristics flow downstream (λ_1, λ_3) and one characteristic flows upstream (λ_2). In the approximate Riemann solver according to Roe the flux Jacobians are linear approximated at the element boundaries using information from both neighboring elements. On every element boundary the three eigenvalues, eigenvectors and wavestrengths are determined. This forms three Roe fluxes which are added to the flow variables in the neighbouring element following the direction of its own characteristic (eigenvalue). In mathematical terms a Roe solver is an upwind scheme. In FINEL2D explicit a first order approach is used to determine the three Roe fluxes. This causes some numerical diffusion, but guarantees strict mass and momentum conservation.

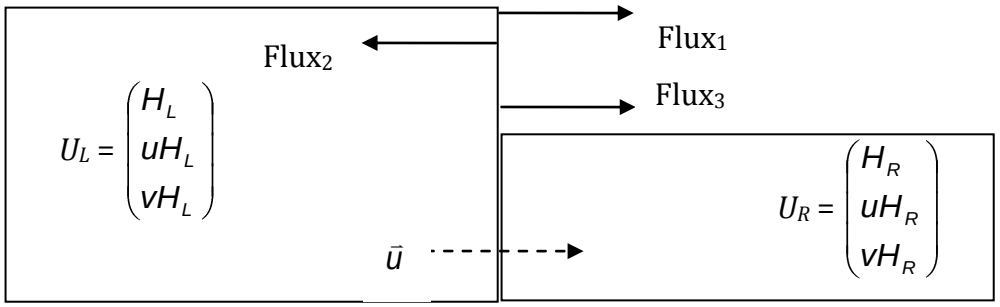

Figure 2.3: Discontinuity at element boundary with Roe fluxes sketched (subcritical)

Roe linearization

The Roe eigenvalues are:

$$\lambda_1 = \tilde{u}_n + \tilde{c}, \qquad \lambda_2 = \tilde{u}_n - \tilde{c}, \qquad \lambda_3 = \tilde{u}_n$$

With the eigenvectors:

$$r_1 = \begin{pmatrix} 1 \\ \tilde{u} + \tilde{c}n_x \\ \tilde{v} + \tilde{c}n_y \end{pmatrix}, \qquad r_2 = \begin{pmatrix} 1 \\ \tilde{u} - \tilde{c}n_x \\ \tilde{v} - \tilde{c}n_y \end{pmatrix}, \qquad r_3 = \begin{pmatrix} 0 \\ -n_y \\ n_x \end{pmatrix}$$

The corresponding wave strengths are given by (with B = width boundary):

$$\alpha_1 = \frac{B}{2}(\Delta H + \frac{\sqrt{H_1}\sqrt{H_2}}{\tilde{c}}\Delta u_n)$$

$$\alpha_2 = \frac{B}{2}(\Delta H - \frac{\sqrt{H_1}\sqrt{H_2}}{\tilde{c}}\Delta u_n)$$

$$\alpha_3 = B\Delta u_s$$

Factors to include the bottom slope:

$$\beta_1 = -\frac{B}{2}\tilde{c}\Delta z_b, \qquad \beta_2 = \frac{B}{2}\tilde{c}\Delta z_b, \qquad \beta_3 = 0$$

With the Roe averages:

$$\tilde{u} = \frac{u_R\sqrt{H_R} + u_L\sqrt{H_L}}{\sqrt{H_R} + \sqrt{H_L}}, \qquad \tilde{v} = \frac{v_R\sqrt{H_R} + v_L\sqrt{H_L}}{\sqrt{H_R} + \sqrt{H_L}}, \qquad \tilde{c} = \sqrt{\frac{g(h_R + h_L)}{2}}, \qquad \tilde{u}_n = \tilde{u}n_x + \tilde{v}n_y$$

And the difference operator is given by:

$$\Delta\cdot = (\cdot)_R - (\cdot)_L$$

With subscript $_R$ and $_L$ representing the right and left neighbour element, respectively. The subscript *n* represents the direction normal to the boundary (with n_x,n_y), subscript $_s$ represents the direction parallel to the boundary:

$$\Delta u_n = (u_R n_x + v_R n_y) - (u_L n_x + v_L n_y), \qquad \Delta u_s = (v_R n_x - u_R n_y) - (v_L n_x - u_L n_y)$$

The Roe solver is used to solve the following differential equation:

$$\frac{\partial}{\partial t}U + A\nabla\cdot U = S_1 \text{ with } A = \left(\frac{\partial F_x}{\partial U}, \frac{\partial F_y}{\partial U}\right)\cdot\vec{n}$$

An explicit time-stepping is used, leading to:

$$U^{n+1} = U^n + \Delta t(S_1 - A\nabla\cdot U)$$

Following the direction of the characteristics, the Roe solution becomes:

$$U_R^{n+1} = U_R^n - \frac{\Delta t}{A_{element}}\sum_{i=1}^{3}(\alpha_i\lambda_i + \beta_i)r_i, \text{ when } \lambda_i > 0$$

$$U_L^{n+1} = U_L^n - \frac{\Delta t}{A_{element}}\sum_{i=1}^{3}(\alpha_i\lambda_i + \beta_i)r_i, \text{ when } \lambda_i < 0$$

Every triangle has three sides where the fluxes are calculated, those fluxes across the three sides determines the total change in flow variables in one time step. The Roe solver can handle both supercritical as sub critical flow, because simply the direction of the characteristics is followed. The integration in time is explicit. As this method restricts the time step, the time step is controlled automatically for optimum performance.

When the Roe solver tries to extract more water from an element than there is available, the first two wave strengths (α_1 and α_2, both used in the continuity equation) are redistributed.

Dry elements in FINEL2D explicit

A special problem in shallow waters like for example in estuaries is the drying and flooding of large areas during a tidal cycle. As a discontinuous discretisation is used in combination with an explicit time-stepping, this flooding and drying of elements can be treated relatively easily. When the water depth in an element becomes less than the dry-criterion (default 0.03 m) it becomes a dry element. The velocities are made zero and next time step no water can be extracted from the dry element. The remaining water in a dry element is not thrown away, instead, all water flowing into a dry element is added to the water already present. In the following two situations the corresponding characteristic waves are reflected on a dry element:

The ROE solver tries to extract water from the dry element
Water elevation of an element next to a dry element < bottom level dry element

In case of reflection on a dry element all characteristic waves are directed away from the dry element.

Bottom friction

Bottom friction takes into account the influence of bottom roughness on the main flow. Bottom roughness can be given as a field with a value for every element or a global value is used. To close the set of equations, the bottom shear stress is expressed in terms of the main flow variables:

$$\frac{1}{\rho}\tau_{x,b} = -u\frac{g\sqrt{u^2+v^2}}{C^2H}$$

$$\frac{1}{\rho}\tau_{y,b} = -v\frac{g\sqrt{u^2+v^2}}{C^2H}$$

The bottom roughness can be given as input in three ways:

1. Nikkuradse roughness k_n→ $C = 10\log(\frac{12H}{k_n})$
2. Chezy value C directly.
3. Manning roughness n → $C = \frac{H^{1/6}}{n}$

Appendix B: Calibration and validation in figures

x, m	y, m	dH, m set-up: 2x2 vs=2.7 m/s ys=50 m		dH, m set-up: 2x2 vs=2.7 m/s ys=100 m		dH, m set-up: 3x2 vs=2.4 m/s ys=50 m		dH, m set-up: 3x2 vs=2.4 m/s ys=100 m	
		scale model	FINEL	scale model	FINEL	scale model	FINEL	scale model	FINEL
668.20	1060	0.225	0.232	0.125	0.148	0.225	0.191	-0.15	0.109
678.20	1040	0.45	0.327	0.175	0.191	0.30	0.265	0.225	0.142
678.20	1050	0.25	0.243	0.15	0.145	0.25	0.184	0.20	0.113
688.20	1050	0.30	0.231	0.15	0.136	0.25	0.177	0.20	0.112
698.20	1050	0.20	0.219	0.10	0.131	0.25	0.166	0.175	0.103
718.20	1050	0.20	0.211	0.10	0.126	0.25	0.159	0.20	0.099
738.20	1050	0.20	0.208	0.10	0.123	0.15	0.156	0.125	0.096
768.20	1020	0.25	0.207	0.15	0.119	0.20	0.158	0.10	0.096
768.20	1030	0.20	0.209	0.15	0.113	0.20	0.149	0.10	0.086
768.20	1040	0.20	0.201	0.15	0.110	0.15	0.145	0.10	0.085
768.20	1050	0.30	0.195	0.15	0.108	0.15	0.145	0.10	0.086
768.20	1060	0.25	0.198	0.15	0.107	0.20	0.146	0.125	0.088
768.20	1070	0.20	0.199	0.15	0.107	0.15	0.148	0.10	0.091
798.20	1050	0.20	0.200	0.15	0.108	0.20	0.152	0.15	0.095
818.20	1050	0.20	0.189	0.15	0.102	0.15	0.144	0.125	0.076
838.20	1050	0.15	0.194	0.15	0.108	0.15	0.144	0.10	0.075
848.20	1050	0.20	0.189	0.10	0.109	0.15	0.144	0.10	0.075
858.20	1040	0.20	0.185	0.15	0.109	0.15	0.140	0.125	0.074
858.20	1050	0.20	0.191	0.15	0.117	0.20	0.142	0.125	0.076
868.20	1060	0.20	0.192	0.15	0.109	0.20	0.136	0.125	0.072
868.20	1070	0.29	0.365	0.225	0.227	0.28	0.297	0.14	0.130

Table 2 Water level drop series from the scale model and FINEL2D

This table summarizes the results of the verification process, by comparing the results to measurements taken in the scale model.

Calibration process

2x2 set-up

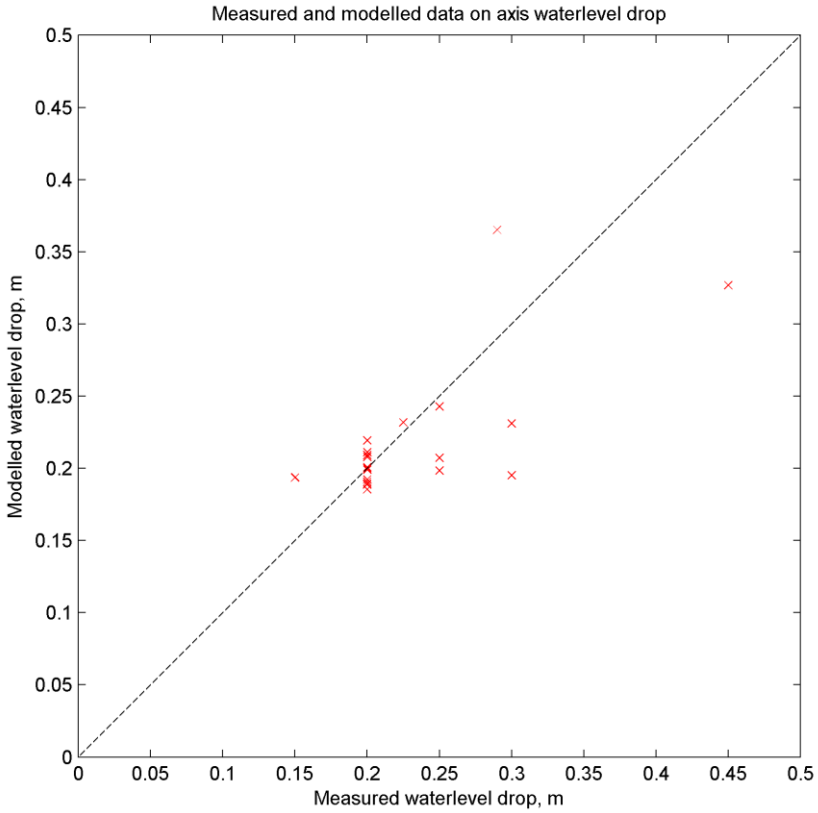

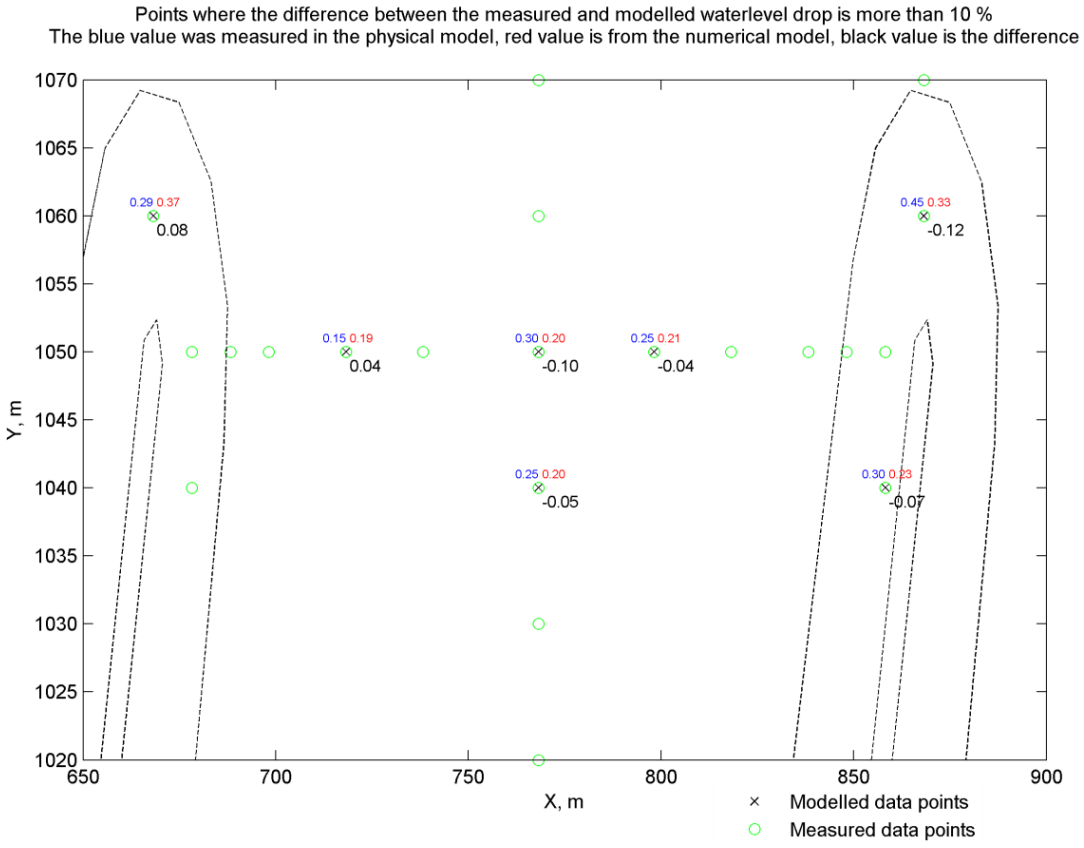

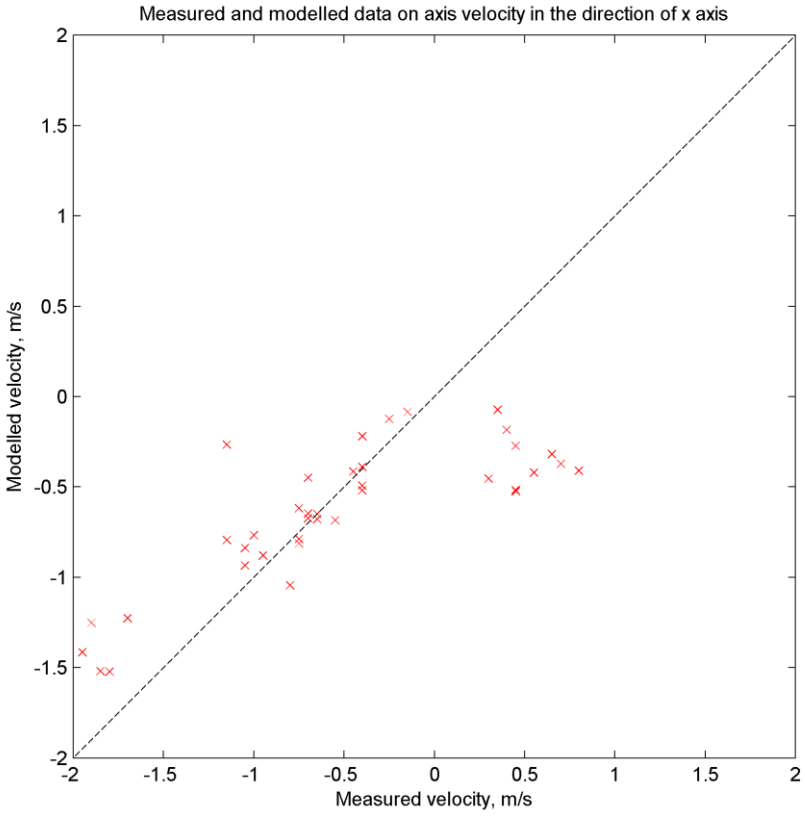
Measured and modelled data on axis velocity in the direction of x axis
Modelled velocity, m/s
Measured velocity, m/s
2
1.5
1
0.5
0
-0.5
-1
-1.5
-2

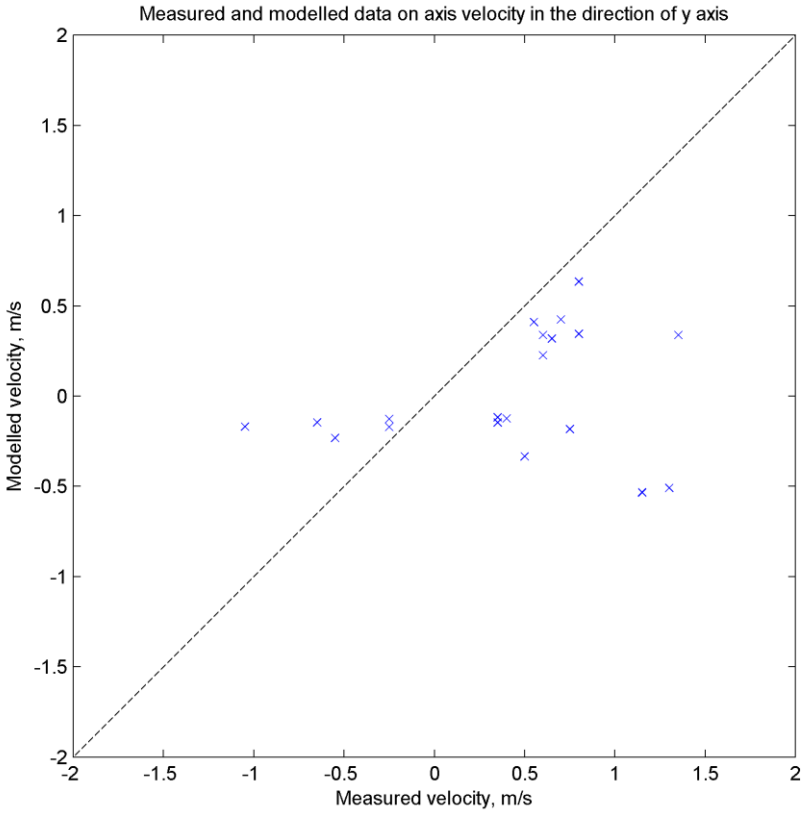
Measured and modelled data on axis velocity in the direction of y axis
Modelled velocity, m/s
Measured velocity, m/s
2
1.5
1
0.5
0
-0.5
-1
-1.5
-2

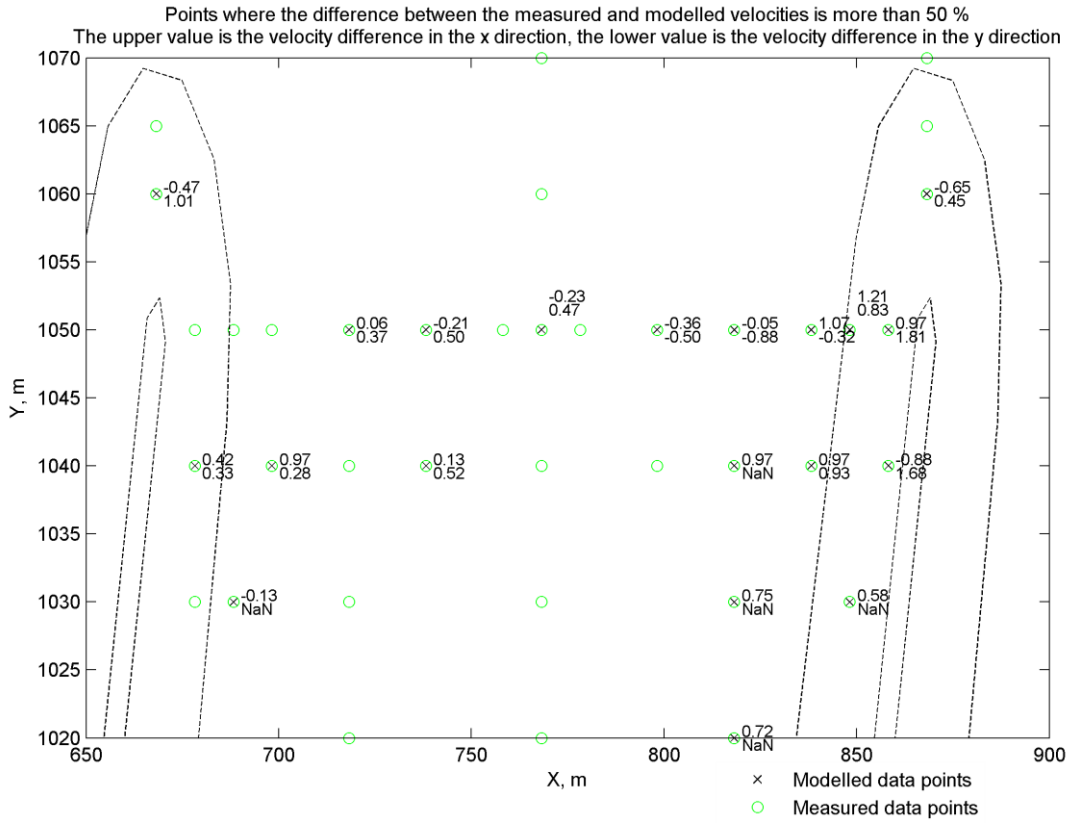
Points where the difference between the measured and modelled velocities is more than 50 %
The upper value is the velocity difference in the x direction, the lower value is the velocity difference in the y direction
Y, m
X, m
Modelled data points
Measured data points
-0.47
1.01
-0.65
0.45
-0.23
0.47
1.21
0.83
0.06
0.37
-0.21
0.50
-0.36
-0.50
-0.05
-0.88
1.07
-0.32
0.97
1.81
0.42
0.33
0.97
0.28
0.13
0.52
0.97
NaN
0.97
0.93
-0.88
1.68
-0.13
NaN
0.75
NaN
0.58
NaN
0.72
NaN

Calibration process

3x2 set-up

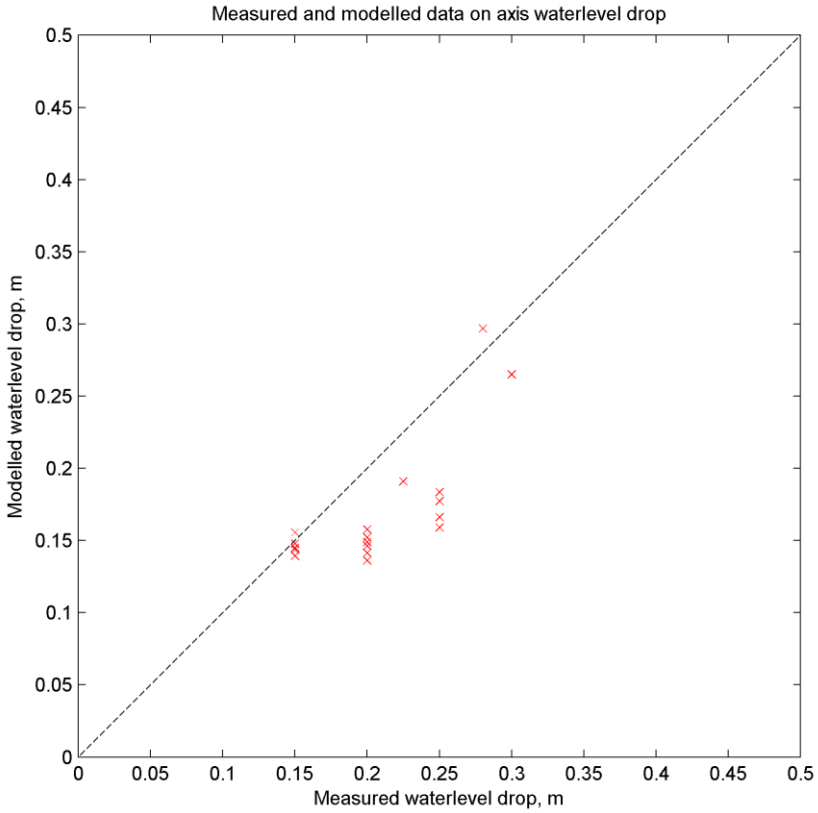

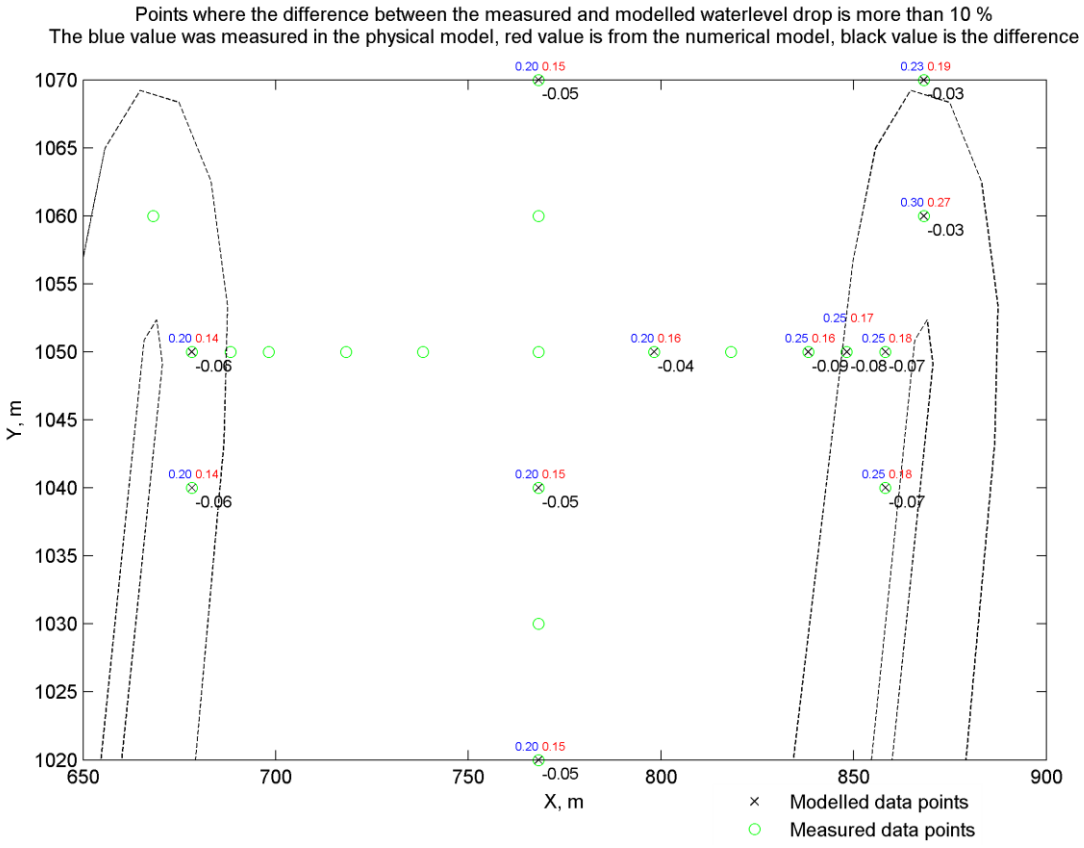

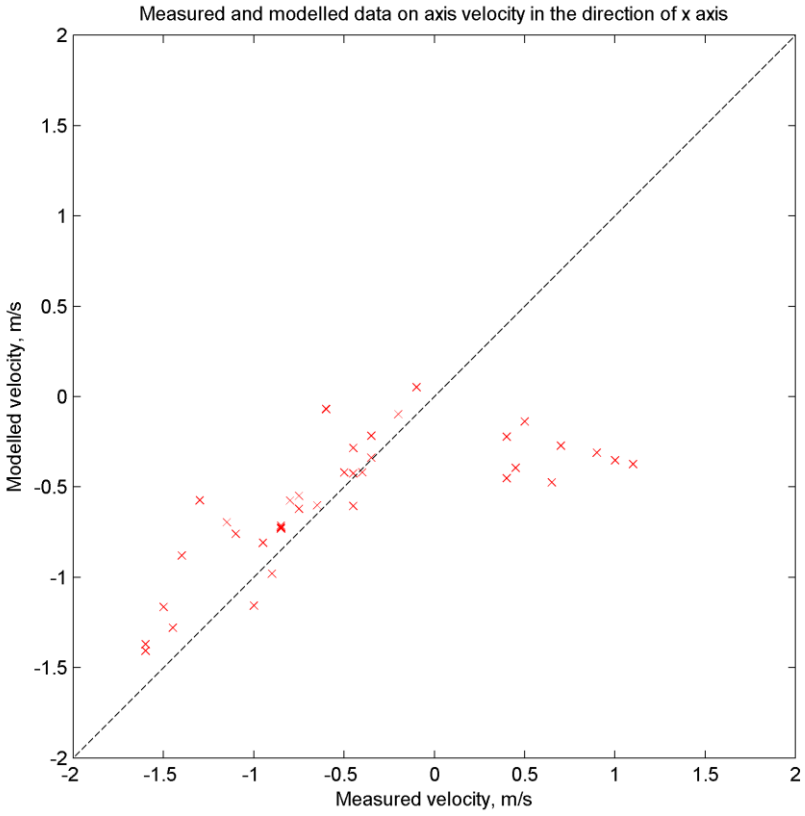
Measured and modelled data on axis velocity in the direction of x axis
Modelled velocity, m/s
Measured velocity, m/s
2
1.5
1
0.5
0
-0.5
-1
-1.5
-2
-2
-1.5
-1
-0.5
0
0.5
1
1.5
2

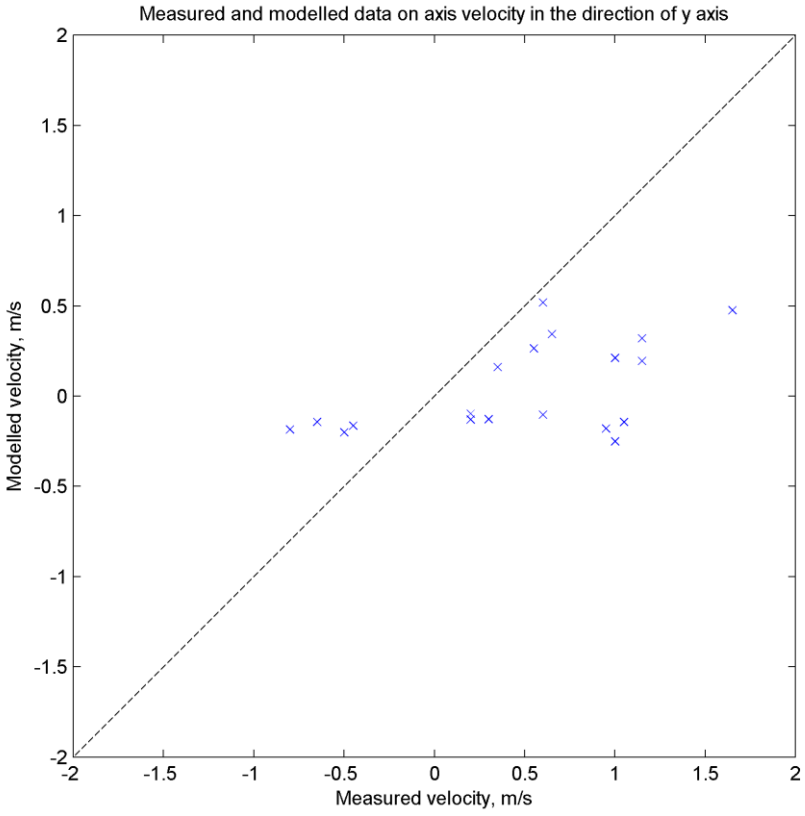
Measured and modelled data on axis velocity in the direction of y axis
Modelled velocity, m/s
Measured velocity, m/s
2
1.5
1
0.5
0
-0.5
-1
-1.5
-2
-2
-1.5
-1
-0.5
0
0.5
1
1.5
2

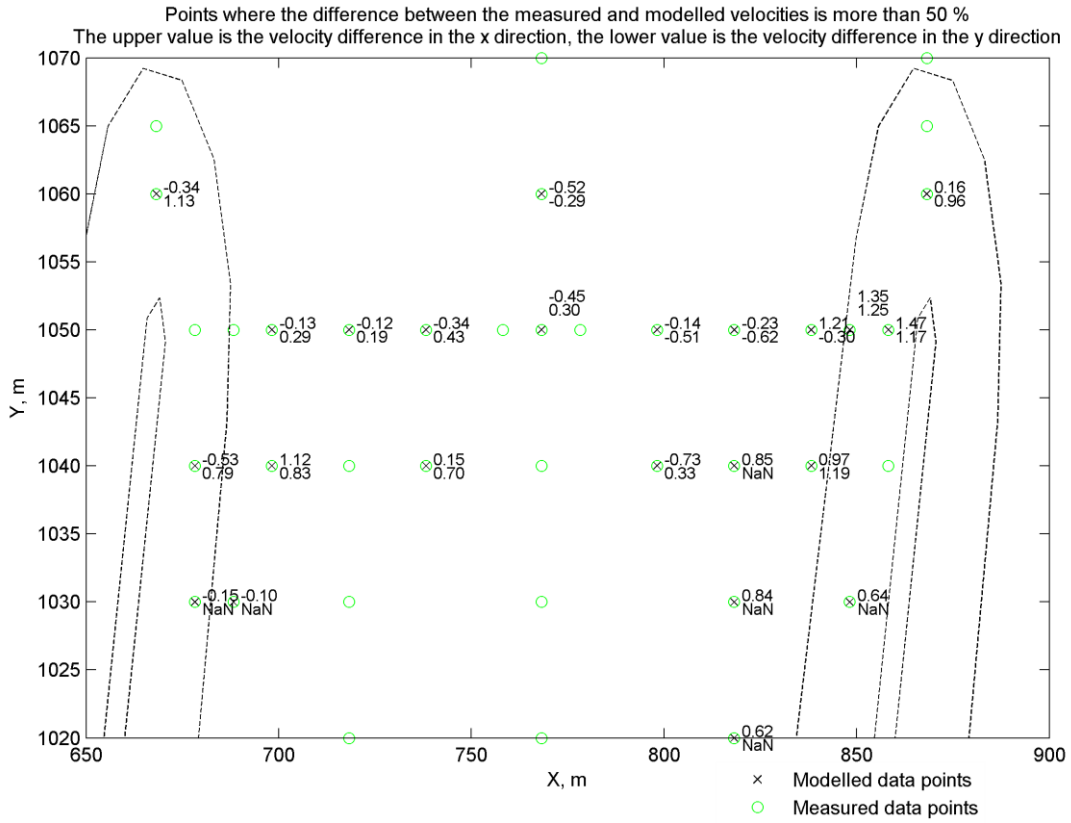
Points where the difference between the measured and modelled velocities is more than 50 %
The upper value is the velocity difference in the x direction, the lower value is the velocity difference in the y direction
Y, m
X, m
Modelled data points
Measured data points

Validation process

2x2 set-up

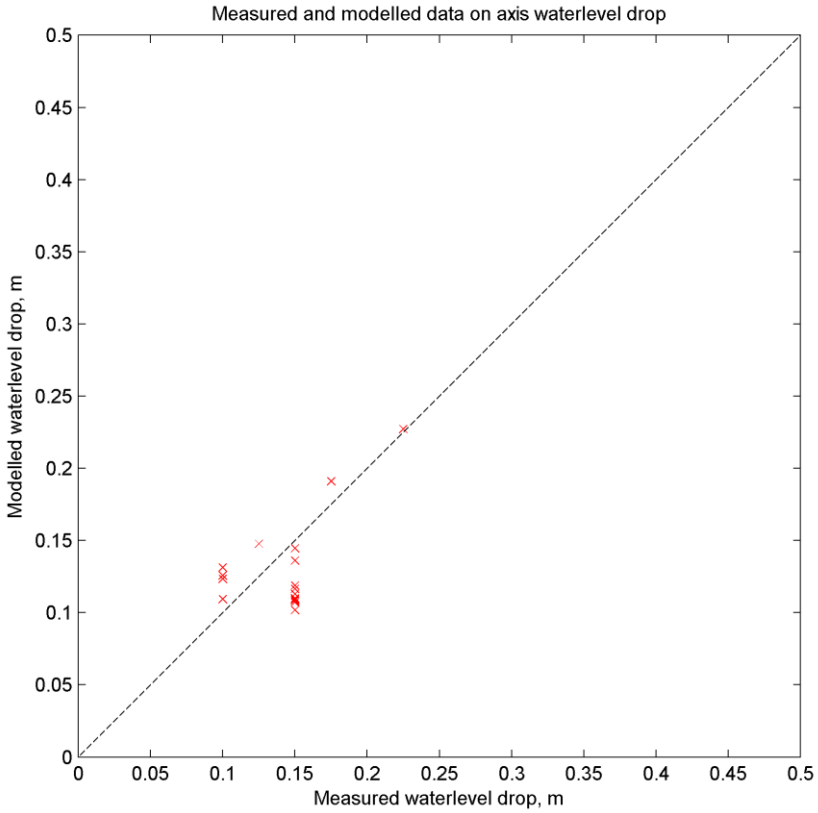

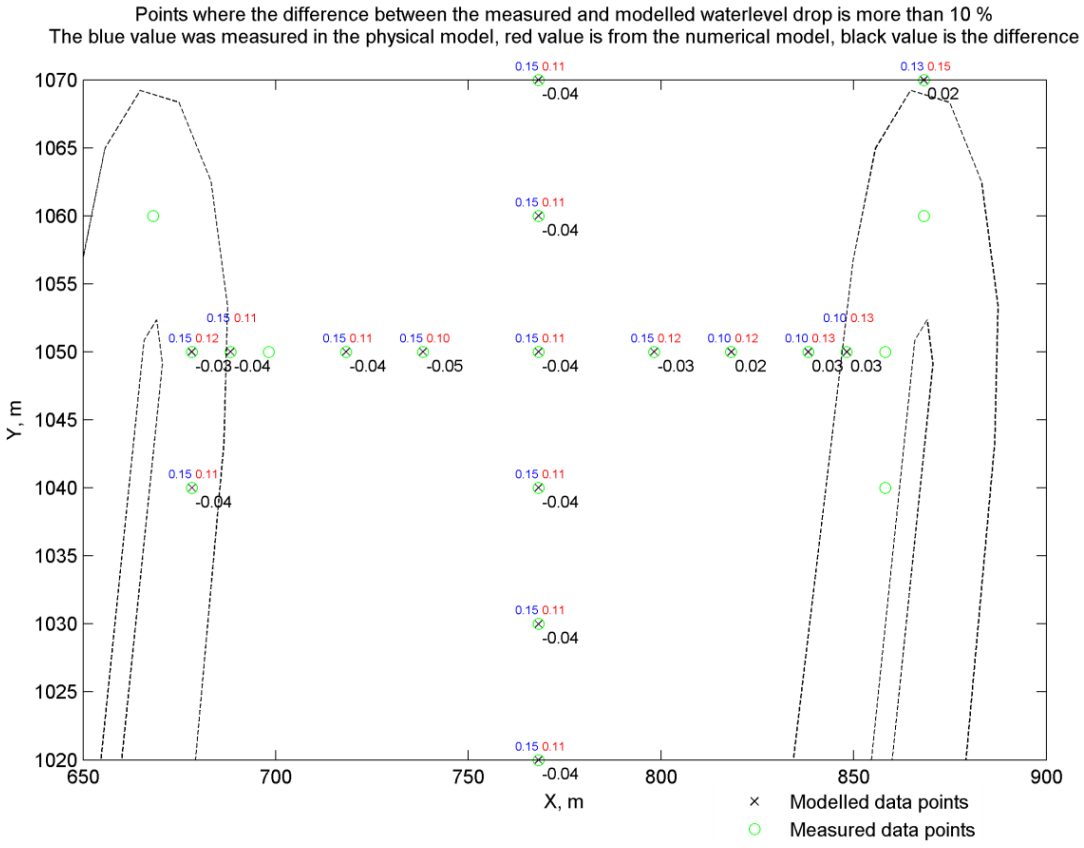

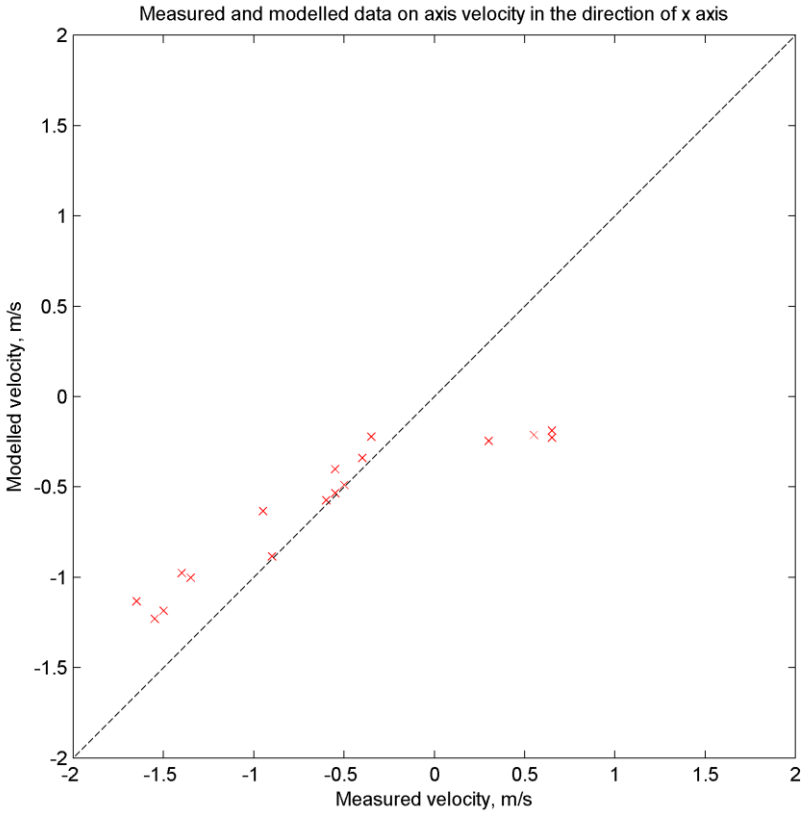
Measured and modelled data on axis velocity in the direction of x axis
Modelled velocity, m/s
Measured velocity, m/s
2
1.5
1
0.5
0
-0.5
-1
-1.5
-2
-2
-1.5
-1
-0.5
0
0.5
1
1.5
2

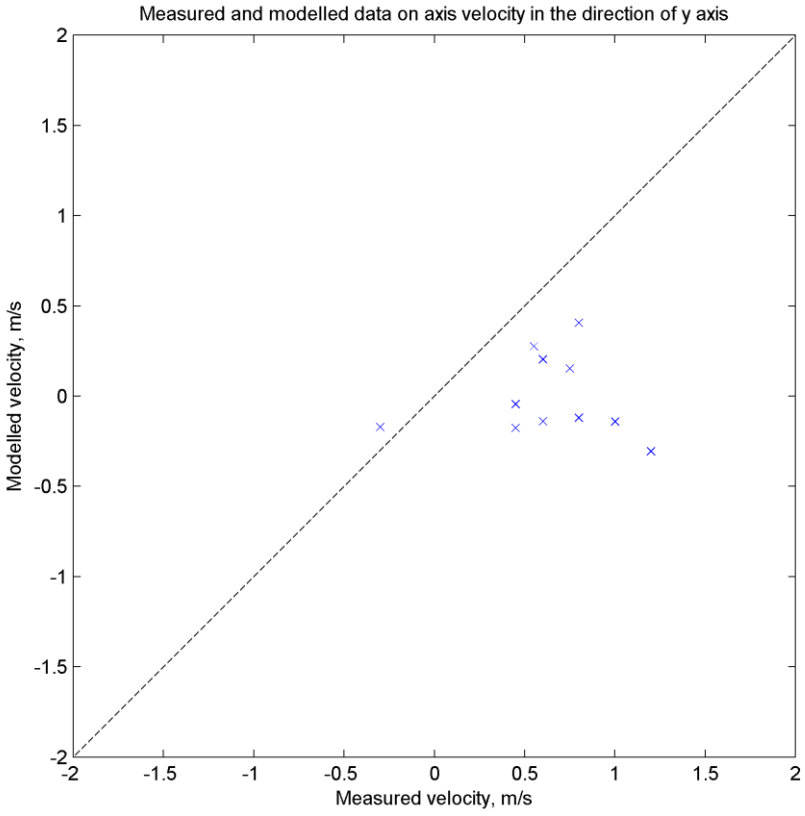
Measured and modelled data on axis velocity in the direction of y axis
Modelled velocity, m/s
Measured velocity, m/s
2
1.5
1
0.5
0
-0.5
-1
-1.5
-2
-2
-1.5
-1
-0.5
0
0.5
1
1.5
2

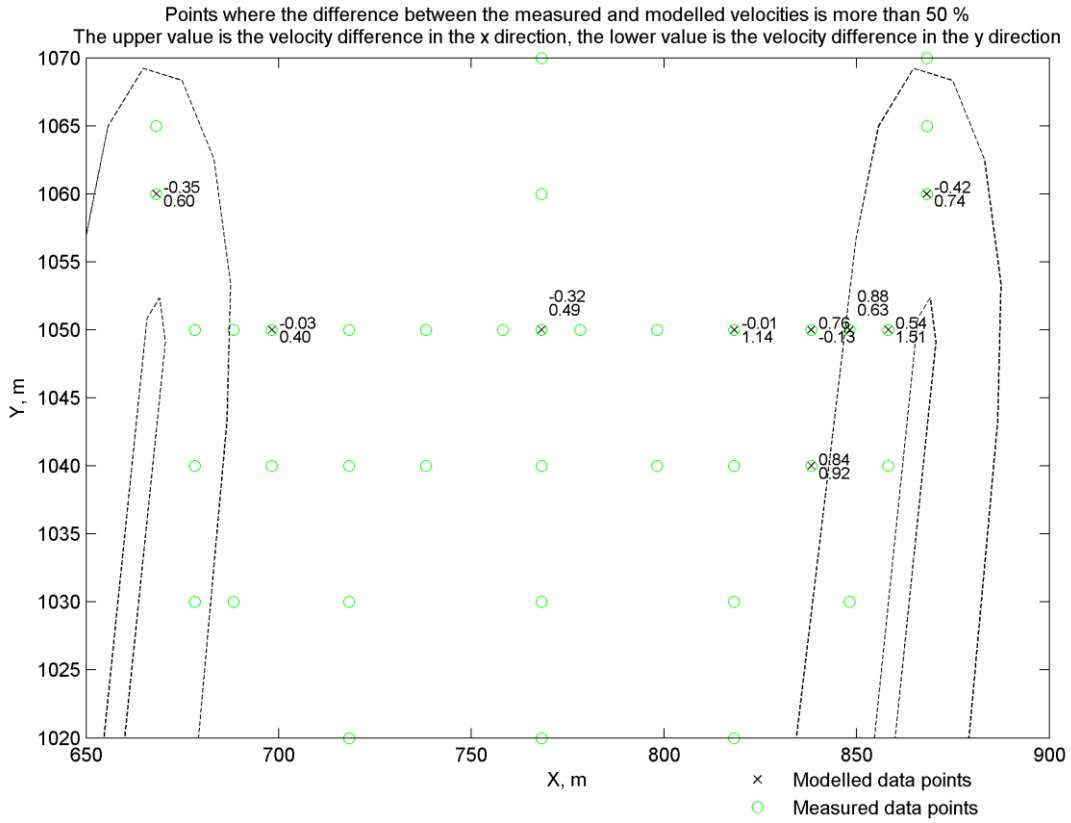
Points where the difference between the measured and modelled velocities is more than 50 %
The upper value is the velocity difference in the x direction, the lower value is the velocity difference in the y direction
Y, m
X, m
1070
1065
1060
1055
1050
1045
1040
1035
1030
1025
1020
650
700
750
800
850
900
-0.35
0.60
-0.03
0.40
-0.32
0.49
-0.01
1.14
0.76
-0.13
0.88
0.63
0.54
1.51
-0.42
0.74
0.84
0.92
Modelled data points
Measured data points

Validation process

3x2 set-up

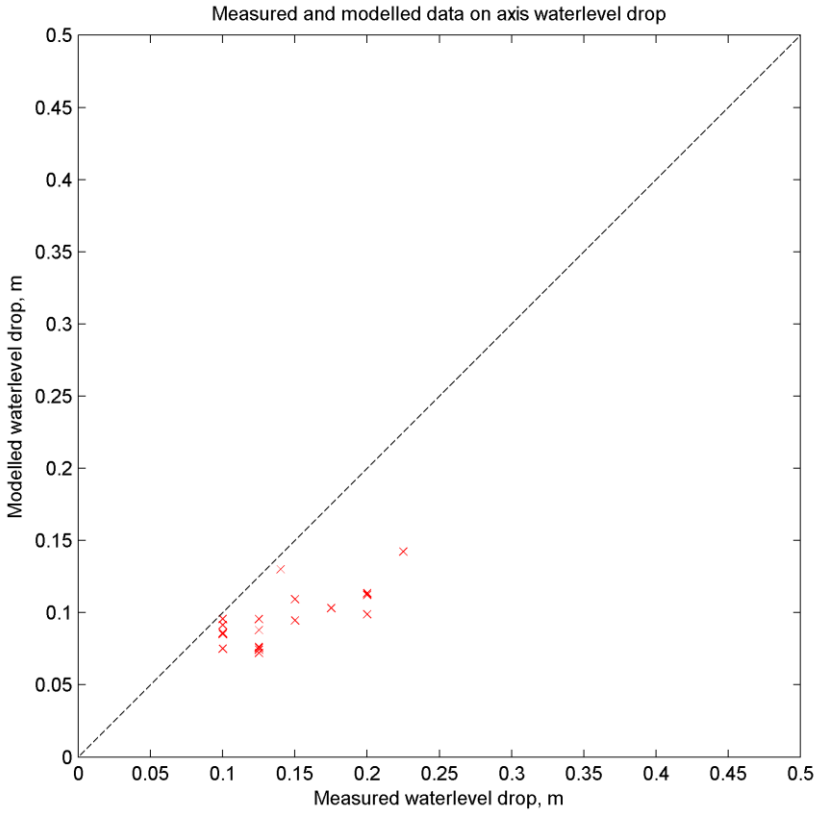

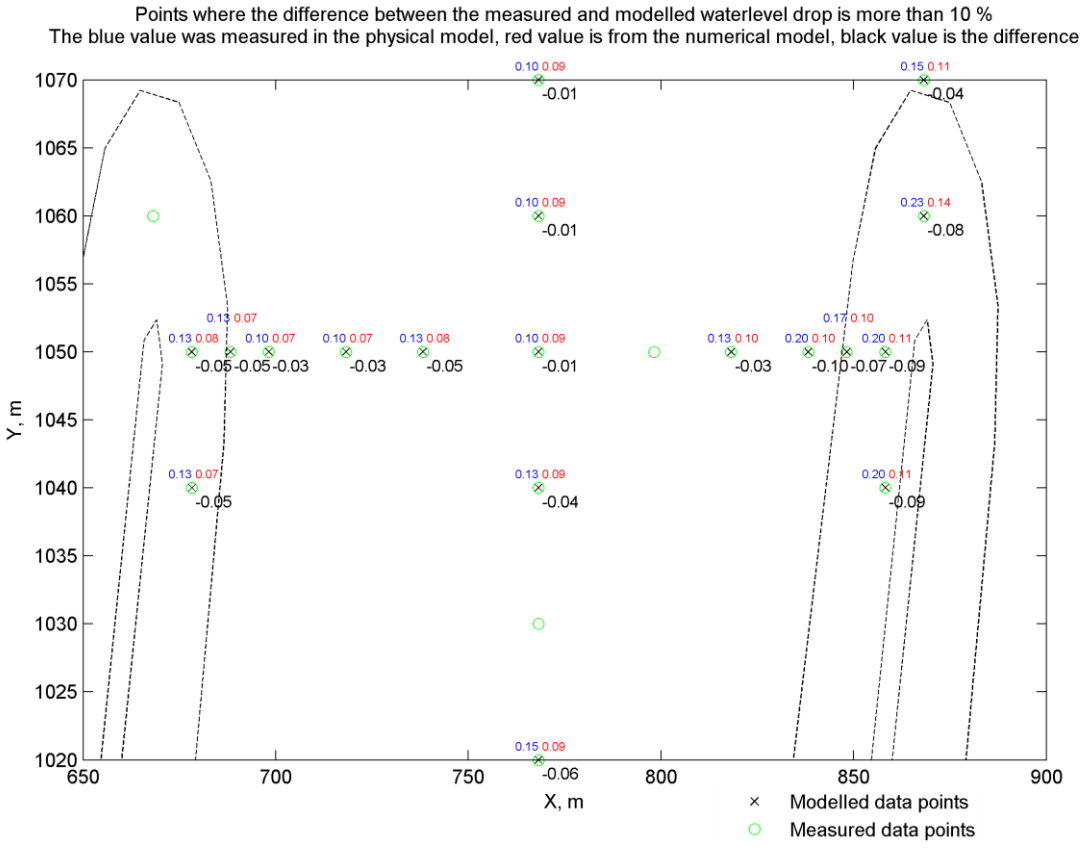

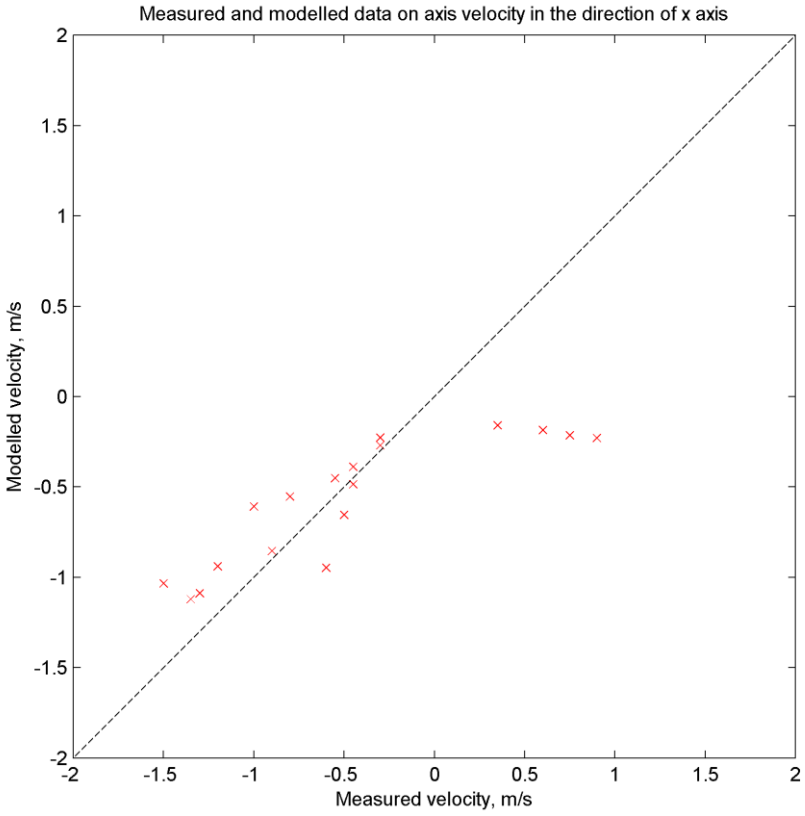
Measured and modelled data on axis velocity in the direction of x axis
Modelled velocity, m/s
Measured velocity, m/s
2
1.5
1
0.5
0
-0.5
-1
-1.5
-2

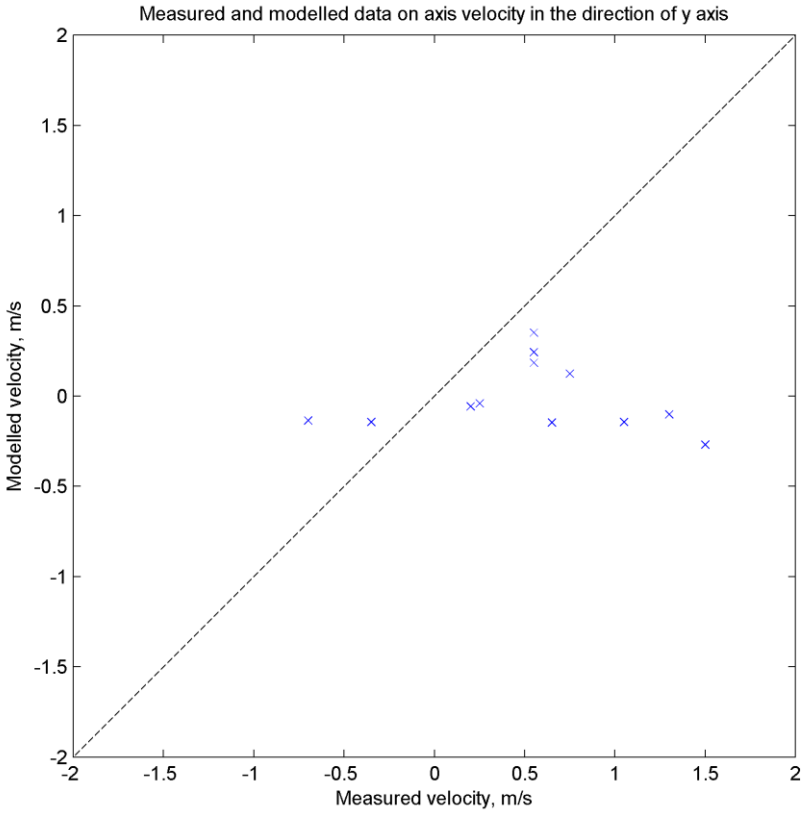
Measured and modelled data on axis velocity in the direction of y axis
Modelled velocity, m/s
Measured velocity, m/s
2
1.5
1
0.5
0
-0.5
-1
-1.5
-2

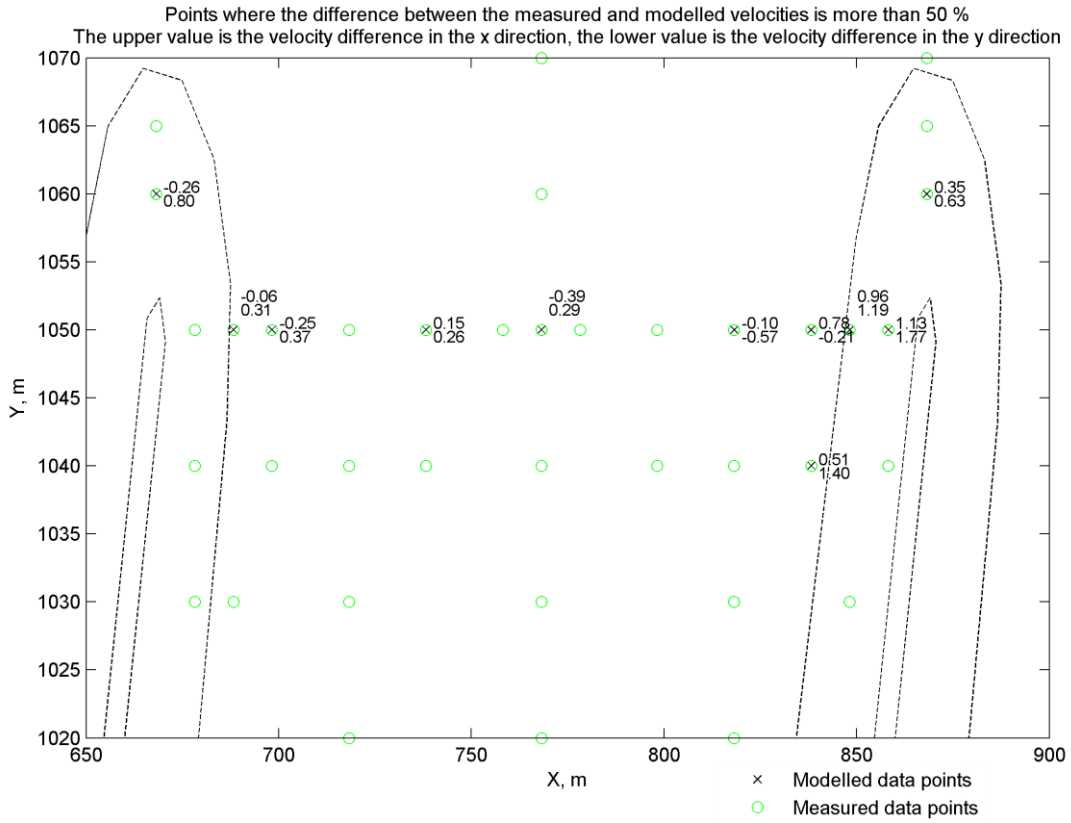
Points where the difference between the measured and modelled velocities is more than 50 %
The upper value is the velocity difference in the x direction, the lower value is the velocity difference in the y direction
Y, m
X, m
Modelled data points
Measured data points
-0.26
0.80
-0.06
0.31
-0.25
0.37
0.15
0.26
-0.39
0.29
-0.10
-0.57
0.78
-0.21
0.96
1.19
1.13
1.77
0.35
0.63
0.51
1.40

Appendix C: FINEL2D simulation results

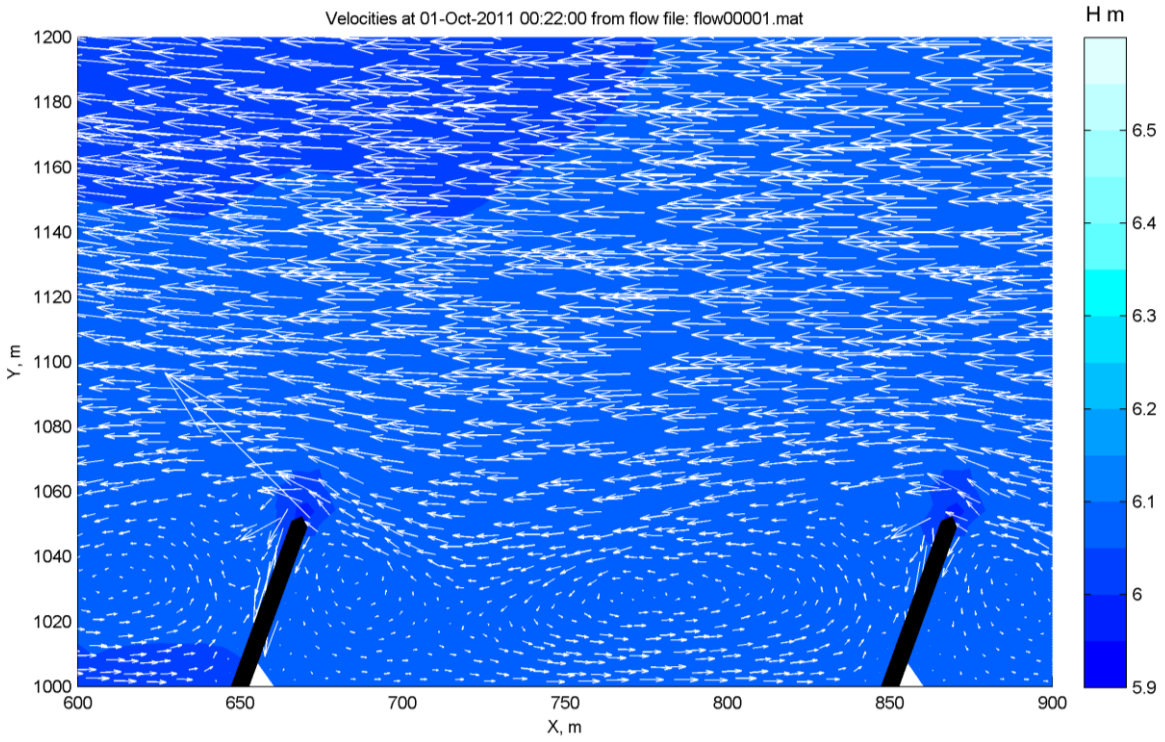

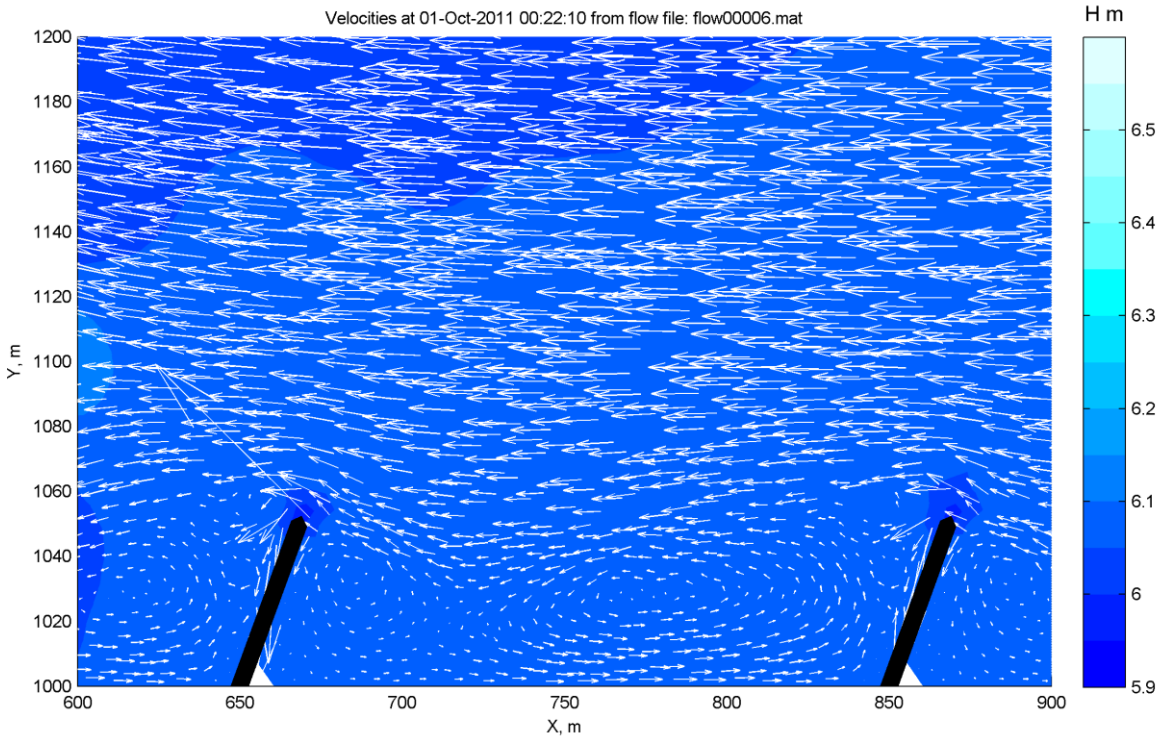

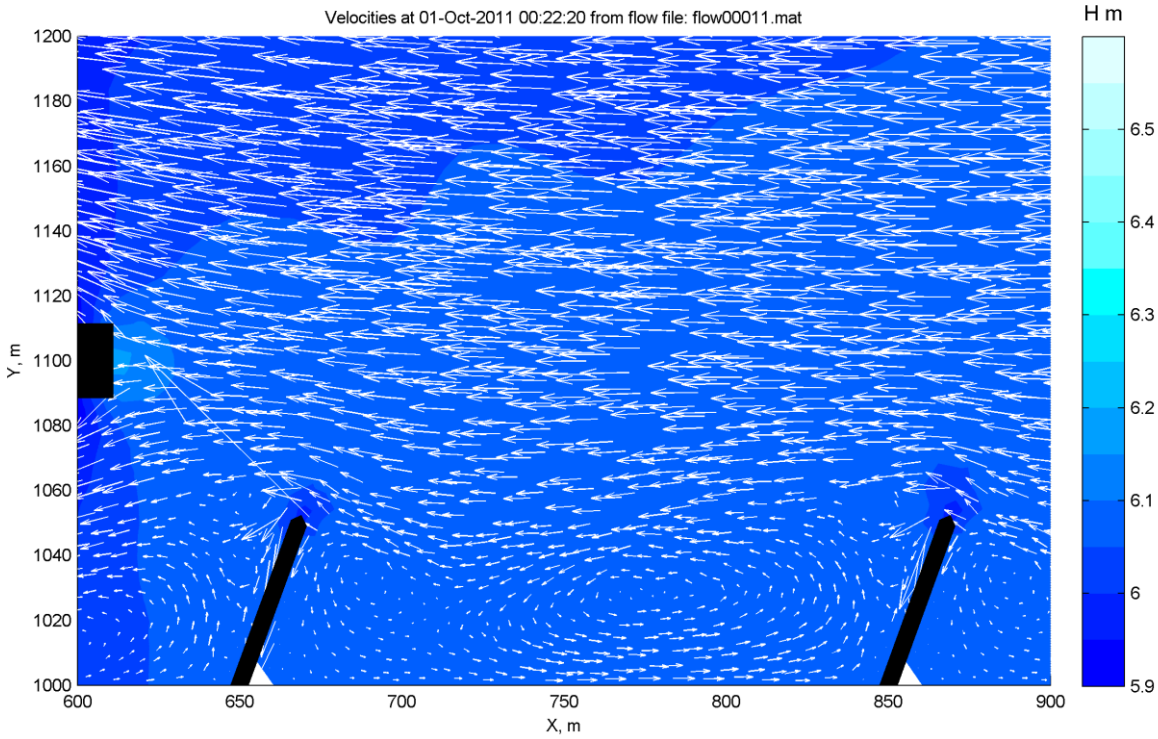
Velocities at 01-Oct-2011 00:22:20 from flow file: flow00011.mat
H m
6.5
6.4
6.3
6.2
6.1
6
5.9
Y, m
1200
1180
1160
1140
1120
1100
1080
1060
1040
1020
1000
600
650
700
750
800
850
900
X, m

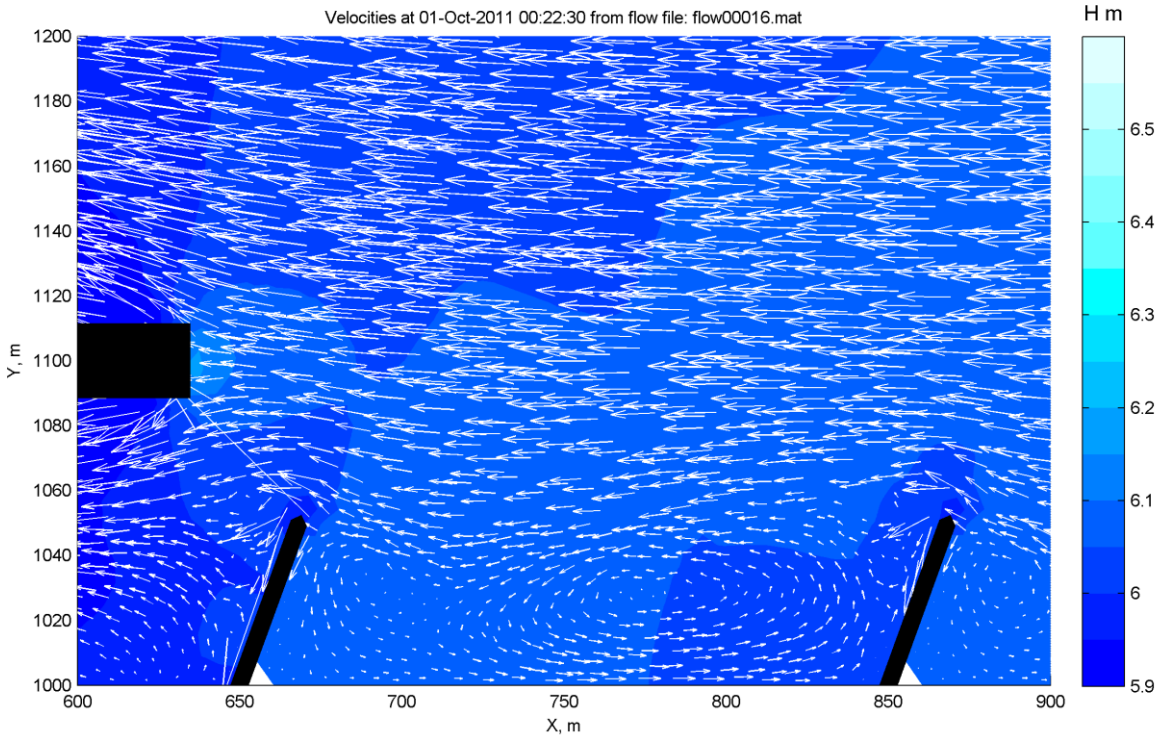
Velocities at 01-Oct-2011 00:22:30 from flow file: flow00016.mat
H m
6.5
6.4
6.3
6.2
6.1
6
5.9
Y, m
1200
1180
1160
1140
1120
1100
1080
1060
1040
1020
1000
600
650
700
750
800
850
900
X, m

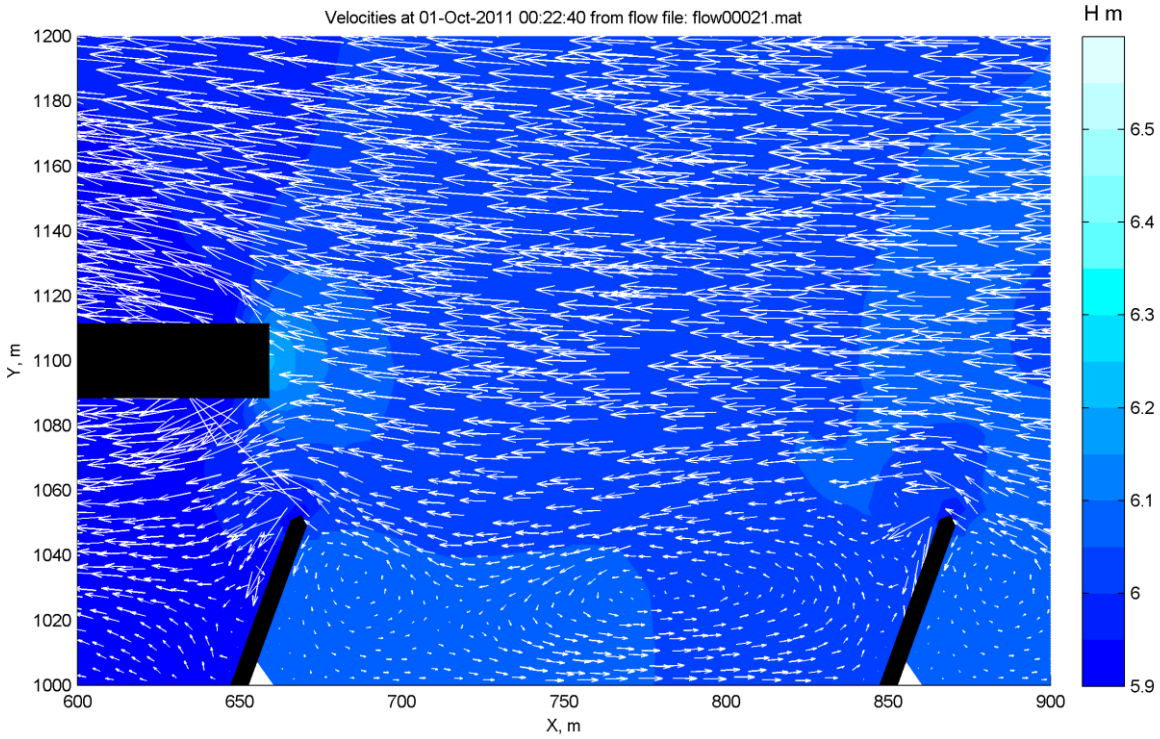
Velocities at 01-Oct-2011 00:22:40 from flow file: flow00021.mat
H m
Y, m
X, m
1200
1180
1160
1140
1120
1100
1080
1060
1040
1020
1000
600
650
700
750
800
850
900
6.5
6.4
6.3
6.2
6.1
6
5.9

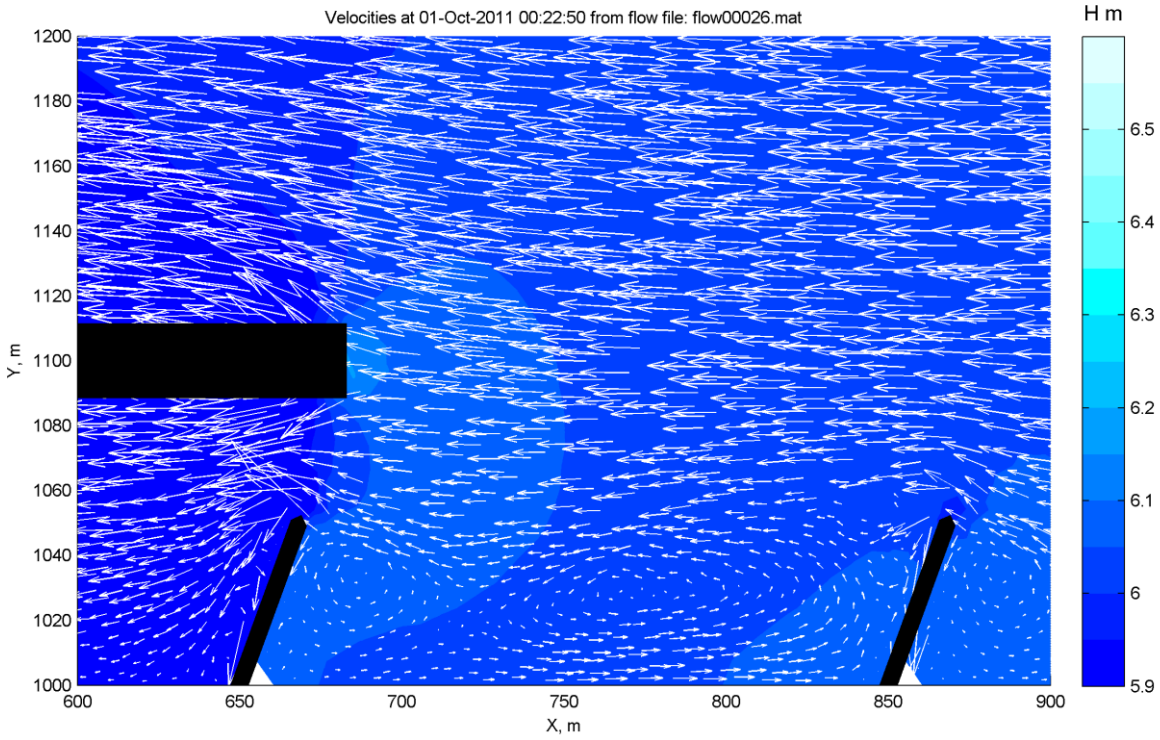
Velocities at 01-Oct-2011 00:22:50 from flow file: flow00026.mat
H m
Y, m
X, m
1200
1180
1160
1140
1120
1100
1080
1060
1040
1020
1000
600
650
700
750
800
850
900
6.5
6.4
6.3
6.2
6.1
6
5.9

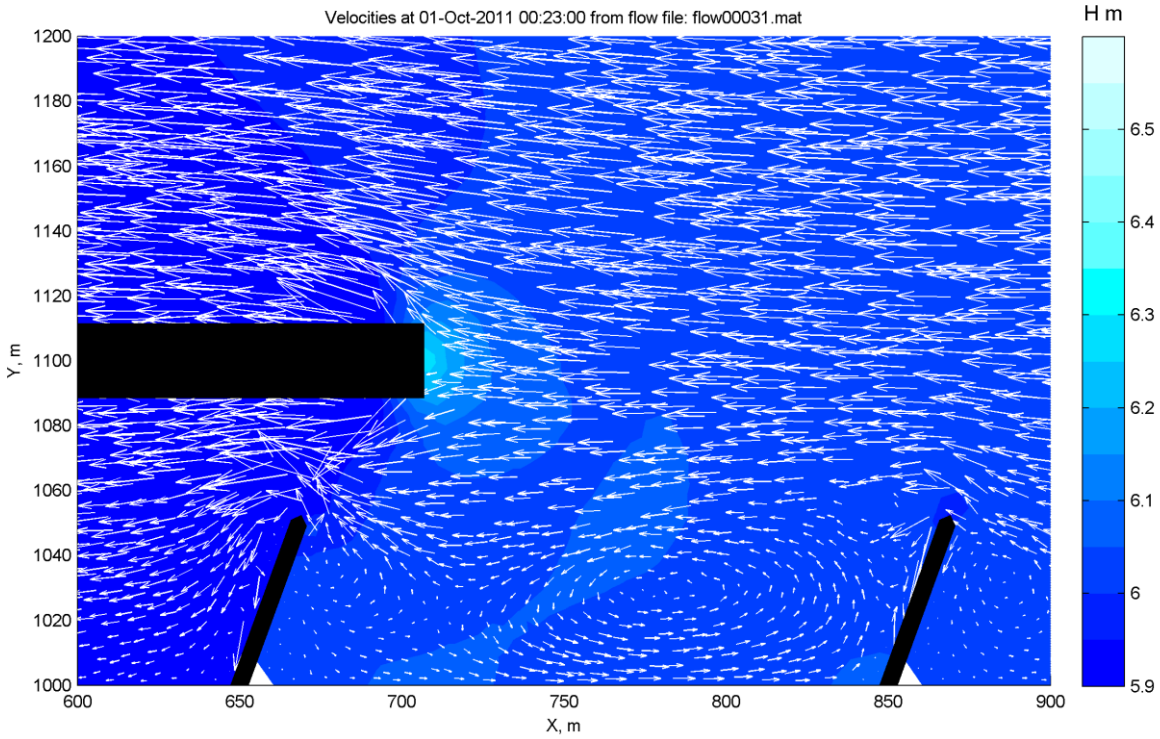
Velocities at 01-Oct-2011 00:23:00 from flow file: flow00031.mat
H m
Y, m
X, m
1200
1180
1160
1140
1120
1100
1080
1060
1040
1020
1000
600
650
700
750
800
850
900
6.5
6.4
6.3
6.2
6.1
6
5.9

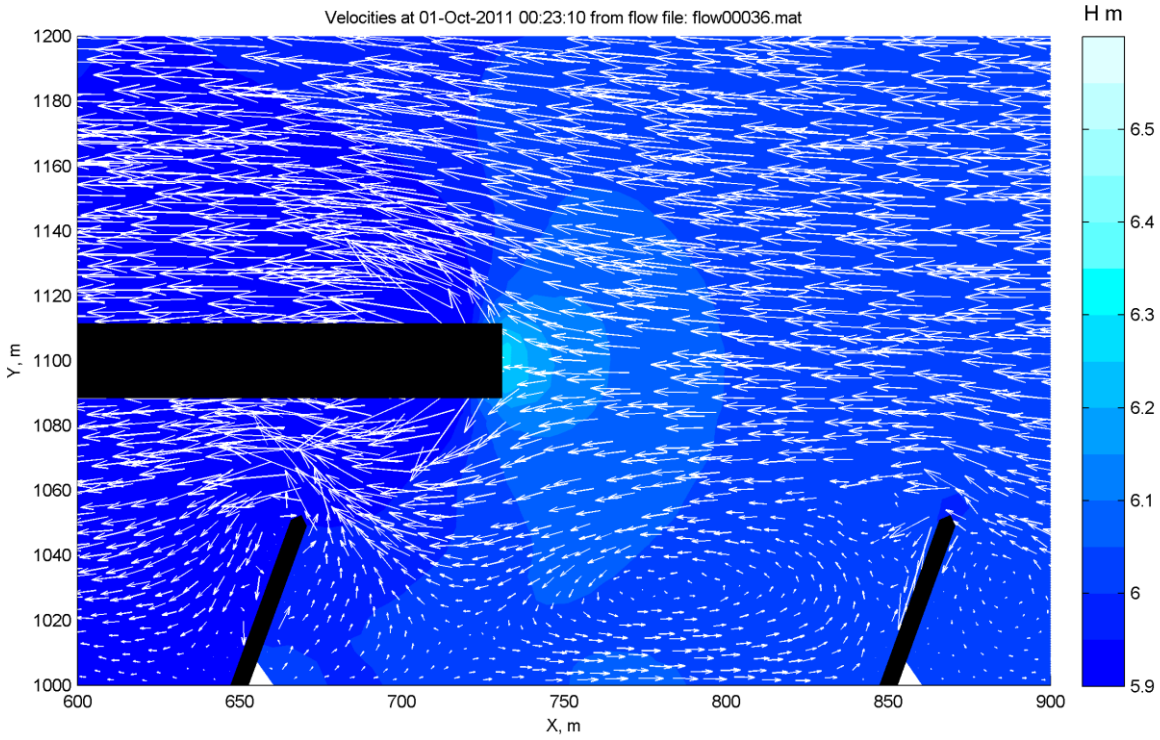
Velocities at 01-Oct-2011 00:23:10 from flow file: flow00036.mat
H m
Y, m
X, m
1200
1180
1160
1140
1120
1100
1080
1060
1040
1020
1000
600
650
700
750
800
850
900
6.5
6.4
6.3
6.2
6.1
6
5.9

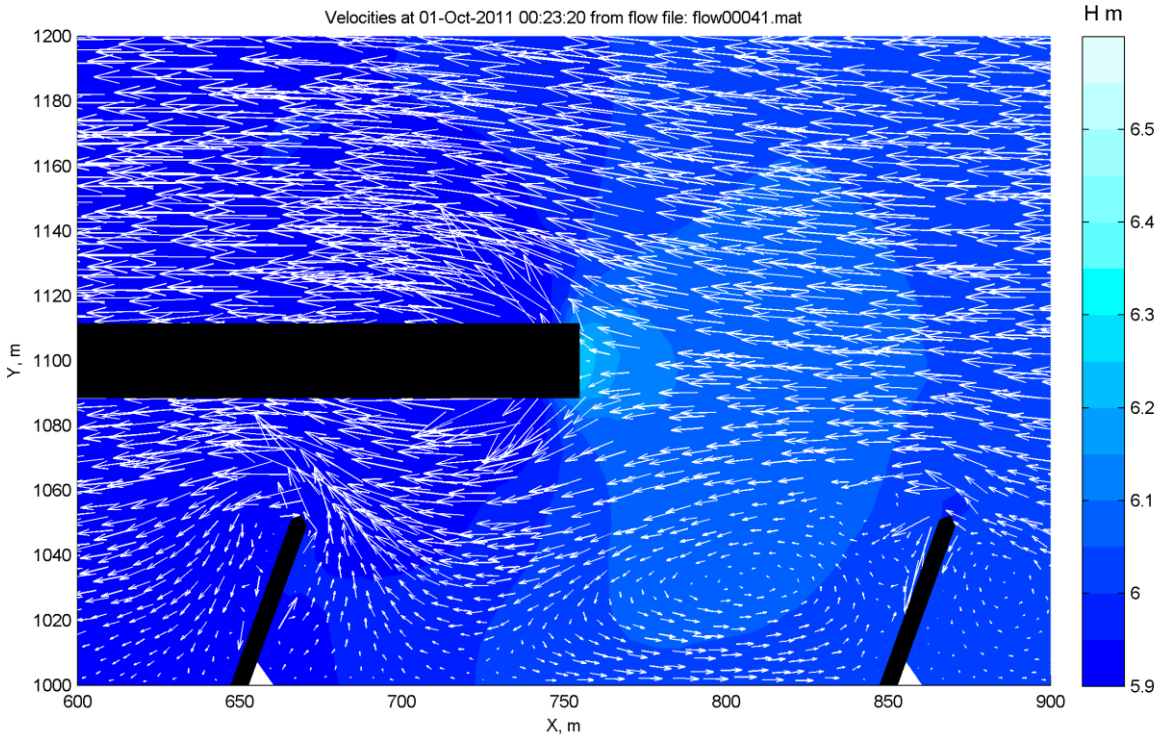
Velocities at 01-Oct-2011 00:23:20 from flow file: flow00041.mat
H m
6.5
6.4
6.3
6.2
6.1
6
5.9
Y, m
1200
1180
1160
1140
1120
1100
1080
1060
1040
1020
1000
600
650
700
750
800
850
900
X, m

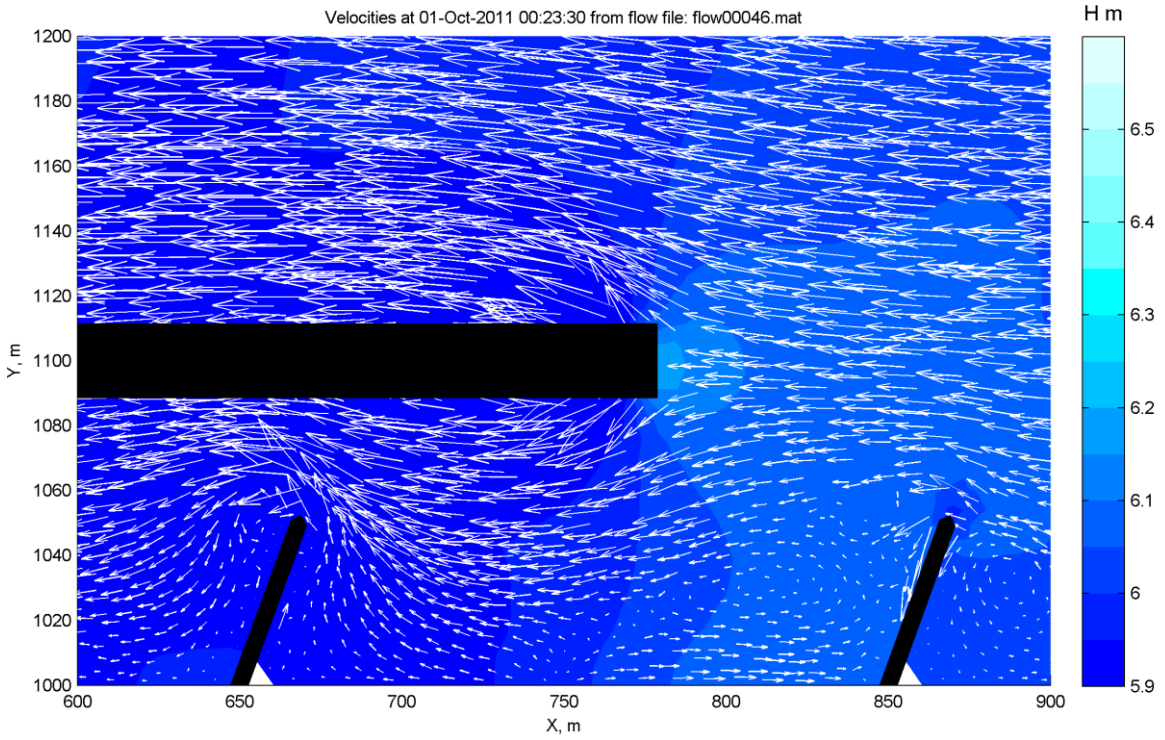
Velocities at 01-Oct-2011 00:23:30 from flow file: flow00046.mat
H m
6.5
6.4
6.3
6.2
6.1
6
5.9
Y, m
1200
1180
1160
1140
1120
1100
1080
1060
1040
1020
1000
600
650
700
750
800
850
900
X, m

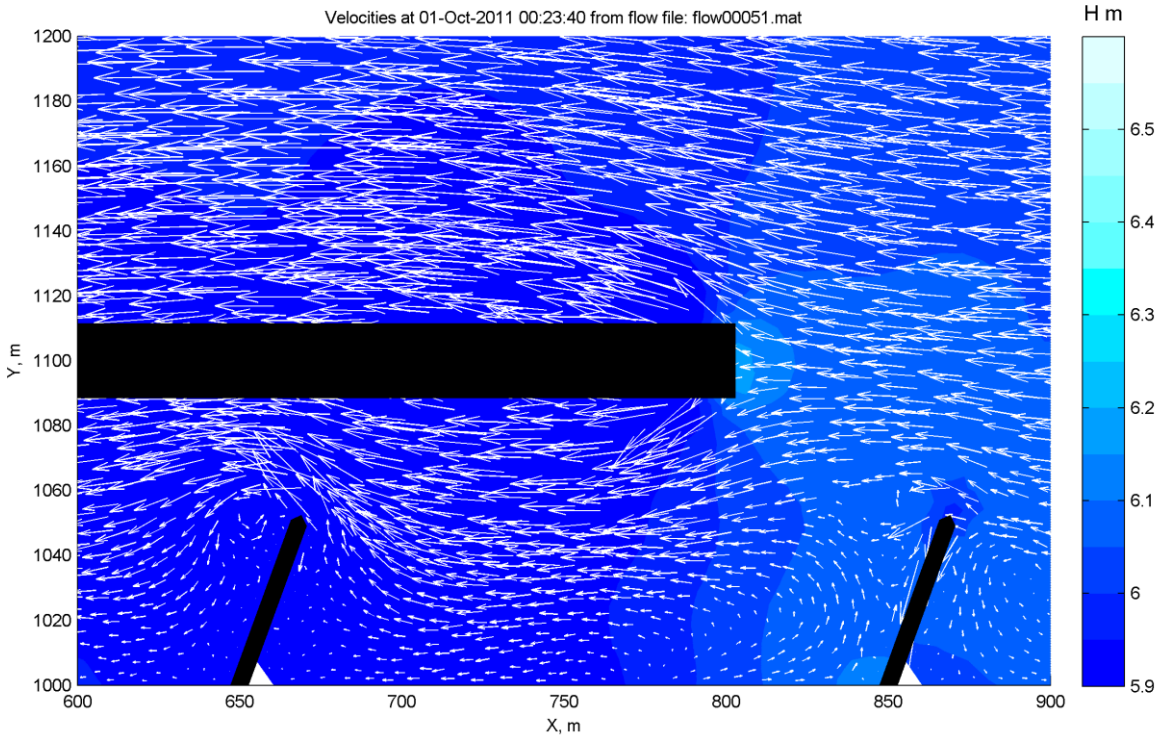
Velocities at 01-Oct-2011 00:23:40 from flow file: flow00051.mat
H m
6.5
6.4
6.3
6.2
6.1
6
5.9
Y, m
1200
1180
1160
1140
1120
1100
1080
1060
1040
1020
1000
600
650
700
750
800
850
900
X, m

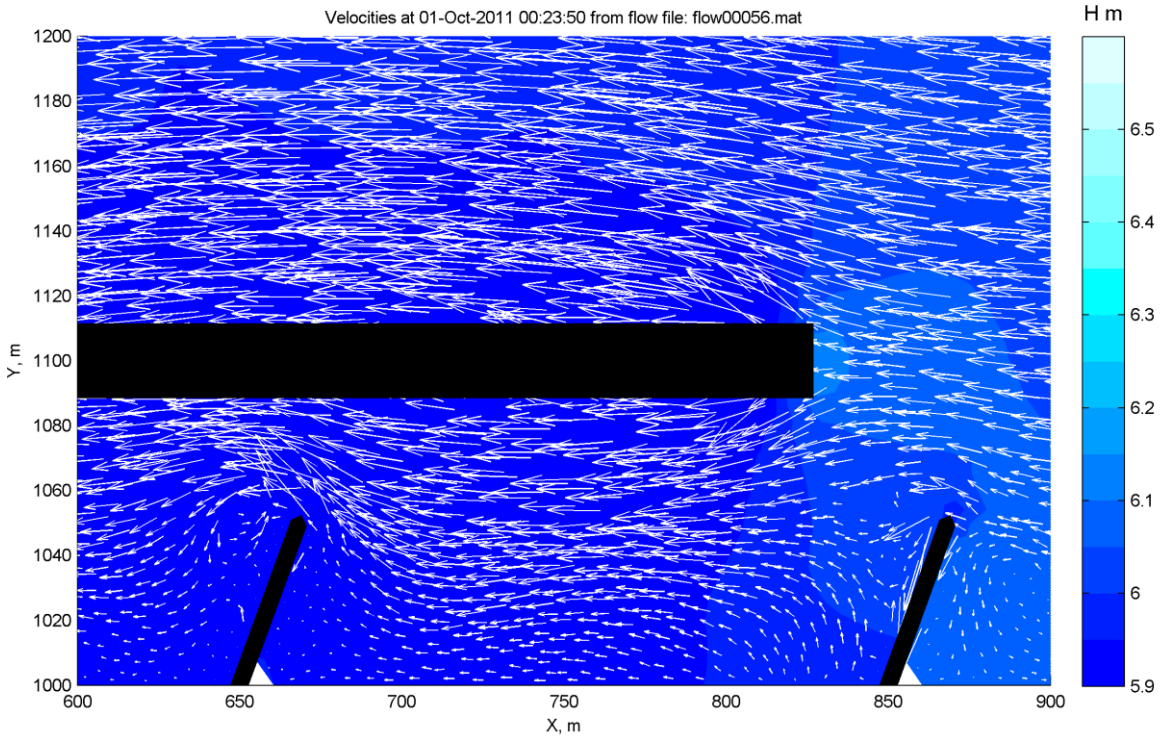
Velocities at 01-Oct-2011 00:23:50 from flow file: flow00056.mat
H m
6.5
6.4
6.3
6.2
6.1
6
5.9
Y, m
1200
1180
1160
1140
1120
1100
1080
1060
1040
1020
1000
600
650
700
750
800
850
900
X, m

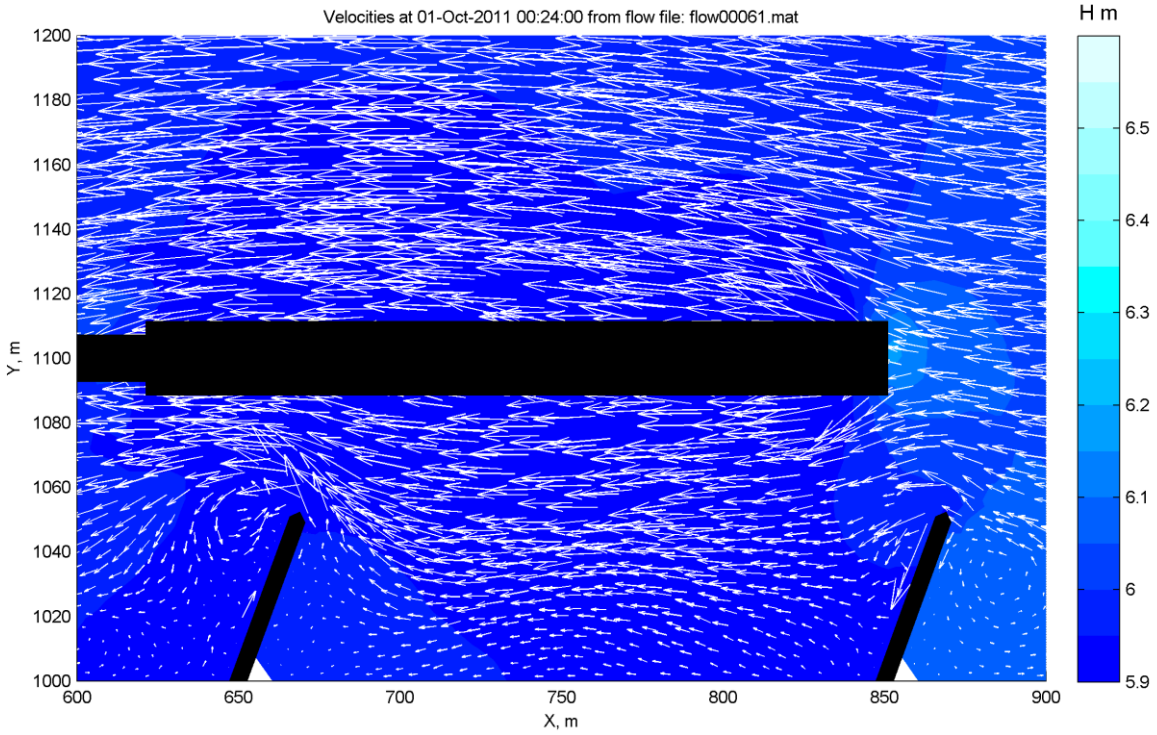
Velocities at 01-Oct-2011 00:24:00 from flow file: flow00061.mat
H m
Y, m
X, m
1200
1180
1160
1140
1120
1100
1080
1060
1040
1020
1000
600
650
700
750
800
850
900
6.5
6.4
6.3
6.2
6.1
6
5.9

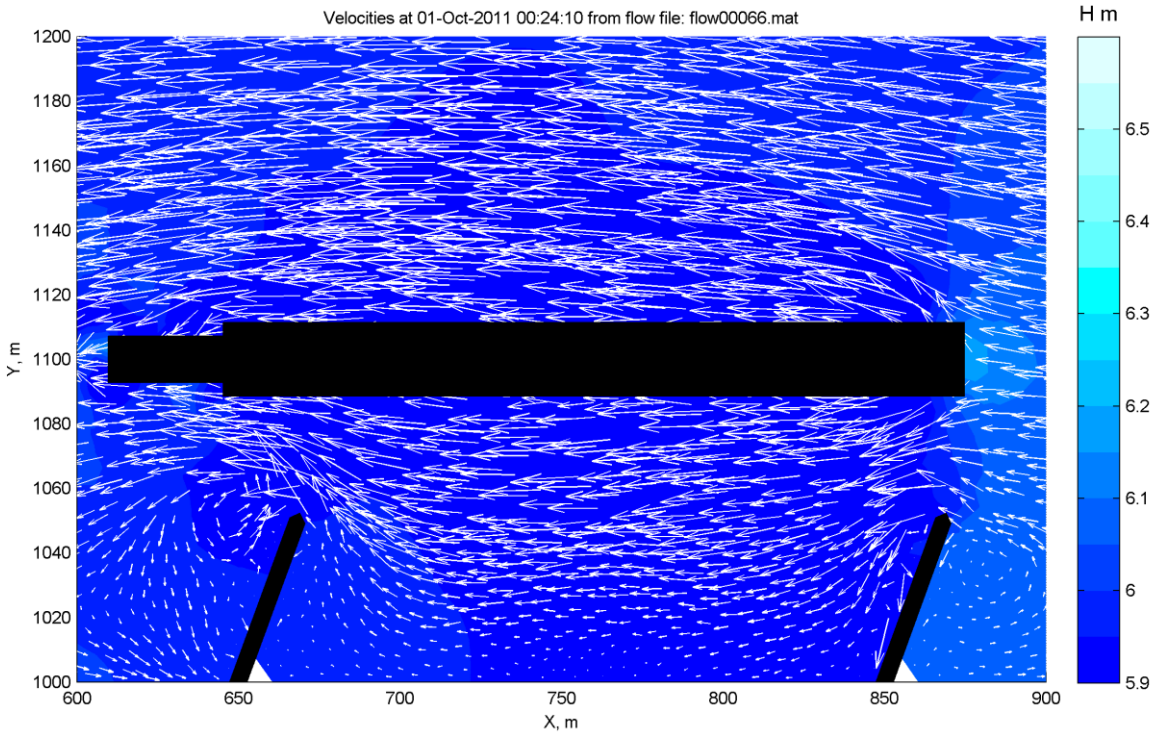
Velocities at 01-Oct-2011 00:24:10 from flow file: flow00066.mat
H m
Y, m
X, m
1200
1180
1160
1140
1120
1100
1080
1060
1040
1020
1000
600
650
700
750
800
850
900
6.5
6.4
6.3
6.2
6.1
6
5.9

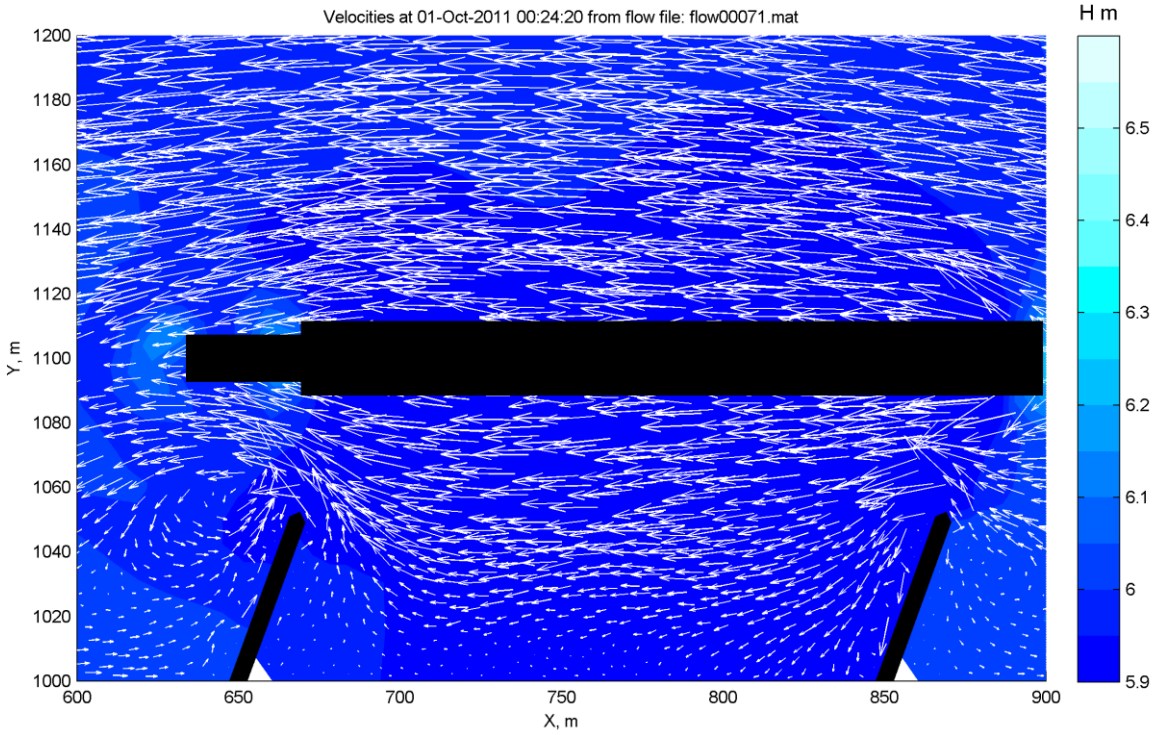
Velocities at 01-Oct-2011 00:24:20 from flow file: flow00071.mat
H m
6.5
6.4
6.3
6.2
6.1
6
5.9
Y, m
1200
1180
1160
1140
1120
1100
1080
1060
1040
1020
1000
600
650
700
750
800
850
900
X, m

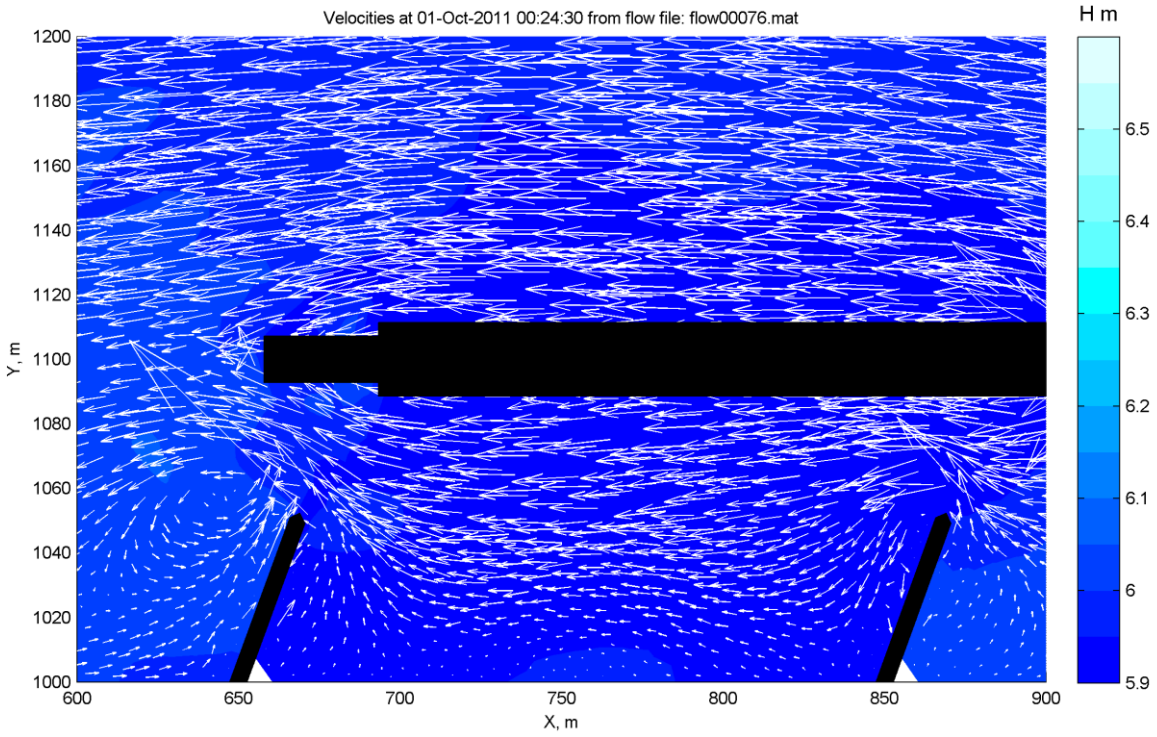
Velocities at 01-Oct-2011 00:24:30 from flow file: flow00076.mat
H m
6.5
6.4
6.3
6.2
6.1
6
5.9
Y, m
1200
1180
1160
1140
1120
1100
1080
1060
1040
1020
1000
600
650
700
750
800
850
900
X, m

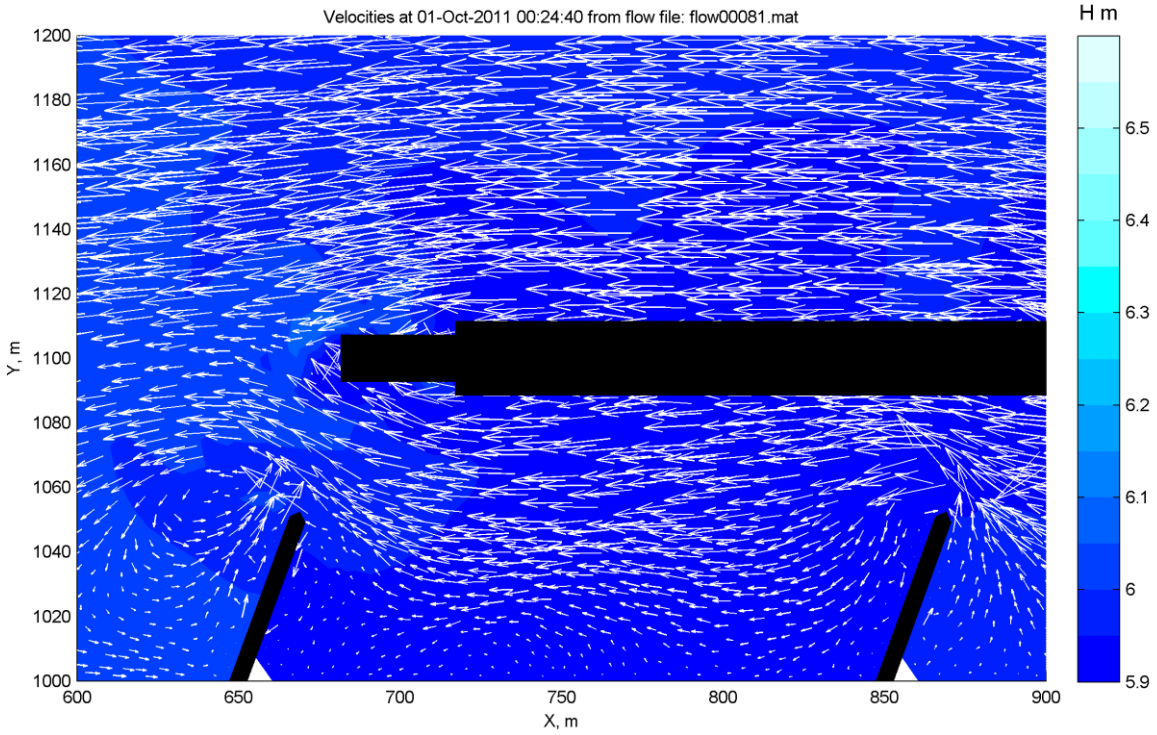
Velocities at 01-Oct-2011 00:24:40 from flow file: flow00081.mat
H m
6.5
6.4
6.3
6.2
6.1
6
5.9
Y, m
1200
1180
1160
1140
1120
1100
1080
1060
1040
1020
1000
600
650
700
750
800
850
900
X, m

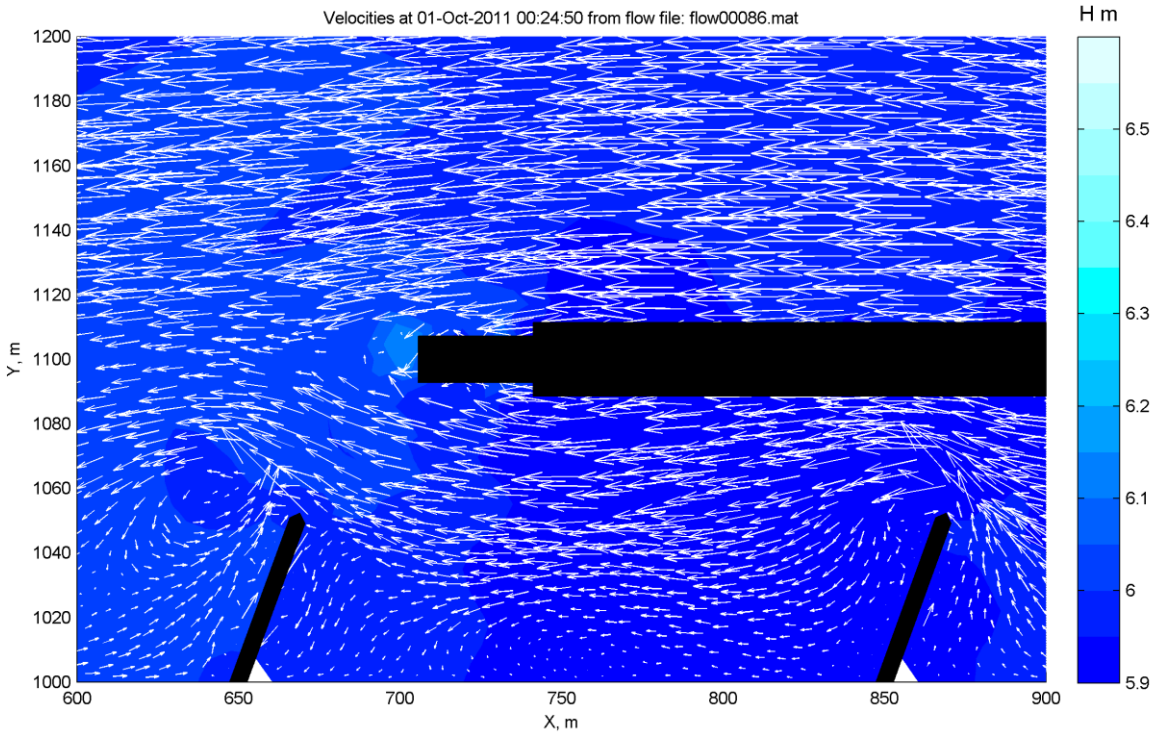
Velocities at 01-Oct-2011 00:24:50 from flow file: flow00086.mat
H m
6.5
6.4
6.3
6.2
6.1
6
5.9
Y, m
1200
1180
1160
1140
1120
1100
1080
1060
1040
1020
1000
600
650
700
750
800
850
900
X, m

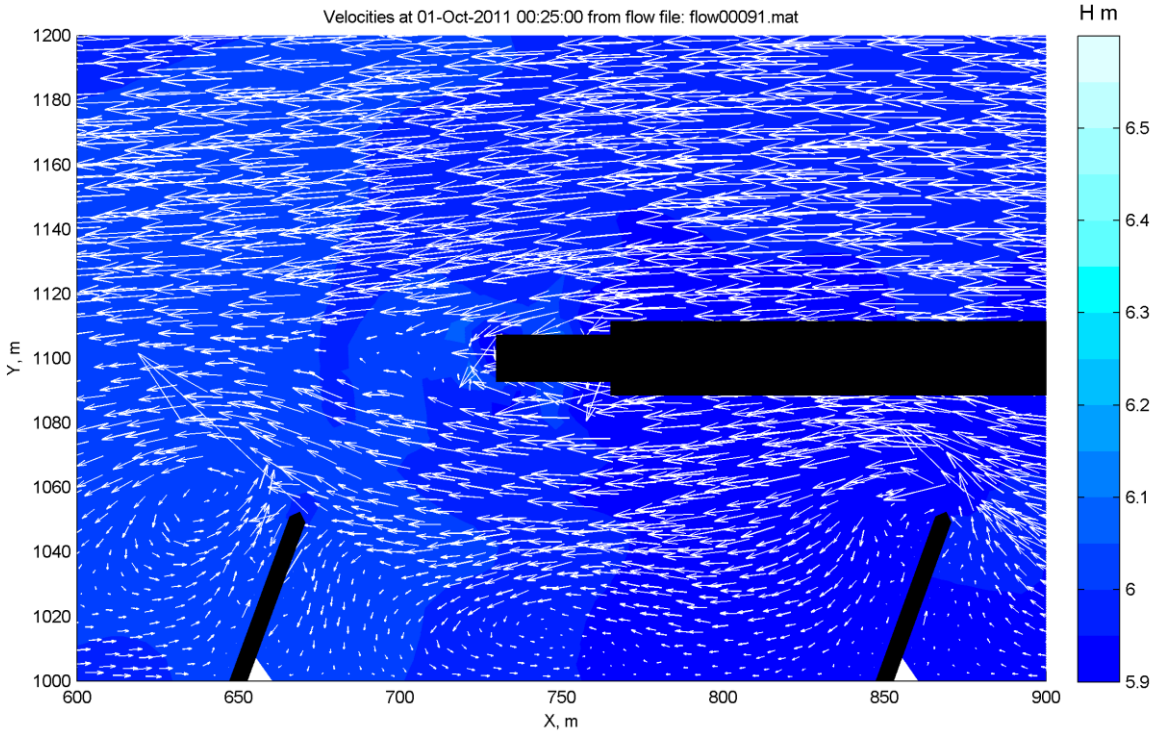
Velocities at 01-Oct-2011 00:25:00 from flow file: flow00091.mat
H m
6.5
6.4
6.3
6.2
6.1
6
5.9
Y, m
1200
1180
1160
1140
1120
1100
1080
1060
1040
1020
1000
600
650
700
750
800
850
900
X, m

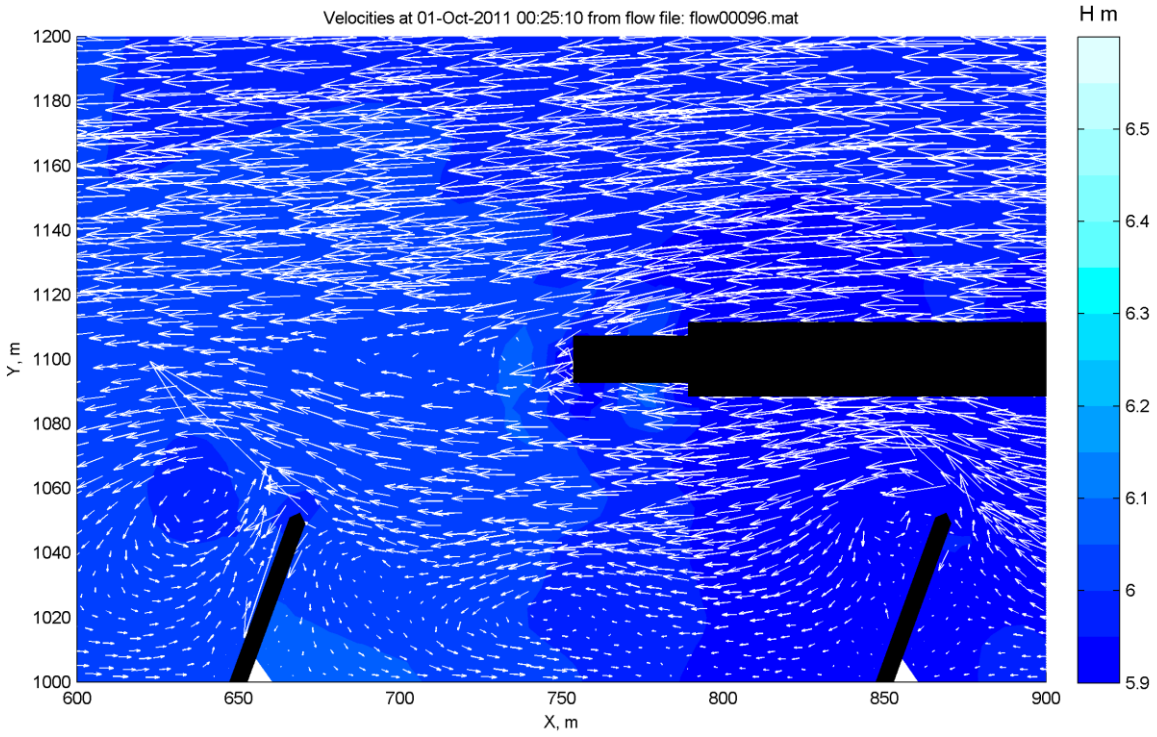
Velocities at 01-Oct-2011 00:25:10 from flow file: flow00096.mat
H m
6.5
6.4
6.3
6.2
6.1
6
5.9
Y, m
1200
1180
1160
1140
1120
1100
1080
1060
1040
1020
1000
600
650
700
750
800
850
900
X, m

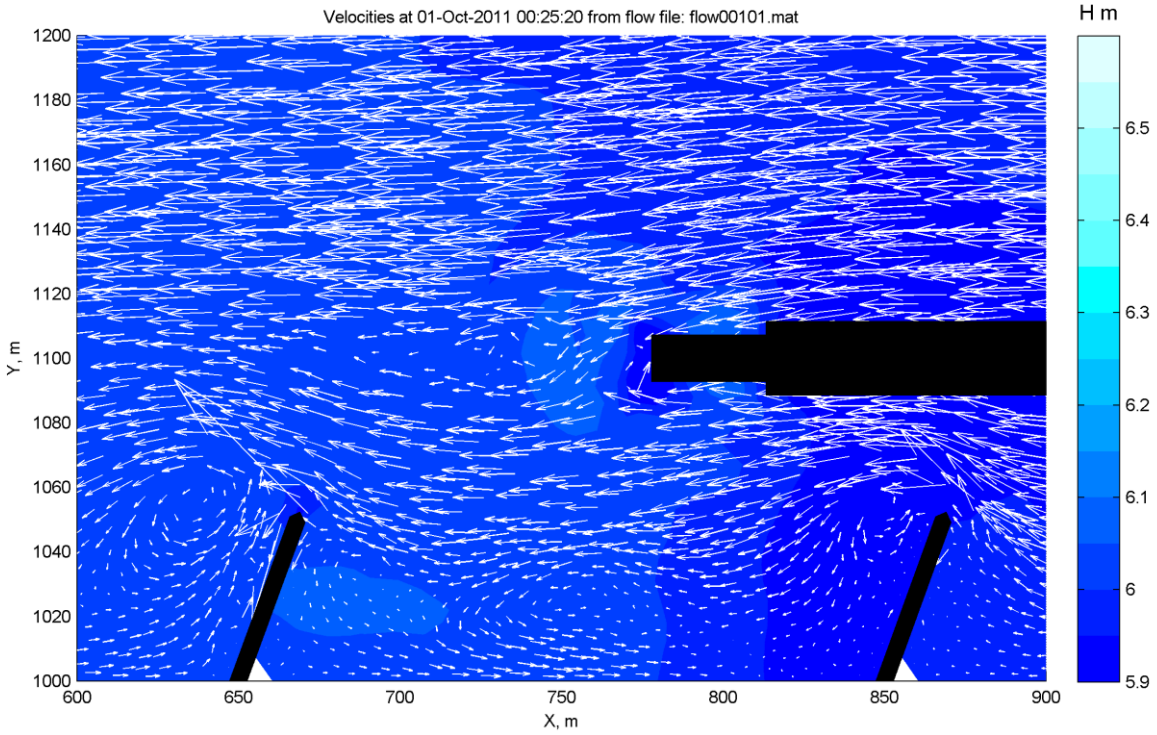
Velocities at 01-Oct-2011 00:25:20 from flow file: flow00101.mat
H m
6.5
6.4
6.3
6.2
6.1
6
5.9
Y, m
1200
1180
1160
1140
1120
1100
1080
1060
1040
1020
1000
600
650
700
750
800
850
900
X, m

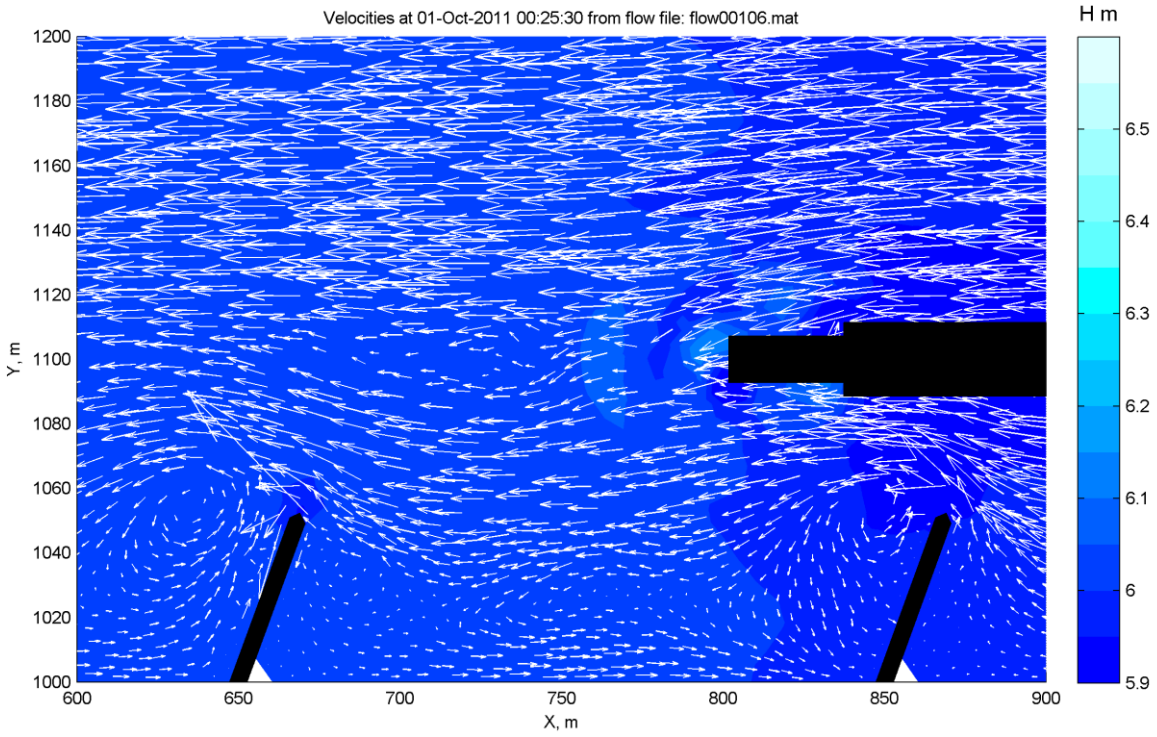
Velocities at 01-Oct-2011 00:25:30 from flow file: flow00106.mat
H m
6.5
6.4
6.3
6.2
6.1
6
5.9
Y, m
1200
1180
1160
1140
1120
1100
1080
1060
1040
1020
1000
600
650
700
750
800
850
900
X, m

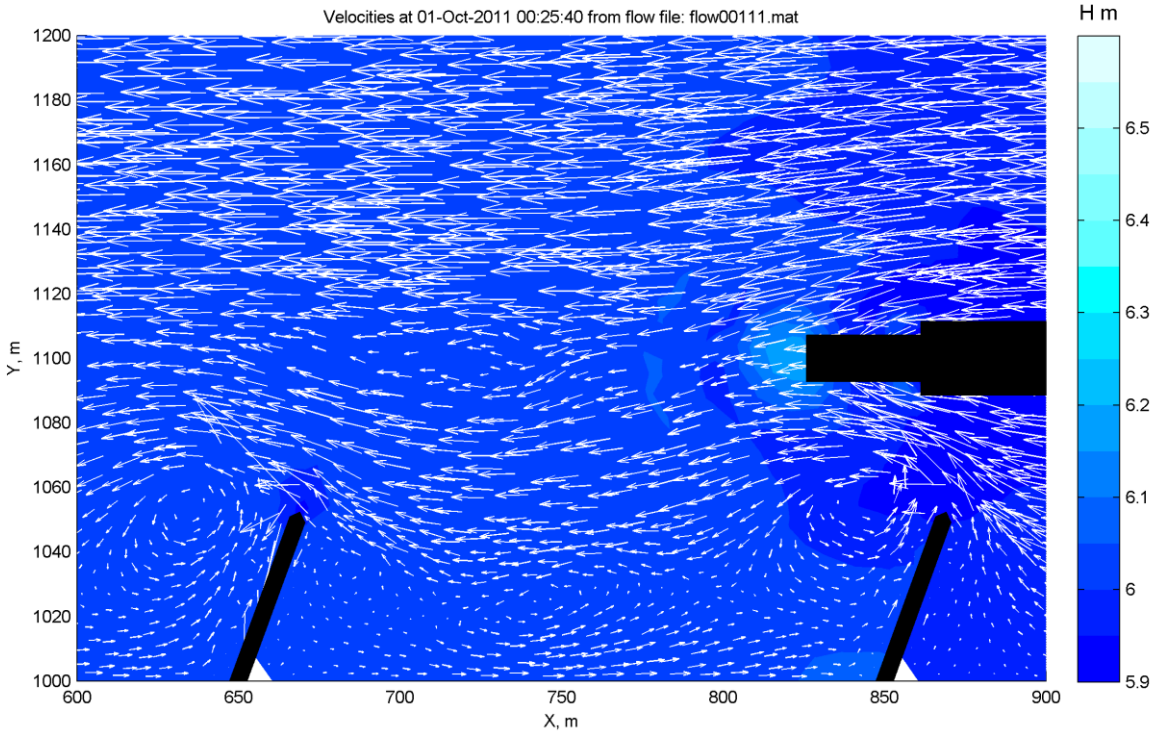
Velocities at 01-Oct-2011 00:25:40 from flow file: flow00111.mat
H m
6.5
6.4
6.3
6.2
6.1
6
5.9
Y, m
1200
1180
1160
1140
1120
1100
1080
1060
1040
1020
1000
600
650
700
750
800
850
900
X, m

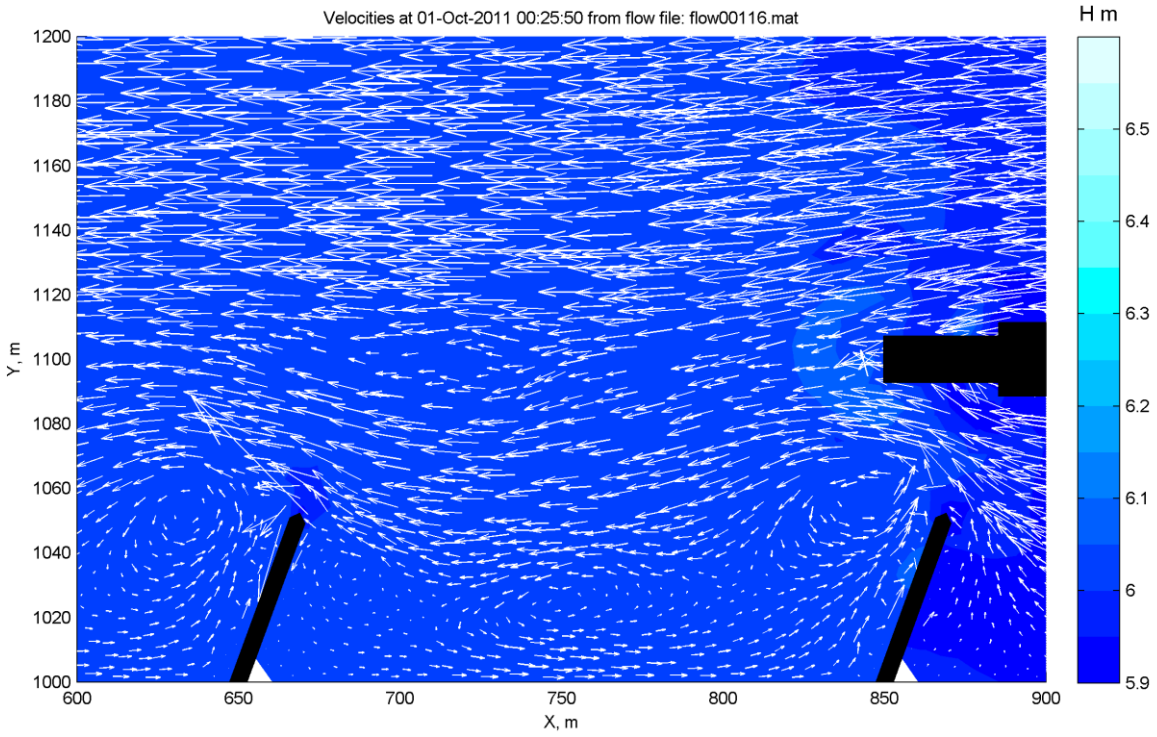
Velocities at 01-Oct-2011 00:25:50 from flow file: flow00116.mat
H m
6.5
6.4
6.3
6.2
6.1
6
5.9
Y, m
1200
1180
1160
1140
1120
1100
1080
1060
1040
1020
1000
600
650
700
750
800
850
900
X, m

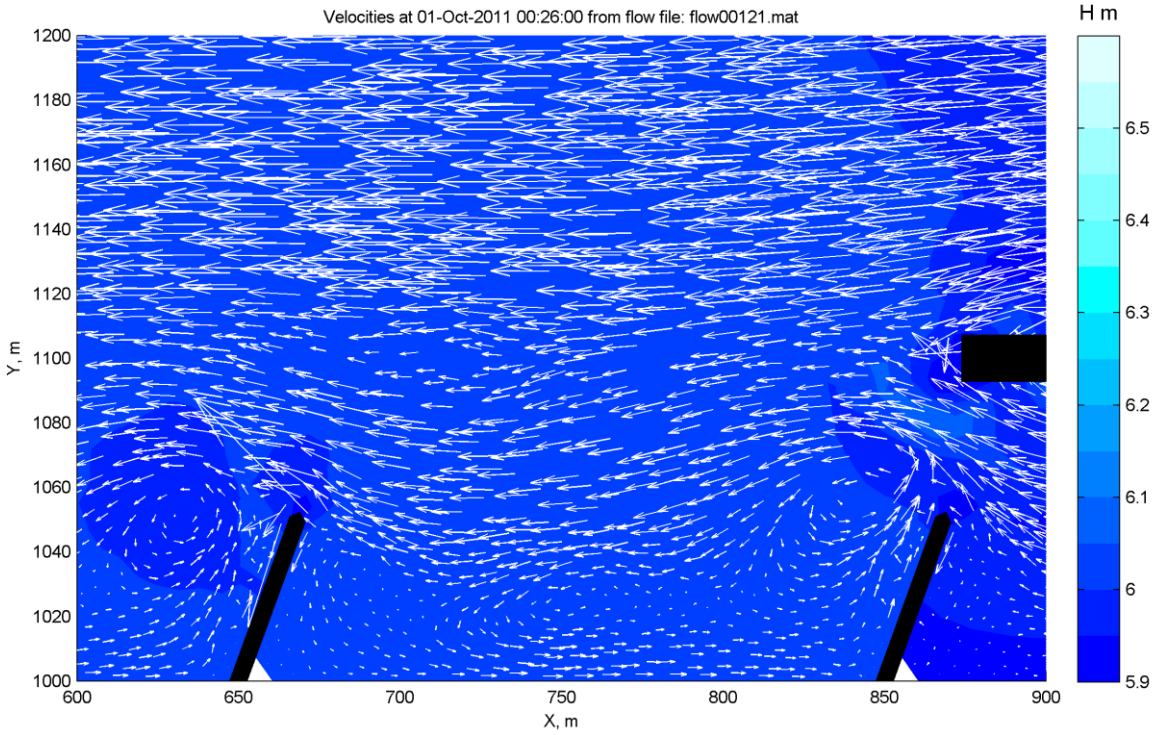
Velocities at 01-Oct-2011 00:26:00 from flow file: flow00121.mat
H m
Y, m
X, m
1200
1180
1160
1140
1120
1100
1080
1060
1040
1020
1000
600
650
700
750
800
850
900
6.5
6.4
6.3
6.2
6.1
6
5.9

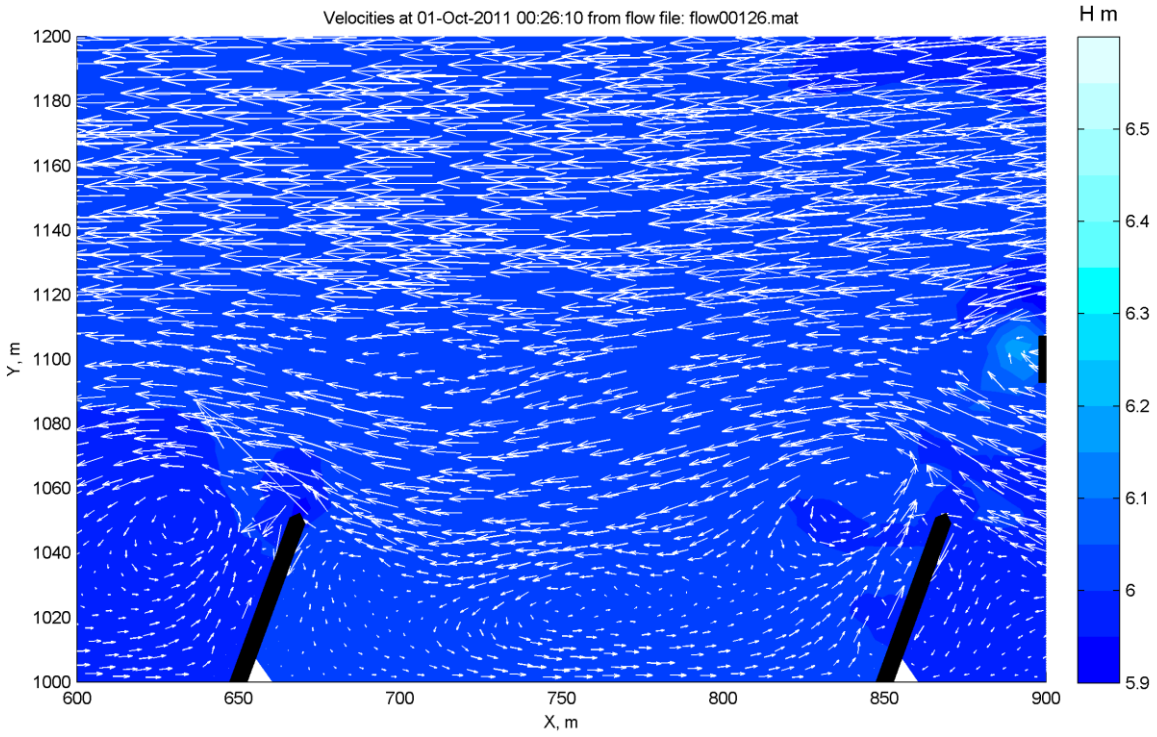
Velocities at 01-Oct-2011 00:26:10 from flow file: flow00126.mat
H m
Y, m
X, m
1200
1180
1160
1140
1120
1100
1080
1060
1040
1020
1000
600
650
700
750
800
850
900
6.5
6.4
6.3
6.2
6.1
6
5.9

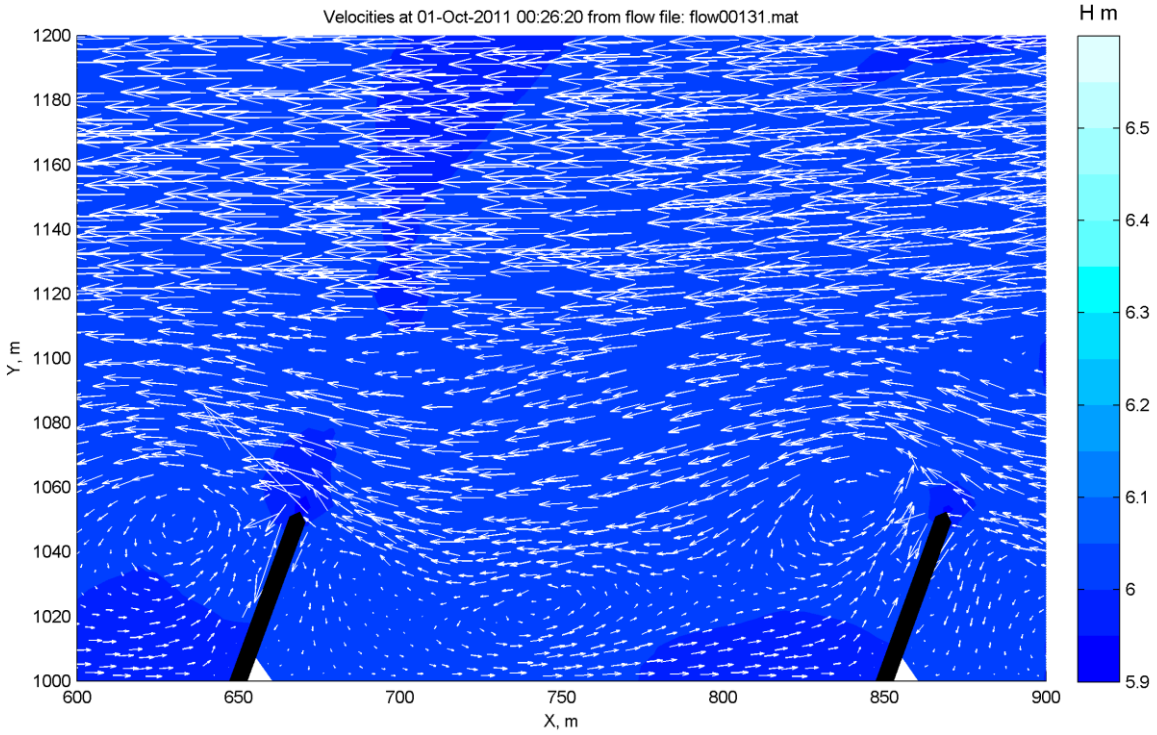
Velocities at 01-Oct-2011 00:26:20 from flow file: flow00131.mat
H m
Y, m
X, m
1200
1180
1160
1140
1120
1100
1080
1060
1040
1020
1000
600
650
700
750
800
850
900
6.5
6.4
6.3
6.2
6.1
6
5.9

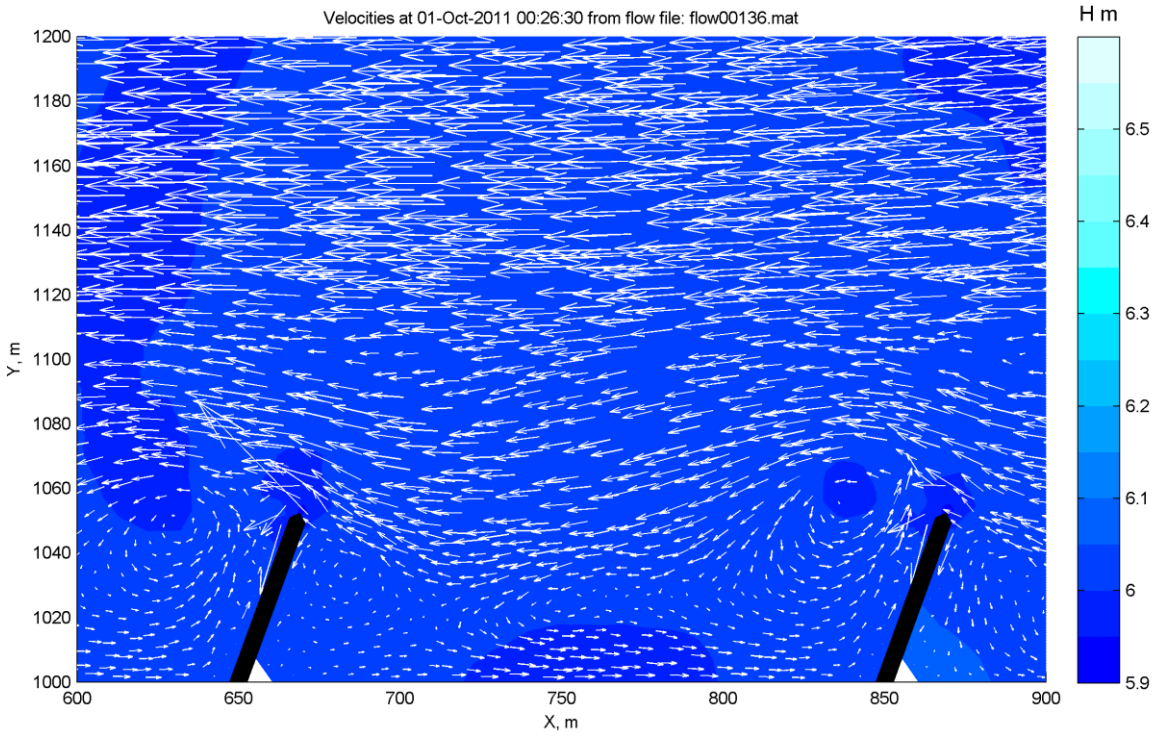
Velocities at 01-Oct-2011 00:26:30 from flow file: flow00136.mat
H m
Y, m
X, m
1200
1180
1160
1140
1120
1100
1080
1060
1040
1020
1000
600
650
700
750
800
850
900
6.5
6.4
6.3
6.2
6.1
6
5.9